2020

Impacts Of Intracellular Localizations Of Full-Length And Defective Viral Genomes On Paramyxovirus Particle Production

Emmanuelle Genoyer
University of Pennsylvania

Impacts Of Intracellular Localizations Of Full-Length And Defective Viral Genomes On Paramyxovirus Particle Production

Abstract

Paramyxoviruses are negative-sense single-stranded RNA viruses that comprise many important human and animal pathogens. During viral replication, paramyxoviruses produce defective viral genomes (DVGs), truncated genomic products that are unable to replicate in the absence of standard virus. DVGs influence the outcomes of infection through interference with standard viral replication and by inducing antiviral immunity. Using the model paramyxovirus, Sendai virus (SeV), we found that full-length (FL) and DVG viral RNA (vRNA) accumulated heterogeneously in cells during infection, with some cells accumulating predominantly full-length genomes (FL-high) and some accumulating predominantly DVGs (DVG-high). Interestingly, in FL-high cells genomes accumulated in a perinuclear region while viral genomes in DVG-high cells remained diffusely distributed throughout the cytoplasm. We sought to address the mechanisms and consequences of the differential intracellular distributions of viral RNA in the presence of DVGs. We found that vRNA in FL-high cells interacts with the host GTPase Rab11a and uses the recycling endosome system for particle production, while viral RNA in DVG-high cells does not interact with the host cell in this way. Consequently, FL-high cells produce both standard virions and defective particles, while DVG-high cells do not produce virions. We next addressed the determinants of this distinct intracellular localization. We reasoned that DVG-high cells, which robustly replicate vRNA but do not progress to virion assembly, fail to accumulate the viral proteins required for interaction between vRNA and Rab11a. We found that neither SeV matrix nor nucleoproteins are sufficient to drive this interaction. We identified the viral polymerase protein L and the accessory protein C as differentiating factors in cells that engage with Rab11a, and found C proteins to be the most enriched proteins in Rab11a immunoprecipitation followed by mass spectrometry. These data suggest that the polymerase complex proteins L and its cofactor C are critical in regulating initial steps in SeV assembly. Overall, this work investigated the intracellular distributions of viral genomes in the presence of DVGs to understand the impact of DVGs on the dynamics of full length and defective particle production, as well as to gain insights into viral proteins required to initiate viral assembly.

Degree Type
Dissertation

Degree Name
Doctor of Philosophy (PhD)

Graduate Group
Cell & Molecular Biology

First Advisor
Carolina B. López

Keywords
Defective particles, Defective viral genomes, Paramyxovirus, Sendai virus, Viral assembly

Subject Categories
Virology

IMPACTS OF INTRACELLULAR LOCALIZATIONS OF FULL-LENGTH AND DEFECTIVE VIRAL GENOMES ON PARAMYXOVIRUS PARTICLE PRODUCTION

Emmanuelle Genoyer

A DISSERTATION

in

Cell and Molecular Biology

Presented to the Faculties of the University of Pennsylvania

in

Partial Fulfillment of the Requirements for the

Degree of Doctor of Philosophy

2020

Supervisor of Dissertation

_____
Carolina B. López, Ph.D.
Associate Professor of Microbiology and Immunology

Graduate Group Chairperson

_____
Daniel S. Kessler, Ph.D.
Associate Professor of Cell and Developmental Biology

Dissertation Committee
Glenn F. Rall, Ph.D., Professor of Blood Cell Development and Function
Susan R. Weiss, Ph.D, Professor of Microbiology
Michael S. Marks, Ph.D., Professor of Pathology and Laboratory Medicine
Paul F. Bates, Professor of Microbiology

IMPACTS OF INTRACELLULAR LOCALIZATIONS OF FULL-LENGTH AND
DEFECTIVE VIRAL GENOMES ON PARAMYXOVIRUS PARTICLE PRODUCTION

To my mom, who always encouraged my curiosity and instilled in me a lifelong love of

learning.

ACKNOWLEDGEMENTS

I also have to thank my friends, near and far, who made life outside of the lab so enjoyable. Particularly thanks to Hannah Greenfeld for being the best friend and roommate I could have ever asked for. I can't imagine my everyday life of the past five years without you in it.

And of course, a mega thank you to Chris Greer, for absolutely everything. For being my go-to when I'm happy or sad, for your unwavering optimism and constant encouragement, and of course for bringing Pickle into my life. You have shaped my life in countless ways and I will always be thankful.

Finally, a very special thank you to Yan Sun and Jie Xu for being the best role models, mentors, and friends. I have grown immensely, personally and scientifically, from working alongside you. Not only did you teach me techniques and advise on experimental design, you also challenged me to ask better questions and to think more deeply. You have also always been there for me when I needed to laugh or needed a friend. Thanks for all the late nights in lab, arguments over hypotheses, silly gossip and coffee. I couldn't have done any of this without you two.

ABSTRACT

IMPACTS OF INTRACELLULAR LOCALIZATIONS OF FULL-LENGTH AND DEFECTIVE VIRAL GENOMES ON PARAMYXOVIRUS PARTICLE PRODUCTION

Emmanuelle Genoyer

Carolina B. López

Paramyxoviruses are negative-sense single-stranded RNA viruses that comprise many important human and animal pathogens. During viral replication, paramyxoviruses produce defective viral genomes (DVGs), truncated genomic products that are unable to replicate in the absence of standard virus. DVGs influence the outcomes of infection through interference with standard viral replication and by inducing antiviral immunity. Using the model paramyxovirus, Sendai virus (SeV), we found that full-length (FL) and DVG viral RNA (vRNA) accumulated heterogeneously in cells during infection, with some cells accumulating predominantly full-length genomes (FL-high) and some accumulating predominantly DVGs (DVG-high). Interestingly, in FL-high cells genomes accumulated in a perinuclear region while viral genomes in DVG-high cells remained diffusely distributed throughout the cytoplasm. We sought to address the mechanisms and consequences of the differential intracellular distributions of viral RNA in the presence of DVGs. We found that vRNA in FL-high cells interacts with the host GTPase Rab11a and uses the recycling endosome system for particle production, while viral RNA in DVG-high cells does not interact with the host cell in this way. Consequently, FL-high cells produce both standard virions and defective particles, while DVG-high cells do not produce virions. We next addressed the determinants of this distinct intracellular localization. We reasoned that DVG-high cells, which robustly replicate vRNA but do not progress to virion assembly, fail to accumulate the viral proteins required for interaction

between vRNA and Rab11a. We found that neither SeV matrix nor nucleoproteins are sufficient to drive this interaction. We identified the viral polymerase protein L and the accessory protein C as differentiating factors in cells that engage with Rab11a, and found C proteins to be the most enriched proteins in Rab11a immunoprecipitation followed by mass spectrometry. These data suggest that the polymerase complex proteins L and its cofactor C are critical in regulating initial steps in SeV assembly. Overall, this work investigated the intracellular distributions of viral genomes in the presence of DVGs to understand the impact of DVGs on the dynamics of full length and defective particle production, as well as to gain insights into viral proteins required to initiate viral assembly.

TABLE OF CONTENTS

LIST OF TABLES

LIST OF FIGURES

CHAPTER 1: Introduction

1.1 Paramyxoviruses

1.1.1 Paramyxoviruses in human and animal disease

Paramyxoviruses are negative-sense single-stranded RNA viruses that infect a wide range of animals causing a broad spectrum of diseases. Paramyxoviruses comprise many important human and animal pathogens that have high global burdens of morbidity and mortality. Some paramyxoviruses including measles, mumps, Rinderpest, and Newcastle Disease Virus are vaccine preventable or have been eradicated (1). However, among paramyxoviruses there are a number of human pathogens which currently lack vaccines and cause a human health burden. These include the human parainfluenza viruses (HPIV), which include the respirovirus genus members HPIV1 and HPIV3, and the rubulavirus genus members HPIV2 and HPIV4. These viruses circulate in the summer and fall of alternating years and cause disease in young children. HPIV1 and HPIV2 are the leading cause of croup in young children and HPIV3 is associated with bronchiolitis, bronchitis, and pneumonia(2). These infections have also been associated with the development or exacerbation of asthma and chronic airway disorders(3). Additionally, a study in 2015 demonstrated that HPIVs were the etiological agent of 7% of hospitalized pneumonia cases in U.S. children(4), and a study of children across five countries in Africa and Asia recapitulated these data in 2018(5). Importantly, there are no direct acting antivirals or prophylactic vaccines for these viruses.

Additionally, there are a number of zoonotic or epizootic paramyxoviruses which have caused small outbreaks in human populations for the past three decades and continue to pose a threat as emerging viruses. The viruses in the henipavirus genus, Hendra virus and Nipah virus, have caused a number of outbreaks with high case fatality rates since the 1990s. Henipaviruses circulate in bats and while little is known about these viruses in bats, they are not thought to cause severe disease in their host species.

2

However, spillover to human populations has proved deadly(6). Hendra virus (HeV) can cause fatal neurological disease in horses and in humans. HeV first appeared in Australia in 1994 and has since caused over 100 equine deaths and 7 human deaths, with spillovers being observed at least once a year(6, 7). While there is evidence that the virus may be transmitted from horse to human there is little evidence of sustained human to human transmission. Additionally, while there is now an efficacious vaccine for horses, there is no approved human vaccine(8). Nipah virus (NiV) was first identified in 1998 in an outbreak in Malaysia and Singapore(9). Since then it has crossed from bats to humans a number of times, presumably via consumption of fruits contaminated with bat urine or feces(9). Unlike HeV, NiV outbreaks have been partially driven by human to human transmission, with some outbreaks recording up to 75% of cases due to human to human transmission chains (6). These outbreaks have had high case fatality rates with some outbreaks reaching a case fatality rate of nearly 95% and there are no approved vaccines or direct acting antivirals(10). A number of other viruses in the henipavirus family that currently circulate in bats are being monitored for their potential transmission to humans, including Cedar virus. Additionally, other paramyxovirus genuses include viruses that circulate in bats, such as the rubulavirus Sosuga virus, and Beilong virus which belongs to its own genus, have shown limited transmissions to humans and are also monitored for their potential to spark outbreaks in human populations(11).

Finally, while vaccines were developed against measles and mumps in the 1950s, and by 1971 there was a licensed combination measles, mumps, and Rubella vaccine licensed in the United States that shows 93% efficacy against measles and 88% efficacy against mumps after two doses(12), challenges with vaccine adherence and

distribution have continued to leave people vulnerable to measles virus infection.

Additionally, waning humoral immunity to the mumps vaccine, even in fully immunized

populations, has led to periodic outbreaks(13). Further, Newcastle disease virus, also

known as avian avulavirus 1, which affects poultry and can be economically devastating

when livestock are infected. While there is an effective vaccine against NDV, not all

animals are vaccinated and there continue to be periodic outbreaks of this virus. Thus,

even in the presence of effective vaccines, these diseases continue to cause economic

and health burdens across the world.

With currently circulating paramyxovirus infections in humans that cause a

significant health burden, as well as potential zoonotic paramyxoviruses that lack

vaccines or treatments, it is particularly important to continue to study the basic biology

of these viruses. Understanding how the virus interacts with the host during infection can

yield various therapeutic targets that are either host or virus directed.

1.1.2 Paramyxovirus Replication

1.1.2.1. Viral genes and genomic replication

Paramyxoviruses are negative-sense single-stranded RNA viruses, which means

that their genomic RNA must be transcribed to positive-sense mRNA before being

translated in cells and the virus relies on a positive-sense intermediate antigenome for

replication (14). Paramyxoviruses code for six essential genes and a number of

accessory proteins. The six genes that comprise the essential genes of paramyxoviruses

in their order on the genome are as follows (**Fig 1.1A**). **1)** The nucleoprotein (NP) is the

most abundant protein product and coats the viral genome during replication and within

the virion. It is reported that there is one nucleoprotein for every six nucleotides in the

4

genome and that this interaction is very strong and stable(15, 16). This complex of viral

RNA coated in nucleoprotein is known as the viral nucleoprotein or vRNP. **2)** The

phosphoprotein (P) is a cofactor for the viral polymerase and is required for viral

replication and efficient nucleocapsid formation(17, 18). **3)** The Matrix protein (M) lines

the inner membrane of the virion and is important for driving contact between the vRNP

and the surface proteins(19, 20). **4+5)** The surface proteins are Fusion (F) and

Hemagglutinin (H) proteins (or Glycoprotein (G) or Hemagglutinin/Neuraminidase (HN),

depending on functionality), and are responsible for cell fusion and cellular attachment

and activation of fusion respectively(20-22). **6)** The polymerase or Large protein (L) is

the RNA dependent RNA polymerase (RdRP) that catalyzes the addition of nucleotides

and includes methyltransferase activity for capping nascent mRNA(14, 23).

Paramyxoviruses also encode a number of accessory proteins from the P gene, the

number and type of which vary by genus, that primarily function as innate immune

antagonists(24).

Paramyxoviruses enter the cell by fusion at the plasma membrane.

Hemagglutinin proteins bind to cell surface receptors and trigger conformational changes

to allow the fusion protein to direct fusion between the viral membrane and the cellular

plasma membrane(25) whereby viral genomic contents are deposited into the host

cell(26). Upon entry, negative sense viral genomes are coated with nucleoprotein and

carry with them L and P proteins. The L-P protein complex, or polymerase complex,

recognizes the leader sequence at the 3' end of the virus and synthesizes short RNA

strands before recognizing a gene start signal, which signals for the polymerase to

create a capped mRNA. The polymerase continues to synthesize mRNA until it reaches

the gene end sequence, where it will stutter along a polyU track to generate a polyA tail

for the mRNA. The polymerase then continues to scan the viral genome until it finds the next gene start sequence and begins to make the following mRNA(14). As the polymerase continues along the viral genome, it may lose processivity and fall off of the template strand. This leads to a gradient of mRNA expression where the first synthesized (3' proximal) mRNAs are in highest abundance and the last synthesized (5' proximal) mRNAs are at the lowest abundance(27) (**Fig. 1.1.A**). Viral mRNA is then translated and post-translationally modified by host cell ribosomes and host proteins.

After several rounds of transcription and the accumulation of viral proteins, the viral RdRP will change from "transcriptase" mode to a "replicase" mode and instead of synthesizing mRNA will begin to synthesize viral RNA (vRNA) genomes. It is hypothesized that the switch between transcriptase and replicase is governed by accumulation of NP proteins, whereby when a sufficient level of NP proteins coat the nascent RNA generated from the 3' end of the leader, the RdRP will bypass gene start events to create a vRNA(28, 29). The processive synthesis of vRNA form the negative strand genome yields a positive sense anti-genome, which is also completly coated in NP. The positive sense anti-genome contains the inverse trailer region which acts as a promoter and can be recognized by the RdRP to initiate replication. Importantly, the trailer region does not initiate any transcription events, and only replication can occur from this promoter. The antigenome is used as a template to generate negative sense genomes, which are able to propagate the viral lifecycle(14, 30). It has been reported that in Sendai virus, the trailer region is about 40 times stronger a promoter than the leader region which drives the synthesis of higher levels of negatives sense genomes during infection(29, 31) (**Fig. 1.1.B**).
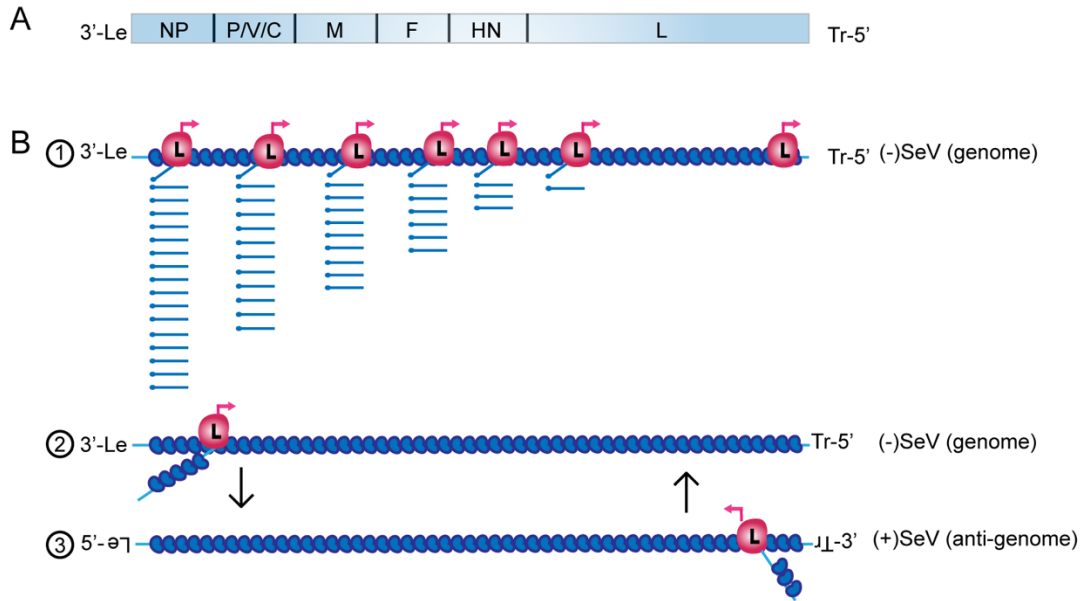
Figure 1.1 General Replication Strategy of Paramyxoviruses (A) Gene organization of SeV **(B)** Replication strategy of paramyxoviruses (1) Upon entry, the viral polymerase synthesizes capped and polyadenelyated mRNA, beginning at the 3' end of the genome. The polymerase progressively loses processivity leading to a gradient of mRNA with high levels of 3' proximal mRNAs and low levels of 5' proximal mRNAs. (2) After initial transcription of viral mRNA and accumulation of viral proteins, the polymerase switches to replication and generates an antigenome that is coated with nucleoprotein as it is synthesized (3) Positive-sense anti-genomes coated in nucleoproteins are replicated by the polymerase beginning at the 3'trailer to generate more negative-sense genomes.

1.1.2.2 Intracellular sites of replication

In contrast to positive sense RNA viruses which form membranous vesicles or associate with the endoplasmic reticulum, paramyxoviruses replicate within the cytoplasm of infected cells. Additionally while the nucleocapsid and matrix proteins of some paramyxoviruses have been reported to transit through the nucleus for post translational modifications such as ubiquitination(32, 33), their genomes do not have a nuclear phase. Viral genomes are replicated freely in the cytoplasm of cells. While inclusion body (IB) formation appears to be a hallmark of other negative sense virus families, including rhabdoviruses(34), filoviruses(35), and pneumoviruses(36, 37), some but not all paramyxoviruses have been reported to form inclusion bodies during

7

replication. For example, formation of inclusion bodies is a hallmark of Canine distemper virus (CDV)infection(38). Additionally, while IBs have been described to form during infection with parainfluenza virus 5 (PIV5)(39), measles virus(40, 41), and NiV(42), these IBs have been characterized as dynamic, forming and diffusing during infection. IBs are protein condensates that form in the cytoplasm and are driven by the accumulation of viral proteins with intrinsically disordered domains. These IBs are often classified as membranelles organelles that form by liquid-liquid condensation(37, 43). IBs are thought to concentrate viral RNA and viral proteins within the cytoplasm to increase rates of replication and to shield viral RNA from host cell sensors(44). However, not all paramyxoviruses replicate using IBs and the factors that dictate the formation of these inclusion bodies is not well understood.

1.1.3 Paramyxovirus Assembly and Virion Components

While viral genomes are replicated in the cytoplasm of infected cells, the virus buds from the plasma membrane and therefore the genome must be trafficked to the plasma membrane for virion assembly(20). Many negative sense RNA viruses have developed strategies to target their genome to the plasma membrane by hijacking the host recycling endosomal pathway(45). Host recycling endosomes travel along actin and microtubules propelled by the small guanine triphosphatase (GTPase) Rab11a. Recycling endosomal networks transport cargo in a bidirectional manner, to and from the perinuclear endosomal recycling center and the plasma membrane(46). This concerted bidirectional movement has been coopted by a number of viruses including paramyxoviruses(47-50), orthomyxoviruses(51, 52), pneumoviruses(53), filoviruses(54), and hantaviruses(55).

The paramyxoviruses Sendai virus(48), measles(50), mumps(49), and human parainfluenza 1 virus(47) have been shown to be dependent on Rab11a and

microtubules for the movement of vRNPs within the cytoplasm and for the production of infectious particles (**Fig. 1.2**). Whereas vRNPs use Rab11a to traffic to the plasma membrane, the surface proteins F and HN are synthesized in the endoplasmic reticulum and trafficked to the plasma membrane via the secretory pathway (22) and are preferentially sorted to lipid rafts(56). F and HN are thought to be trafficked independently of each other and recent work has shown that NiV surface proteins are stochastically incorporated into virions, rather than being incorporated at a fixed stoichiometric ratio, supporting the idea that these proteins reach the plasma membrane independently of each other.
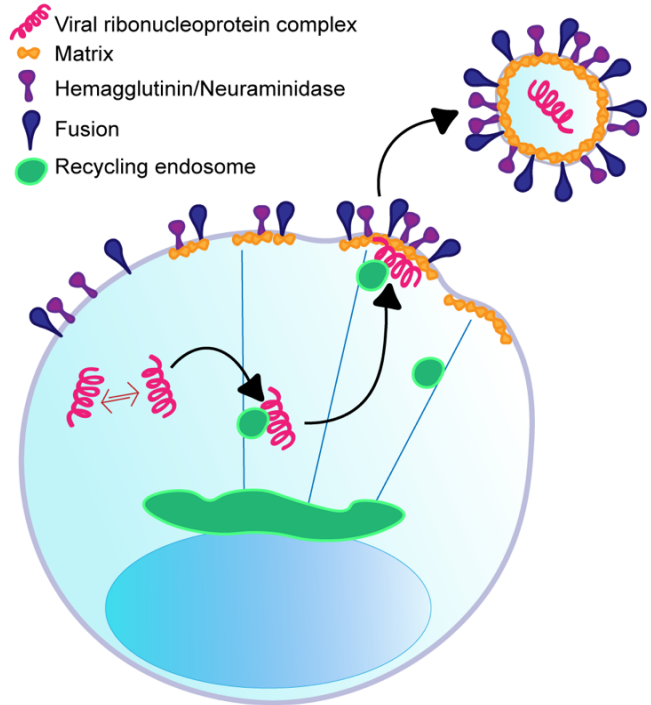
Figure 1.2. Schematic of Paramyxovirus Assembly
Viral ribonucleoprotein complexes are replicated in the host cell cytoplasm. After accumulation of viral proteins, vRNPs use recycling endosomes to transit to the plasma membrane where they interact with matrix, Fusion and hemagglutinin/neuraminidase proteins distributed on the cell surface.

The oligomeric matrix protein which forms a matrix along the plasma membrane serves to bridge the contacts between the surface proteins and the vRNPs(19). The incorporation of NiV F and G protein into virion occurs by interactions with matrix

9

protein(57). Matrix is also thought to direct specificity of vRNP incorporation into virions.

For example, while NP proteins from closely related SeV and HPIV1 are able to coat the

others genomes, they are not able to interact with their orthologous matrix protein and

form viral particles, indicating that NP-matrix contacts are important for producing

virions(58).

While the expression of matrix protein alone is sufficient to drive the production of

virus like particles in cells for most paramyxoviruses, including SeV(59) and HPIV1(60),

the association between the vRNPs and matrix is thought to enhance budding as vRNPs

induce curvature of the host membrane to induce scission(61). While many viruses

including retroviruses, filovirus, and rhabdoviruses use ESCRT proteins to drive

membrane scission and produce particles, the use of ESCRT by paramyxoviruses is not

universal(62). Viruses that use ESCRT for particle production include NiV(63), PIV5 (64)

and mumps(65). These viruses recruit ESCRT proteins via PPXY-like late domains in

their matrix proteins. However, other paramyxoviruses including measles bud in an

ESCRT independent manner(66). In addition, other membrane scission proteins

involved in vesicle formation such as Aip1/Alix have been shown to be recruited by

matrix and C proteins to enhance particle production in SeV(67, 68), but their

requirement for particle production remains contested(69). The accessory protein C,

generated from the P gene mRNA in SeV, HPIV1, MeV, NiV and others, has also been

implicated to play a role in particle production, either by enhancing the recruitment of

Aip1/Alix or Tsg101, an ESCRT component, to the plasma membrane(63, 68) or by

driving vRNP migration to the plasma membrane(70).

Though particle production has been long studied and the identification of the

involvement of Rab11 endosomal pathway has illuminated mechanisms of virus

trafficking to the plasma membrane, there are still a number of questions surrounding

the assembly of paramyxoviruses. First, the viral and host proteins that are critical for

vRNP interaction with Rab11a are unknown. It is clear that vRNPs interact with Rab11a,

but, the elements of the vRNP that interact with Rab11a are unknown. In addition, it

remains to be determined if another viral protein or other host factors are involved in this

interaction. Further, the mechanisms of transport of matrix proteins and the involvement

of C protein in particle production remain contested despite having been studied for a

long time. Finally, differences amongst paramyxoviruses, particularly in those that

express different accessory proteins, remains to be explored. The identification of

specific mechanisms of either virus or host proteins involved in virion assembly could

provide targets for the development of antivirals for a number of important diseases.

1.1.4 Sendai Virus

Sendai virus (SeV), recently renamed murine parainfluenza virus 1, is a member

of the respirovirus genus of the paramyxovirus family. The SeV genome is approximately

15kb in length with enveloped virions ranging in size from 110-540nm in diameter, based

on the amount of viral RNA that has been packaged(71). As a prototypical

paramyxovirus, SeV expresses the six common genes, as well as a large number of

accessory proteins from the P gene. These accessory proteins include four C proteins

(C, C', Y1, and Y2), which have been described to antagonize the interferon response by

binding to STAT1 and preventing its nuclear translocation(72), as well as having roles in

particle production as discussed above(70), and regulating the polarity of genome

synthesis(73). C proteins are generated from the P mRNA by translation initiations at

alternate start sites downstream of the primary AUG(74). V proteins are expressed from

mRNA generated by the insertion of a G during P mRNA synthesis which creates a

frame shift. Therefore V proteins share N terminus amino acid sequences with P but have a unique C terminus. The V protein is an innate immune antagonists and functions by blocking MDA5 activation to prevent IRF3 activation(75), blocking NLRP3 inflammasome activation to prevent IL1b secretion(76), and binding to RIG-I/TRIM25 to prevent RIGI ubiquitination and subsequent activation(77). These proteins are dispensable for replication in vitro but are required for pathogenesis in animal models(78, 79).

SeV infects rodents and causes a respiratory disease, with virus restricted to replication in the lung in the presence of tryptase Clara, a specific trypsin secreted by Clara (or Club) cells in the lung(80). While the virus has a strong organ specific tropism, and primarily replicates in bronchial epithelial cells, type I and type II pneumocytes, and alveolar macrophages, there are no entry specific factors that restrict this virus to rodents or to respiratory tissues, as SeV enters via binding to sialic acid(81). In natural hosts, SeV causes an acute disease and spreads rapidly amongst outbred and wild animals primarily via contact, with peak virus titers occurring 4 to 5 days post infection(82). Disease is characterized by roughened coat hair, dyspnea and, weight loss(1). Viral clearance is dependent on CD8+ T cells that are recruited to the lung by strong innate immune responses initiated by cell intrinsic immunity(83, 84). Mice will clear detectable SeV by day 10 or 11 and develop immunity characterized by a robust CD8+ T cell and antibody response. However, SeV can cause long term damage to lungs of infected animals(85, 86) and there is long standing evidence that SeV can remain as a persistent infection and be reactivated throughout the lifetime of hamsters(87).

SeV is most closely related to human parainfluenza virus 1, with 69% sequence homology at the nucleotide level. In fact, their high degree of similarity leads to cross reactivity of neutralizing antibodies both in humans and mice(88). Other respiroviruses closely related include HPIV3 and bovine parainfluenza virus. Because SeV can be easily studied in its natural host, it provides an excellent model system for studying these important human diseases. Additionally, SeV has been a longstanding model for paramyxoviruses and for negative sense single stranded RNA viruses as a whole with which many fundamental discoveries regarding the replication of RNA viruses have been made.

1.2 Defective Viral Genomes

DVGs exist across many viral families including DNA viruses, retroviruses, and RNA viruses(89-91). Defective viral genomes (DVGs) are viral replication products derived from the parental genome that in the absence of coinfection with a standard virus are unable to carry out a full replication cycle. DVGs can have small to large internal substitutions, deletions, and/or insertions that make the genome unable to produce one or more critical proteins while retaining their replication and packaging potential. Replication strategies of viruses are diverse, and the species of DVGs generated during replication are just as diverse within and across viral families. However, DVGs may be produced whenever a virus replicates.

1.2.1 Types and Generation of defective viral genomes

Among RNA viruses there are two dominant types of DVGs: deletion DVGs and snapback or copy-back DVGs. Both types of DVGs maintain the ability to complete a full replication cycle when complemented by a standard virus.

1.2.1.1 Deletion Defective Viral Genomes

Deletion DVGs retain both genomic termini that contain replication promoters but lack internal regions of the viral genome (**Figure 1.3**). Deletions can range from a few nucleotides, leading to alterations in or loss of certain
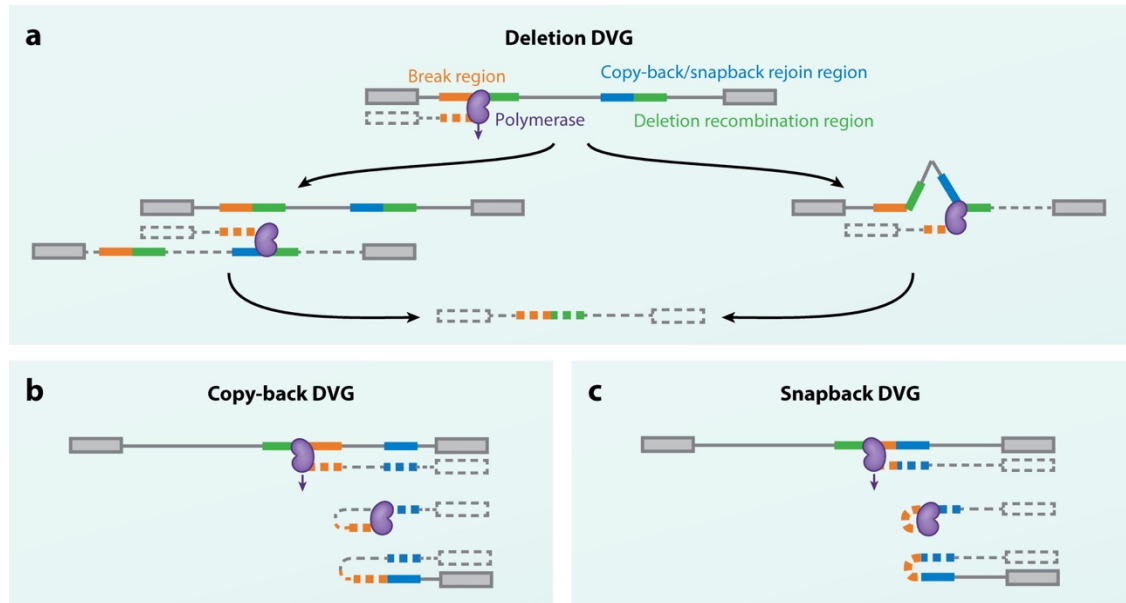
Figure 1.3. Types of DVGs and their proposed mechanisms of generation. Deletion DVGs are generated when the polymerase falls off a template strand at a break region and either switches to a new template strand or continues along the same template strand while skipping internal regions, rejoining at a deletion rejoin region that may have sequence homology to the region immediately following the break point. Copy-back DVGs are generated when the polymerase releases the template strand at a break point and rejoins the nascent strand at a nonhomologous region, creating a nonhomologous theoretical loop structure flanked by complementary ends. Snapback DVGs are formed similarly to copy-back DVGs but lack significant nonhomologous regions because the rejoin points are proximal to the break points. Abbreviation: DVG, defective viral genome. Figure published in (92).

viral proteins, to large truncations that preserve only the minimum amount of genome required to undergo replication by the viral polymerase(93, 94). Deletion DVGs are often found in positive-sense RNA viruses, including flaviviruses(95), alphaviruses(96), coronaviruses(97), and picornaviruses(98). Deletion DVGs are hypothesized to be formed when the viral polymerase begins to copy the template strand but falls off from the template at a break point and continues replication at a distal rejoin point on a new

14

template, skipping internal regions of the genome. Identification of small degrees of sequence homology at the break and rejoin regions of deletion DVGs led to the hypothesis that DVG generation may be driven by homologous recombination(96, 99). This hypothesis is supported by evidence that mutations in the viral polymerase that enhance recombination lead to more DVG generation in alphaviruses(96). Additionally, analysis of poliovirus DVGs indicated that predicted secondary structures in the genome encourage copy-choice recombination around sites frequently found in DVGs(100).

The majority of DVGs described from the negative-sense RNA influenza viruses and bunyaviruses are also deletion-type DVGs(101-103). Like in positive-strand RNA viruses, sequences in the break and rejoin regions of influenza virus DVGs share nucleotide similarities(104, 105). However, unlike in positive-strand viruses, homologous recombination events are rare in negative-strand viruses including influenza(106). Mutations in the influenza virus polymerase acidic (PA) protein enhance DVG generation(107, 108), and it has been hypothesized that tertiary structures of influenza viral ribonucleoproteins may underlie the relationship between break and rejoin points(105), indicating that DVG generation in these viruses may be driven by different mechanisms.

1.2.1.2 Copy-Back and Snapback Defective Viral Genomes

The predominant species of DVGs found in negative-sense RNA viruses are copy-back and snapback genomes. These DVGs are generated from the 5′ end of the viral genome and consist of a theoretical loop with complementary ends(109) (**Figure 1.3**). Snapback DVGs, differently from copy-back DVGs, do not contain much of a loop and are predominantly complementary with as little as a single noncomplementary nucleotide (110). Mechanisms for the generation of this type of DVG are still poorly understood. The prevailing model is that during viral replication the polymerase falls off

the template strand at a break point, rejoins the nascent strand at a rejoin point, and begins to copy back. Unlike minimally complementary regions found in break and rejoin points in deletion DVGs, there does not seem to be homology between break and rejoin points in copy-back DVGs. Because of the lack of a discernable pattern of copy-back DVG generation, it was thought to be a random process driven by an error-prone viral polymerase. However, sequence analysis of DVGs from the rhabdovirus vesicular stomatitis virus (VSV) found that some sequences may act as signals to the polymerase and may be more prone to act as break or rejoin points(111). Additional work from our laboratory shows that there are conserved regions in the genome of the pneumovirus respiratory syncytial virus (RSV) that act as rejoin points during infection and that a specific nucleotide composition is required in these regions for optimal DVG formation (112). The molecular mechanisms underlying the use of these specified break and rejoin points are the subject of current investigation.

1.2.1.3 Other Types of Defective Viral Genomes

While deletion and copy-back DVGs are the most prevalent, a wide range of viral genomic products can be classified as DVGs. A recently described type of DVG in influenza virus does not contain any deletions; rather, a viral segment is heavily mutated in promoter regions and packaging signals so that it interferes with replication of the standard virus(113). Other types of DVGs include mosaic or complex DVGs, which include viral genomes from different segments of segmented viruses, different viruses coinfecting a single host cell, or parts of the host genome(105, 114).

1.2.2 Defective Particles and Their Defective Viral Genomes

It is important to make the distinction between DVGs and defective particles (DPs) (historically referred to as DIPs) when interpreting literature and considering the

effects that defective viruses have during an infection. DVGs are, as described, viral genomes lacking regions of the genome that render them replication incompetent in the absence of a standard virus. These genomes may be either inside cells or inside viral particles. DPs are virions that contain a DVG. DIPs, as historically referred to, necessitate the function of interference, as is stated in their name; however, not all DPs are necessarily interfering.

DVGs may be generated de novo within an infected cell by the mechanisms discussed above. While specific conditions that facilitate either the generation or the accumulation of DVGs are unknown, there is evidence that host factors including host species and cell type can influence DVG generation. For example, avian influenza virus strains are more likely to generate aberrant replication products when they replicate in mammalian hosts and vice versa(115, 116), and West Nile virus (WNV) DVG generation and accumulation are affected by the host cell type and mouse strain used to expand the virus(117). Additionally, viral factors are implicated in DVG generation. Various mutations in the polymerase that alter fidelity can encourage DVG generation(96, 107), and different viral accessory proteins are implicated in regulating DVG generation in paramyxoviruses and orthomyxoviruses(118-120). Regardless, DVGs are generated when infections occur at a high multiplicity of infection(109, 121). DVGs generated de novo within an infected cell may impact the rate of standard virus replication and the accumulation of viral proteins, and they may have different functional consequences within the cell (**Fig. 1.4**).

DPs can spread to other cells during infection. To create a DP, a DVG must be packaged into a virion, and for some viruses this process requires a specific packaging signal. If deletion DVGs fail to retain packaging signals, they will not be transmitted as DPs. Examples include deletion DVGs generated during Semliki Forest virus, which
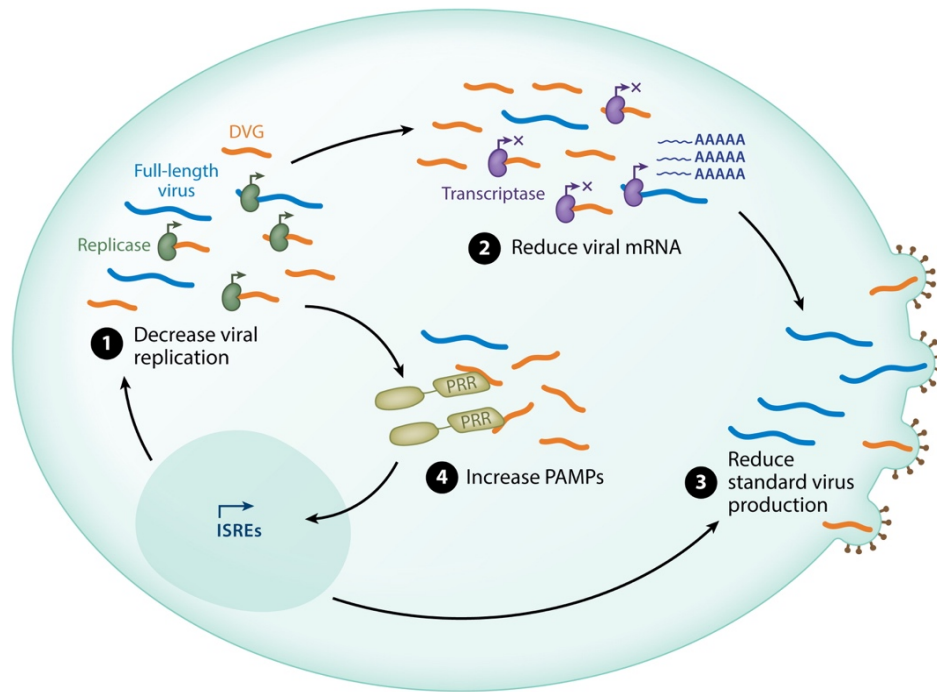
Figure 1.4 Impact of DVGs during infection. DVGs can limit standard viral replication through interference in a number of different ways within an infected cell, often with one type of interference leading to multiple levels of restriction on the standard virus. (1) DVGs can compete with standard virus for viral replication machinery including polymerase and nucleoproteins and may be at an advantage to standard virus due to their size or their promoters, leading to a decreased ratio of standard virus to DVGs. (2) Increased levels of DVGs compared to standard virus can decrease available templates for viral mRNA synthesis either because deletion DVGs lack coding regions for certain mRNAs or because copy-back and snapback DVGs are unable to code for any mRNA and thereby lead to reduced accumulation of viral proteins in the cell. (3) The limited amount of viral proteins can lead DVGs to compete with standard virus for surface proteins for assembly, compete with standard segments for incorporation into virions in segmented virus, or even induce degradation of surface proteins, leading to a decrease in virion production. (4) Increased accumulation of DVGs within the cell can trigger pattern recognition receptors to initiate signaling cascades leading to the upregulation of interferons and interferon-stimulated genes, which can in turn have inhibitory effects on viral replication or particle production. Abbreviations: DVG, defective viral genome; ISRE, interferon-sensitive response element; PAMP, pathogen-associated molecular pattern; PRR, pattern recognition receptor. Figure published in (92)

helped define critical packaging signals in the viral nonstructural protein nsp2(122), as well as clinically isolated DVGs identified in Middle East respiratory syndrome coronavirus that contain large deletions between ORF5 and the E gene and, therefore, may be unable to be packaged(123). These types of DVGs may affect the cell in which they arise de novo but might not be transmitted or amplified in other cells, except

potentially by mechanisms of virion-free cell-to-cell transmission(124).

For DVGs that can be packaged into virions, not all types of DVGs may be efficiently packaged and transmitted. Competition assays between the paramyxovirus Sendai virus (SeV) DVGs of different sizes show that larger DVGs have a packaging advantage over smaller DVGs, likely because they are better at inducing the membrane curvature required for particle formation(61, 125). However, these findings do not exclude the possibility that high levels of replication of smaller DVGs interfere with virion production in other ways. Similarly, different alphavirus DVGs are more or less efficiently packaged into DPs when propagated or produced in different cell lines(122). Furthermore, DVGs may have additional requirements for budding, as is the case for lymphocytic choriomeningitis virus (LCMV) DVGs. The PPXY domain of the matrix protein, Z, can be reversibly phosphorylated, and this posttranslational modification can either enhance or restrict production of DPs depending on which residue is phosphorylated, indicating a potential mechanism for the virus to regulate DP generation. Interestingly, production of LCMV DPs relies on the endosomal sorting complex required for transport (ESCRT) pathway, whereas standard virus particles can be produced in the absence of ESCRT and do not require the PPXY domain(126, 127).

1.2.3 Defective viral genomes and Disease

1.2.3.1. Defective Particles and Disease Outcome

Many early studies of the role of DVGs during infection were performed in the context of DPs. Most notably, the first studies using influenza virus showed that smaller noninfectious particles could influence the outcome of infection by reducing viral titers when the virus was grown in cell cultures or in eggs(128-130). After that, DPs for many other viruses were described including the negative-strand viruses SeV(131) and

19

VSV(132) and the positive-strand viruses Semliki Forest virus(133), Sindbis virus(134), and poliovirus(135).

Work in the 1970s and 1980s showed that DPs influenced infection outcomes in mice. In infections with Semliki Forest virus(136, 137) or with influenza virus(138, 139), mice that received an inoculum containing high levels of DPs in addition to the standard virus were protected from disease and had reduced levels of viral replication and virus dissemination compared to those receiving standard virus alone. Production of virus stocks with higher levels of DPs was observed when virus was grown to high titers or when animals were infected with viruses that contained high levels of DPs during initial infection. However, because the de novo production of DPs was observed only in viruses grown to high titers in tissue culture, the presence of DPs in natural infections was questioned and progress in the field slowed.

Work in the past decade has reexamined the role of DPs in disease outcome, and the original findings with orthomyxoviruses and alphaviruses have been confirmed and expanded to a number of additional viral families. Mice infected with stocks of SeV containing high amounts of DPs were protected from weight loss early during infection and induced stronger immune responses compared to mice infected with virus containing low amounts of DVGs. These findings were replicated by supplementing low DVG virus stocks with purified DPs, indicating that this protective effect is due to the addition of DPs(140). Similar observations were obtained in infections with influenza virus (140) or the pneumovirus RSV(141).

The role of DPs in viral infections was also expanded to arboviruses and nonvertebrate hosts. Infections of Drosophila with Sindbis virus with a high content of DVGs survived longer than flies infected with virus with a low content of DVGs(142). Additionally, mosquitos infected with stocks of WNV that contained high amounts of

DVGs had reduced infection, viral replication, and dissemination compared to those infected with stocks with low levels of DVGs. Interestingly, WNV findings in mosquitos were not recapitulated in mice, indicating that there may be different effects of DVGs or DPs in different host species(143).

Whether conclusions from infections of animal models using inocula with high initial levels of DPs apply to human infections is unclear. Models of interhost transmission describe high bottlenecks for infection where the production of thousands of virions from a transmitting host can lead to founding virus populations as small as a single virion in the receiving host(144). It therefore seems unlikely that during transmission a cell in a naive receiving host would be coinfected with a DP and a standard virus particle as this would require inoculation with a high DP to standard virus particle ratio. However, infections of hosts that are immunosuppressed or have comorbidities may increase sizes of founding populations, thereby increasing the probability of cells coinfected with a DP and a standard virus particle. However, initial infections may also occur with virions that have packaged both a DVG and a standard viral genome inside a single virion(71), or virions may aggregate during infection to enhance co-transmission, as reported for VSV(145) and poliovirus(146). Additionally, it is possible that DPs are independently transmitted during infection and that DVGs remain silent within a cell until that cell becomes infected with a standard virus before replicating. For paramyxoviruses, defective ribonucleoprotein complexes are stable within cells, in the absence of replication for up to 96 hours(147, 148). Evidence that DVGs are transmitted between hosts during natural infection with influenza virus comes from finding the same DVG RNAs in patients infected with pandemic H1N1 linked by direct contact(104), although this does not exclude that the same DVGs were present in patients due to sequences in the viral genome that promote the generation of DVGs at

specific regions.

<u>*1.2.3.2 Defective Viral Genomes and Disease Outcome in Natural Infections*</u>

DVGs have been detected in tissues and fluids of humans and animals infected with influenza(104), dengue(95), hepatitis C(149), hepatitis A(150), WNV(143), or measles(151). However, due to a generalized belief that DVGs did not play an important biological role, the literature on this topic was limited to descriptive rather than mechanistic studies. Recently, DVGs were identified in clinical samples from respiratory secretions of children infected with RSV, and, importantly, their presence correlated with stronger innate immune responses in these patients(152). These observations demonstrated for the first time that naturally occurring DVGs may play an important role during natural infections. Further, during natural infections with influenza virus, patients infected with a virus containing a mutation in the polymerase basic 2 subunit of the polymerase were more likely to accumulate DVGs. Importantly, this variant was found more often in patients who recovered from the infection compared to those who were categorized as severely ill(107).

<u>1.2.4 Mechanisms of DVG Impacts on Infection</u>

DVGs and DPs were first discovered for their ability to interfere with standard virus replication and production. DVGs were first described in influenza virus infection in the late 1940s by Preben von Magnus and termed von Magnus particles (128, 129). Upon infection of the same cell as a standard virus, von Magnus particles reduced the production of standard virus presumably by competing for resources with the parental virus. Interference has been demonstrated for DVGs and DPs from a number of viruses, and in many cases an impact on infection outcome has been demonstrated.

<u>*1.2.4.1 Mechanisms of interference*</u>

DVGs can exert interfering pressure at multiple levels during the production of progeny virus (**Fig. 1.3**). During replication, DVGs can compete for the viral polymerase as well as consume the nucleocapsid proteins for coating its genome. The small size of DVGs confers a replication advantage. In addition, in negative-sense RNA viruses the 5′ trailer promoter is approximately 40 times more favorable than the 3′ leader promoter, and as snapback or copy-back DVGs are flanked by trailer promoters, they are replicated at an advantage to a leader-trailer–flanked virus(153). Additionally, DVGs may accumulate mutations in their promoter regions, which can confer advantages over the standard virus. DVGs may also compete for structural proteins to be packaged into virions, thereby limiting the number of infectious particles produced. Particularly for segmented viruses, the packaging of DVGs into particles can limit levels of infectious particles(154). Additionally, DVGs may lead to degradation or increased turnover of viral proteins or suppress structural proteins required for assembly, as is the case in SeV, where the presence of DVGs associated with increased degradation of the viral matrix protein and decreased surface expression of the hemagglutinin-neuraminidase protein(155, 156). t

Although the mechanisms of interference have been hypothesized and studied, we do not know the exact ratios of DPs that are required to completely interfere with standard virus replication and particle production. Additionally, it is likely that not all DVGs exhibit similar interfering abilities. For example, multiple types and sizes of DVGs from VSV can efficiently interfere with some strains of parental virus, while other parental strains can replicate these DVGs but do not seem to be subject to interference(157). Interestingly, not all types of DVGs can interfere with replication of standard virus. Particularly, certain strains of WNV seem to be insensitive to interference by DVGs (158). DVGs from WNV also show differing abilities to interfere with virus replication in a

23

host-dependent manner, with interference occurring in mosquito hosts but not mouse hosts(117). These differences in interference ability may be due to host intrinsic factors that limit DVG replication or to changes in viral replication between hosts.

1.2.4.2 Interference and Disease Outcomes

The role of DVGs in modulating outcome of infection can be attributed in part to the ability of DVGs to interfere with the standard virus and prevent damage to the host from viral replication. Data from influenza virus suggest that one DP is sufficient to temper levels of standard virus replication to levels that limit cytopathology, although the role that interferon induction plays in this system may confound these interpretations(159). Interference may play a critical role in determining disease outcome when animals are infected with high levels of DP-containing virus stocks or when DPs are given therapeutically or prophylactically. For naturally arising DVGs, the role of interference and how this dictates host outcome are less clear. Although interference could certainly play a role within an infected cell that generates a de novo DVG, whether there will be high-enough DPs produced in a naturally infected host is unclear. The levels of DPs generated in a particular host and the ratio of DPs to infectious particles within local foci of infection may critically determine if interference occurs at biologically relevant levels in vivo.

1.2.4.3 Innate Immune Activation

One of the best-characterized functions of DVGs during infection is their ability to induce innate immune responses, including expression of interferons, interferon-stimulated genes, cytokines, and chemokines. The primary descriptions of DVGs as inducers of antiviral immunity were during infections with negative-sense RNA viruses. In the absence of DVGs, there was no immune activation, while in the presence of DVGs at the onset of infection in the form of DPs, or after de novo generation in a natural

infection, there was strong induction of the antiviral immune response(121, 140, 141, 160-164). In addition, not all cells engage in an immune response during viral infections, corresponding with the heterogeneous accumulation of DVGs within infected cells(140, 165). In infections with SeV, cells that accumulated high levels of DVGs were the primary inducers of interferon as measured by interferon regulatory factor 3 nuclear translocation(166) and antiviral innate immune signatures obtained by transcriptome analysis of infected cell populations(165).

DVGs are strong inducers of the innate immune response by acting as strong pathogen-associated molecular patterns (PAMPs) during viral infection. The addition of purified DPs to SeV or RSV infections promotes the induction of the antiviral immune responses in an RLR-dependent manner(141, 163). This response is DVG specific, as addition of increasing amounts of standard virus is not sufficient to induce interferon to similar levels(140, 163, 164). Additionally, immunoprecipitation of retinoic acid-inducible gene-I (RIG-I) followed by RNA-seq revealed that most of the ligands bound to RIG-I correspond to segments within the 5′ terminus of the virus, the region from which copy-back DVGs are formed(167). Moreover, analysis of the RNA structure of the predominant SeV DVG, DVG-546, found a molecular motif that enhanced binding of RIG-I and MDA5 to the RNA(166). DVGs produced from measles have also been shown to bind to RLRs (168, 169), and similar principles apply to other negative-sense RNA viruses. While certain well-characterized DVGs have been shown to interact directly with binding partners during infection, this may not be true for all DVGs. First, not all DVGs are equally good at inducing immune responses, as studies with SeV have shown that specifically copy-back DVGs induced innate immune responses compared to deletion DVGs or truncated DVGs(170). Second, it is unknown whether these principles described for negative-sense RNA virus DVGs will translate to positive-sense RNA

25

viruses.

The features that make some DVGs such powerful PAMPs have been investigated. Because DVGs share most, but not all, sequence homology with standard virus, sequences within the DVG may facilitate RLR binding and activation, presumably in an RNA-secondary structure dependent manner. Data using the strongly immunostimulatory SeV Cantell DVG-546 support this argument(166). However, viral RNA from negative-sense RNA viruses is thought to be coated in nucleoprotein within an infected cell, as encapsidation is required for replication, thereby preventing RLRs from accessing the viral RNA. Analysis of measles virus indicated that the lack of encapsidation is critical for the induction of innate immune response by DVGs(168), suggesting that non-encapsidated viral RNA may exist in infected cells. Further, it has been suggested that SeV DVGs are generated by viruses that encode a variant of the nucleoprotein that binds viral RNA less tightly(171), potentially exposing viral RNA to pattern recognition receptors. To reconcile the need for encapsidation for replication and the lack of encapsidation for immune stimulation, a subset of DVGs may be uncoated and stimulate immunity and another subset may be fully coated and replicate potentially exerting interfering pressure. Whether this occurs in the same cell or there are certain cells that contain non-encapsidated DVGs is unknown, but as only a subset of cells elicits an interferon response upon infection, it may be that only a subset of DVGs is able to elicit immune responses.

Another explanation for the ability of DVGs to rapidly induce the antiviral immune response is their ability to interfere with the expression of viral-encoded antagonists. Lack or low expression of viral-encoded antagonists allow the virus to trigger an immune response. However, induction of interferon by DVGs during SeV infections occurs before viral-encoded antagonists accumulate to high levels(163, 164). Additionally, comparison

between antagonist proteins in different strains of SeV that differ in their interferon-inducing abilities showed no difference in ability to antagonize interferon induction in transfection-based assays, further supporting the claim that absence of viral antagonism is not responsible for DVG induced immune responses(171).

Interestingly, interferon antagonists of paramyxoviruses have been shown to limit DVG generation. The accessory protein C found in paramyxoviruses such as measles, Human parainfluenza viruses type 1 and 3, and SeV antagonizes the innate immune response by preventing signal transducer and activator of transcription 1 (STAT1) phosphorylation. The presence of C limits DVG accumulation, as recombinant viruses that lack expression of these proteins produce very high levels of DVGs even when passaged at low multiplicity of infection(118, 119). How C proteins act to limit DVG generation or accumulation is not known, but it may be related to the role that C proteins play in altering polymerase preferences for RNA templates(31). Unpublished data from our lab show that cells that accumulate high levels of DVGs during infection have very low levels of C expression, but whether a lack of C leads to the accumulation of DVGs or whether the accumulation of DVGs limits expression of C is yet to be determined. In fact, these two options are not mutually exclusive, and antagonist or accessory proteins and DVGs may have multiple levels of coregulation.

1.2.5 Defective Viral Genome–Induced Heterogeneity in Infection

During infections with virus stocks containing DPs some cells accumulate high levels of DVG RNA while others accumulate predominantly full-length virus RNA(165). The causes of this heterogeneity are not fully understood but it may be related to the initial input ratio of DPs to standard virions. (**Figure 1.5**). Additionally, there is heterogeneity among cells infected with standard virus that go on to produce de novo

DVGs(172). This type of heterogeneity may also be driven by input virus levels (as

DVGs are more prone to generation under high multiplicity of infection conditions) or by

host intrinsic factors that regulate DVG production.

The heterogeneity in viral nucleic acid accumulation during infection is important

due to the differing functional outcomes of infected cells. In infections with SeV and

RSV, cells that accumulate high levels of DVGs induce a potent immune response

through retinoic acid-inducible gene-I-like receptors (RLRs) signaling and produce
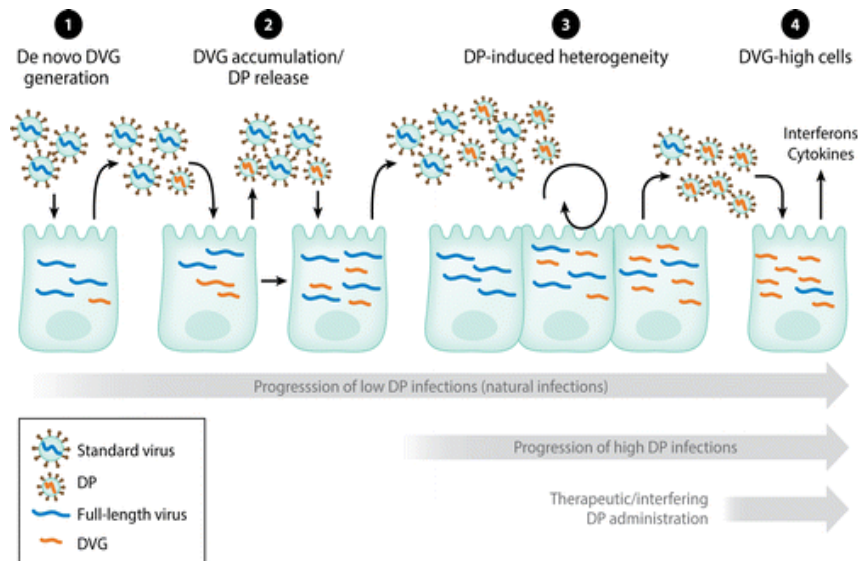
Figure 1.5 DVG and standard virus dynamics during infection progression. (1) Low DVG infections will eventually lead to the de novo generation of DVGs within a cell, presumably in cells infected at a high multiplicity of infection or supporting high levels of viral replication. (2) Once DVGs are generated, they will accumulate and be released from the cell as DPs. DVG will then propagate in neighboring cells infected with standard virions. (3) Once high levels of DVGs have accumulated and sufficient DPs have been released, local foci of infection will become heterogeneous, with cells having low, intermediate, or high levels of DVGs depending on infection ratios of DPs to standard virions. (4) As DVGs and DPs accumulate, some cells receiving high levels of DPs will become DVG high and induce the production of interferons and cytokines but fail to produce virus or DPs. Progression of low DP infections, presumably upon natural transmission, will occur from stages 1 to 4. Infection with viral stocks containing high levels of DVGs or during high particle transmission events will progress from 3 to 4. Therapeutic or prophylactic administration of DPs will likely result uniquely in stage 4. Abbreviations: DP, defective particle; DVG, defective viral genome. Figure published in (92).

interferons, interferon-stimulated genes, cytokines, and chemokines(165, 166). The triggering of RLRs also stimulates the expression of pro-survival tumor necrosis factor (TNF) family member proteins and protects these cells from TNF-mediated cell death, while cells that are enriched in full-length virus are killed by TNF released from DVG-high cells(165). Heterogeneity in induction of immune responses has also been shown for other viruses, such as influenza, through single-cell RNA sequencing of cellular mRNA and viral RNA (172, 173).

In addition to heterogeneity of initiation of immune responses, there is also heterogeneity in the ability of infected cells to produce standard and defective viral particles. During infections with VSV, virus particle production is variable when single cells are examined compared to a bulk population(174). When DPs are added at varying amounts, the heterogeneity in standard virus production increases. Examination of single cells revealed that cells vary from producing no virus to producing low or high levels of virus depending on the input ratio of DPs to standard virus(174, 175). Taken in concert with the idea that these full-length high cells die promptly in infections, while DVG-high cells survive, these observations raise intriguing questions as to the dynamics at play within cells with different contents of DVGs during virus persistence and virus transmission.

1.3 Experimental Questions

The López lab has long used the murine parainfluenza virus, Sendai virus, as a model to study the impact of defective viral genomes during infection particularly on the initiation of the immune response and on the outcomes of infection in mouse models(140, 141, 163-166). In order to study the impact of DVGs on paramyxovirus infection at an intracellular level, we developed an RNA fluorescence in situ hybridization

29

(FISH) approach that enabled us to distinguish full-length from defective viral genome RNA. This approach allowed for the visualization of DVGs during infection, which had previously been difficult due to their sequence homology with the standard virus. Using this technology, we observed that upon infection with SeV viral stocks containing high levels of defective particles, there is heterogeneity in the accumulation of DVGs amongst cells, with some cells accumulating high levels of DVGs and some cells accumulating high levels of full-length virus. These distinct cellular phenotypes were characterized by RNA-seq and indicated that these cells engage distinct transcriptional profiles with DVG-high cells having a pro-inflammatory and pro-survival pathway upregulated in contrast to FL-high cells which had cellular stress and unfolded protein response pathways upregulated(165).

In addition to distinct transcriptional status and cell fates of these cells, we observed that the intracellular localization of viral RNAs in these cells was distinct. While full-length virus high cells have viral RNA that clusters in a perinuclear region, DVG-high cells display viral RNA diffusely throughout the cytoplasm. This observation led to several questions that are the driving motivation for this work, including what the mechanisms of this differential localization are and how does this differential localization impact the viral lifecycle during infection. *We hypothesized that discrete localizations of viral RNA would impact viral particle production due to differential engagement with pathways coopted for virion assembly and that this differential engagement with the host is driven by different levels of accumulation of viral proteins.*

In Chapter 2, I will discuss the characterization of the intracellular localizations of viral genomes in these two distinct cell populations. We asked which host factors viral genomes engage with in these cellular subsets and found that viral genomes in FL-high

cells engage with the Rab11a marked recycling endosomes, while viral genomes in DVG-high cells do not. I will then explore how these differences in localization impact particle production, as the Rab11a pathway is critical to initial steps in virion assembly.

In Chapter 3, I will take advantage of the heterogeneity in viral engagement with the host cell to parse replication and particle assembly to identify critical viral proteins required for engagement with Rab11a. I will examine the role of M and NP proteins as well as C protein and the viral polymerase L in during SeV infection in order to better understand which viral proteins are required for interaction with Rab11a.

Overall, this work seeks to understand the impacts of heterogeneous distributions of DVGs in SeV infections on particle production and infection dynamics and harness these differences to understand the role of viral proteins during paramyxovirus assembly.

CHAPTER 2: Defective viral genomes alter how Sendai virus interacts with cellular trafficking machinery leading to heterogeneity in the production of viral particles among infected cells

The contents of this chapter have been published as:

2.1 Abstract

Defective viral genomes (DVGs) generated during RNA virus replication determine infection outcome by triggering innate immunity, diminishing virulence, and, in many cases, facilitating the establishment of persistent infections. Despite the critical role of DVGs during virus-host interactions, the mechanisms regulating production and propagation of DVGs are poorly understood. Visualization of viral genomes using RNA fluorescent *in situ* hybridization revealed a striking difference in the intracellular localization of DVGs and full-length viral genomes during infections with the paramyxovirus Sendai. In cells enriched in full-length virus, viral genomes clustered in a perinuclear region and associated with cellular trafficking machinery, including microtubules and the GTPase Rab11a. However, in cells enriched in DVGs, defective genomes distributed diffusely throughout the cytoplasm and failed to interact with this cellular machinery. Consequently, cells enriched in full-length genomes produced both DVG and full-length genome-containing viral particles, while DVG-high cells poorly produced viral particles, yet strongly stimulated antiviral immunity. These findings reveal the selective production of both standard and DVG-containing particles by a subpopulation of cells during infection that can be differentiated by the intracellular localization of DVGs. This study highlights the importance of considering this functional heterogeneity in analyses of virus-host interactions during infection.

2.2 Significance

Defective viral genomes (DVGs) generated during Sendai virus infections accumulate in the cytoplasm of some infected cells and stimulate antiviral immunity and cell survival. DVGs are packaged and released as defective particles and have a significant impact on infection outcome. This chapter shows that the subpopulation of

DVG-high cells poorly engages the virus packaging and budding machinery and do not

effectively produce viral particles. In contrast, cells enriched in full-length genomes are

the primary producers of both standard and defective viral particles during infection. This

study demonstrates heterogeneity in the molecular intracellular interactions occurring

within infected cells and highlights distinct functional roles for cells as either initiators of

immunity or as producers and perpetuators of viral particles depending on their content

and intracellular localization of viral genomes.

2.3 Introduction

Defective viral genomes (DVGs) are the primary immunostimulatory molecules

during infection, both *in vitro* and *in vivo,* and stimulate a cellular pro-survival program

that facilitates the establishment of persistent infections (140, 164, 165, 176).

Additionally, DVGs occur in natural infections in humans, likely impacting the infection

outcome (107, 141). However, despite their critical role during virus-host interactions, the

mechanisms regulating DVG production and propagation are poorly understood. The

presence of DPs within viral stocks amplified in the laboratory is nearly ubiquitous and

for decades it has been assumed that all infected cells produce DPs upon reaching a

high titer of virus replication (95, 177-183). However, we have reported remarkable

heterogeneity in the accumulation of DVGs within a subset of cells during infection with

the model paramyxovirus Sendai (SeV). This heterogeneity is associated with distinct

functions of the DVG-high cell population, including the induction of antiviral immunity

(140, 164, 166) and the facilitation of viral persistence via the induction of a pro-survival

cellular program (165). In contrast, cells containing low or no DVGs had a negligible

contribution to these processes. This evidence, together with recent evidence of

heterogeneity in both viral replication and particle production of other RNA viruses (172,

174, 184-186) led us to investigate how DVGs impacted the production of both DPs and standard viral particles.

Using RNA fluorescent *in situ* hybridization (FISH) that allows us to distinguish defective and full-length (FL) viral genomes within infected cells, we discovered that in addition to heterogeneity in the amount of DVGs among infected cells, viral genomes localized to different intracellular spaces in DVG-high and FL-high cells. Importantly, this differential localization critically impacted the ability of viral RNPs to interact with the cellular machinery used to produce viral particles. As a result, DVG-high cells had a drastically reduced production of both standard and defective viral particles compared to FL-high cells. This study reveals two functionally distinct populations during SeV infection that can be distinguished by the amount and intracellular localization of DVGs. In addition, together with published evidence of a critical role for DVGs in driving innate immunity, this study highlights the critical importance of considering the remarkable division of labor among infected cells in the study of virus-host interactions.

2.4 Results

2.4.1 DVGs alter the intracellular distribution of viral ribonucleoprotein (vRNP) during infection

To investigate if the presence of DVGs altered the interactions of vRNPs with cellular components, we first assessed whether DVGs changed the localization of viral ribonucleoproteins (vRNPs) in infected cells. To do this, we infected cells with stocks of SeV strain Cantell depleted of DVGs (SeV-LD) at MOI 1.5 $TCID_{50}$/cell (HAU of 3 per 5×10^5cells) and supplemented the infections with increasing HAU doses of purified DPs containing the SeV Cantell DVG-546 (**Fig 2.1A-E**). Sendai virus Cantell strain naturally

produces one specific DVG 546 nucleotides in length, making this an ideal system for identifying DVGs by PCR (140, 170). We measured the levels of DVG-546 in infected cells by RT-qPCR and found that amount of DVG-546 increased corresponding to greater doses of DP as expected (**Fig 2.1B**). Since viral RNA is associated with nucleoprotein (NP) to form vRNPs (187), visualization of NP protein was used as an initial proxy for vRNPs. Using a stock of virus with low contents of DVGs (SeV-LD + pDP HAU 0), we noted that NP accumulates in a perinuclear region of the infected cell. However, upon addition of increasing doses of DPs during infection, there was a dose-dependent increase in cells that display a cytoplasmic and diffuse NP staining with a corresponding loss of cells that have predominantly perinuclear NP (**Fig 2.1A**). To quantify these differences, we assessed the size of the area occupied by NP per infected cell and determined that NP became more spread out throughout the cell cytoplasm with increasing amounts of DVG (**Fig 2.1C**). Importantly, we also used immunofluorescence to quantify amount of NP within infected cells and determined that presence of DVGs did not decrease the amount of NP within infected cells when imaged at a per cell basis (**Fig 2.1D**). However, the number of cells that were productively infected decreased significantly with the addition of increasing amounts of DPs (**Fig 2.1E**), likely explaining the reported reduction in NP production in cell populations infected in the presence of DVGs (140).

Next, we examined the localization of SeV NP in the presence of DVGs over time. To do this we infected cells with SeV-LD (**Fig 2.1F**) or with SeV containing DVGs at levels similar to SeV-LD + pDP HAU 20 (SeV-HD), and compared NP distribution. Distinct intracellular distributions were seen starting at 12 h when NP accumulated to
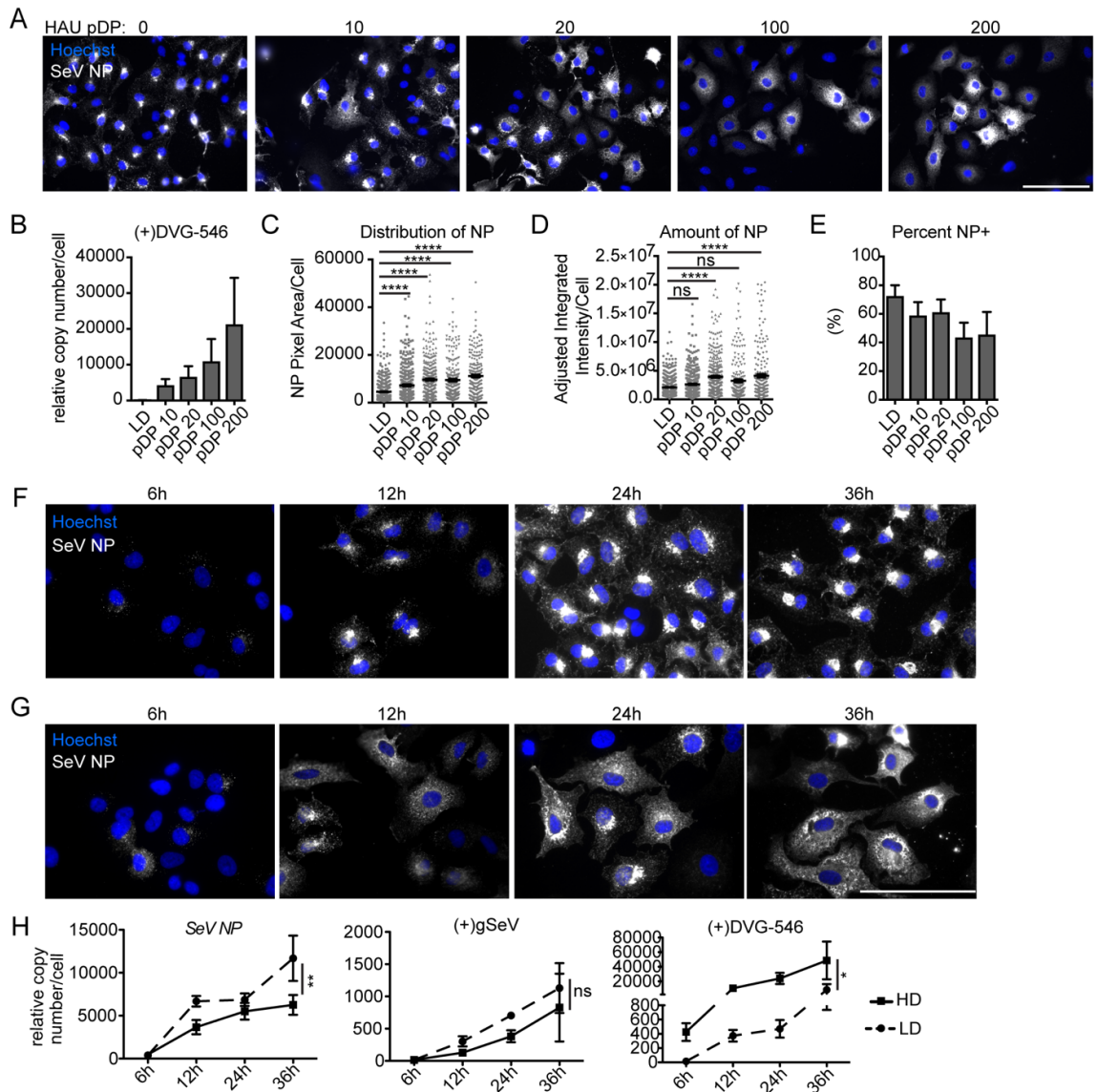
Figure 2.1. Defective viral genomes alter viral nucleoprotein distribution within infected cells. (A) A549 cells infected with SeV-LD MOI 1.5 TCID$_{50}$/cell supplemented with purified DPs at indicated HAU, for 24 h and stained for SeV NP (grey) and nuclei (blue). Images captured at 40X, wide field. Images are representative of 3 independent experiments. Scalebar = 100µm. **(B)** RT-qPCR of SeV (+)DVG-546 relative to *GAPDH*. **(C)** Percentage of cells per field that are NP+ as determined by level of fluorescence above background **(D)** Quantification of SeV NP amount by fluorescence intensity and **(E)** distribution of NP by Pixel area within individual cells at 24 h post infection. Results show sum of 3 independent experiments with >250 individual cells analyzed per condition. Individual cells are plotted with a line at mean, error bar represents ± SEM **** = p < 0.0001 by Kruskal-Wallis test, with Dunn's multiple comparisons test. **(F)** A549 cells infected with SeV-LD and **(G)** SeV-HD for indicated time points and stained for SeV NP (grey) and nuclei (blue). Images captured at 63X, wide field. Images are representative of four independent experiments. Scalebar = 100µm. **(H)** RT-qPCR for SeV NP, (+)gSeV and (+)DVG-546 relative to *GAPDH*. Data is represented as mean ± SEM of three independent experiments, ** = p< 0.005, * = p<0.05 by two-way ANOVA with significance indicated between viral infections.

detectable levels. At this time point, in cells infected with SeV-LD, NP began to uniformly accumulate in a perinuclear region. This distribution was maintained until at least 36 h post infection **(Fig 2.1F)**. In contrast, SeV-HD infections demonstrated heterogeneity in the distribution of NP throughout the time points analyzed **(Fig 2.1G)**. As expected for bulk population analysis, HD infections showed lower levels of FL genomes and SeV NP mRNA and higher levels of DVGs compared to LD infections **(Fig 2.1H),** though as mentioned earlier bulk population analysis may confound the interpretation of these data, artificially lowering values of SeV NP levels on a per cell basis. These data demonstrate that the presence of DVGs during infection alter the intracellular distribution of NP independent of changes on its transcription.

<u>2.4.2 DVGs and full-length genomes localize disparately in infected cells.</u>

Because the addition of DPs to viral infections altered the intracellular localization of viral NP, we next investigated and differentiated the intracellular distribution of DVG-containing vRNPs and FL-genome containing vRNPs using RNA fluorescent *in situ* hybridization (RNA FISH). Probes targeting the 5'- end of the (+)-sense genome colored red and probes targeting the 3'- end of the (+)-sense genome pseudo-colored green were used to distinguish DVGs in green and FL viral genomes as orange (hybridizing both red and green probes), as we have described (165) **(Fig 2.2A)**. RNA-FISH of cells infected with SeV-LD or SeV-LD plus increasing amounts of purified DPs confirmed that FL genomes and DVGs accumulate in different cells and that their intracellular distribution is distinct **(Fig 2.2B)**. In SeV-LD infections, FL genomes were clustered in a perinuclear region and addition of DPs resulted in the appearance of DVG-high cells with DVGs present throughout the cytoplasm. As the amount of DPs added to an infection
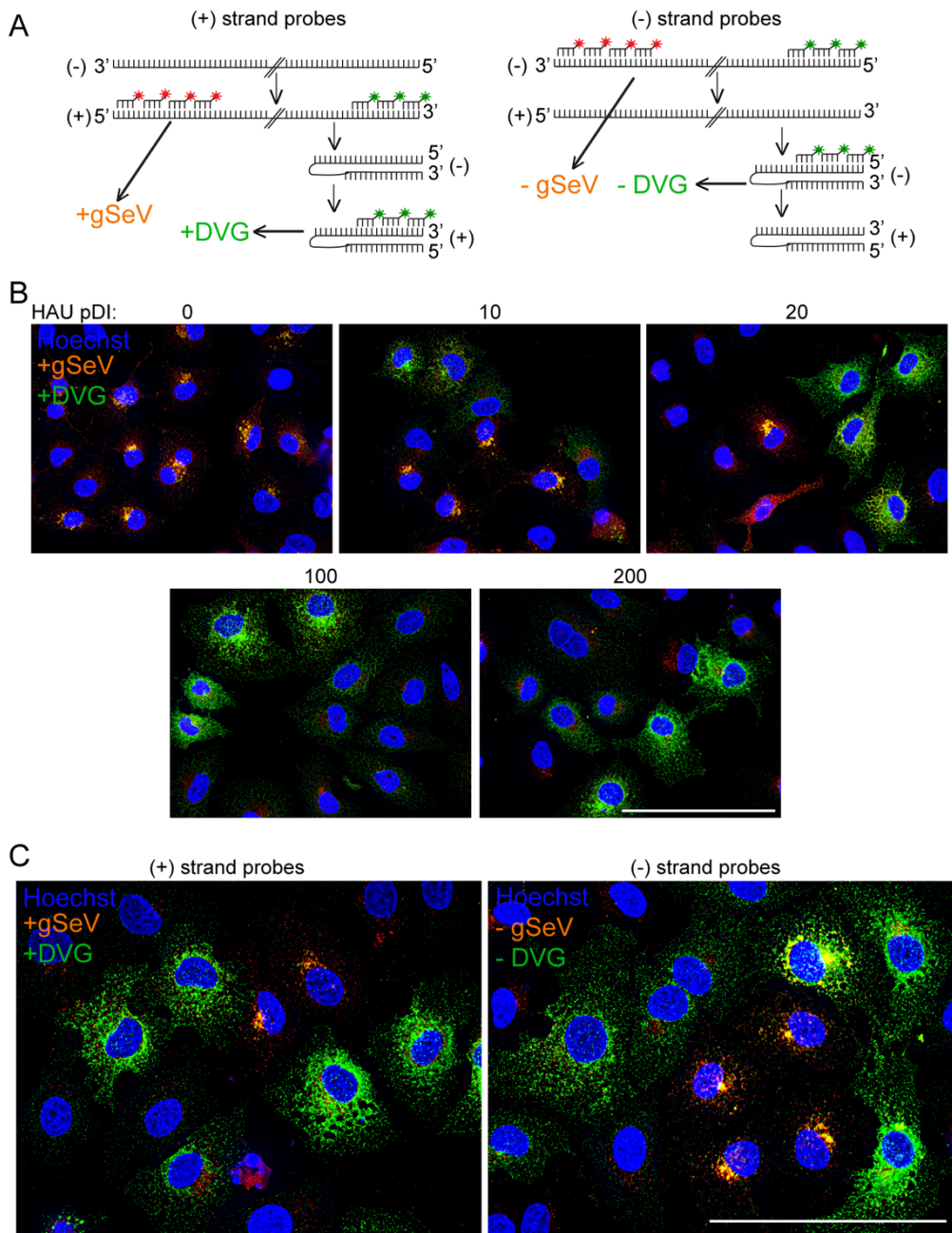
Figure 2.2. FL genomes accumulate in a perinuclear region while DVGs are distributed throughout the cytoplasm. (A) Schematic of (+) and (-) sense probe sets binding to SeV genomes and anti-genomes. For (+) sense FISH: probes targeting the 5' end of (+) genome are shown in red, probes targeting the 3' end of (+) genome are shown in green, interpreted as: +gSeV (orange), +DVG (green). For (-) sense FISH: probes targeting the 3' end of (-) genome are shown in red, probes targeting the 5' end of (-) genome are shown in green, interpreted as: -gSeV (orange), -DVG (green). **(B)** A549 cells infected with SeV-LD MOI 1.5 $TCID_{50}$/cell supplemented with purified DPs at indicated HAU for 24 h followed by (+)-sense viral RNA FISH. Images captured at 40X, wide field. Images are representative of 3 independent experiments, scalebar = 100μm. **(C)** A549 cells infected with SeV-HD for 24 h then subjected to (+)-sense viral RNA FISH or (-)-sense viral RNA FISH. 63X wide field, deconvolved, extended focus is shown. Images are

representative of three independent experiments, scalebar = 100µm.

increased, the number of FL-high cells decreased while the number of DVG-high cells with cytoplasmically distributed DVGs increased.

Because probes targeting (+)-sense viral RNA may also hybridize to mRNA, a set of probes targeting the negative sense genome was used to confirm a distinct distribution of DVGs and FL genomes in the absence of mRNA labeling. Probes targeting the 3'- end of the (-)-sense genome colored red and probes targeting the 5'-end of the (-)-sense genome pseudo-colored green were used to distinguish DVGs in green and FL viral genomes as orange (hybridizing both red and green probes) **(Fig 2.2A)**. During infection with SeV-HD (+)-strand probes identified a heterogeneous population of cells, those that accumulate viral genomes in a perinuclear region and those that accumulate DVGs diffusely in the cytoplasm, similar to what was observed in infections with SeV-LD plus DPs (**Fig 2.2B-C**). Infections with SeV-HD generate distinct subpopulations comprising ~30% DVG-high cells and 30% FL-high cells in A549 cells at 24 h post infection. Similarly, (-)-strand probes identified perinuclear viral genomes and cytoplasmic DVGs **(Fig 2.2C)** indicating that the observed disparate distributions apply to viral genomes regardless of their sense.

2.4.3 DVG cytoplasmic distribution is independent of their size or sequence

In order to address whether the cytoplasmic distribution of DVGs was due to properties of the viral genomes, we asked whether this distribution was unique to SeV Cantell DVGs. This virus strain produces a single 546-nt long cbDVG that is strongly immunostimulatory (164, 166, 170). Other strains of SeV produce cbDVGs of different lengths and sequence and their immunostimulatory activity vary (140, 170). SeV 52

40

produces larger and less immunostimulatory DVGs than SeV Cantell. We generated a

stock of SeV 52 enriched with DVGs (SeV-52-HD) by passaging the parental strain

undiluted in eggs. This stock had two major DVGs, both longer than DVG-546 and show

as two larger amplicons when amplified with a common set of primers **(Fig 2.3A)**. Infections with SeV-52-HD revealed cytoplasmic distribution of DVGs similar to SeV Cantell infections (**Fig 2.3B**), indicating that the differential distribution of FL genomes and DVGs is common to multiple cbDVG types and independent of size or sequence.
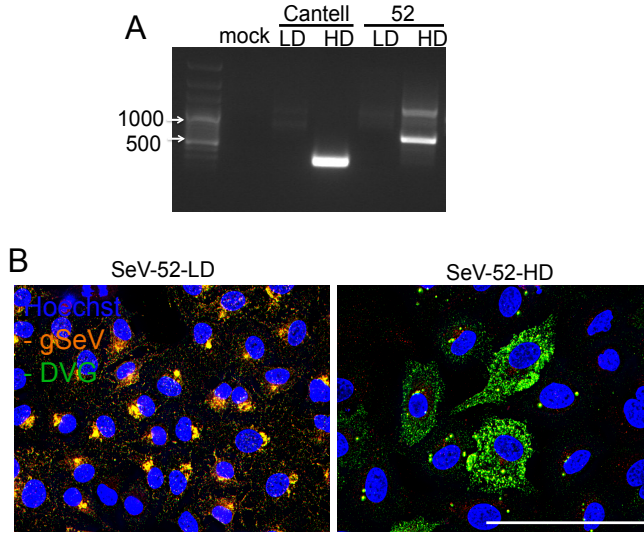
Figure 2.3. Different species of SeV DVGs are cytoplasmically distributed. A549 cells were infected with indicated virus for 24 h. **(A)** Agarose gel electrophoresis of PCR amplification of DVGs using common primers targeting all copy-back DVGs. **(B)** A549 cells infected with SeV- 52-LD or -HD then subjected to (-) sense-viral RNA FISH. Images captured at 63X, widefield, deconvolved. Extended focus is shown. Images are representative of three independent experiments, scalebar = 50μm.

2.4.4 Cytoplasmic diffusively distributed DVGs RNPs do not interact with the Rab11a / microtubule intracellular trafficking machinery

vRNPs from paramyxoviruses and orthomyxoviruses interact with Rab11a and

utilize microtubules to facilitate particle production (45). To test whether SeV DVGs and

FL genomes interacted similarly with this intracellular trafficking machinery, we

performed immunofluorescence for SeV NP as a proxy for vRNPs, in conjunction with

antibodies targeting a variety of cellular organelles and cytoskeletal components in FL-high cells or DVG-high cells. FL-high cells (shown as cells with perinuclear distributed NP) showed strong colocalization of vRNP with Rab11a and microtubules. However, DVG-high cells (cells with cytoplasmically distributed NP) showed almost no colocalization between SeV NP and Rab11a or microtubules (**Fig 2.4**). These data suggest that vRNPs in DVG-high cells do not interact with the host intracellular trafficking machinery in the same manner as in FL-high cells. Further, cytoplasmically distributed NP did not colocalize with mitochondria, the cis-golgi, or the endoplasmic
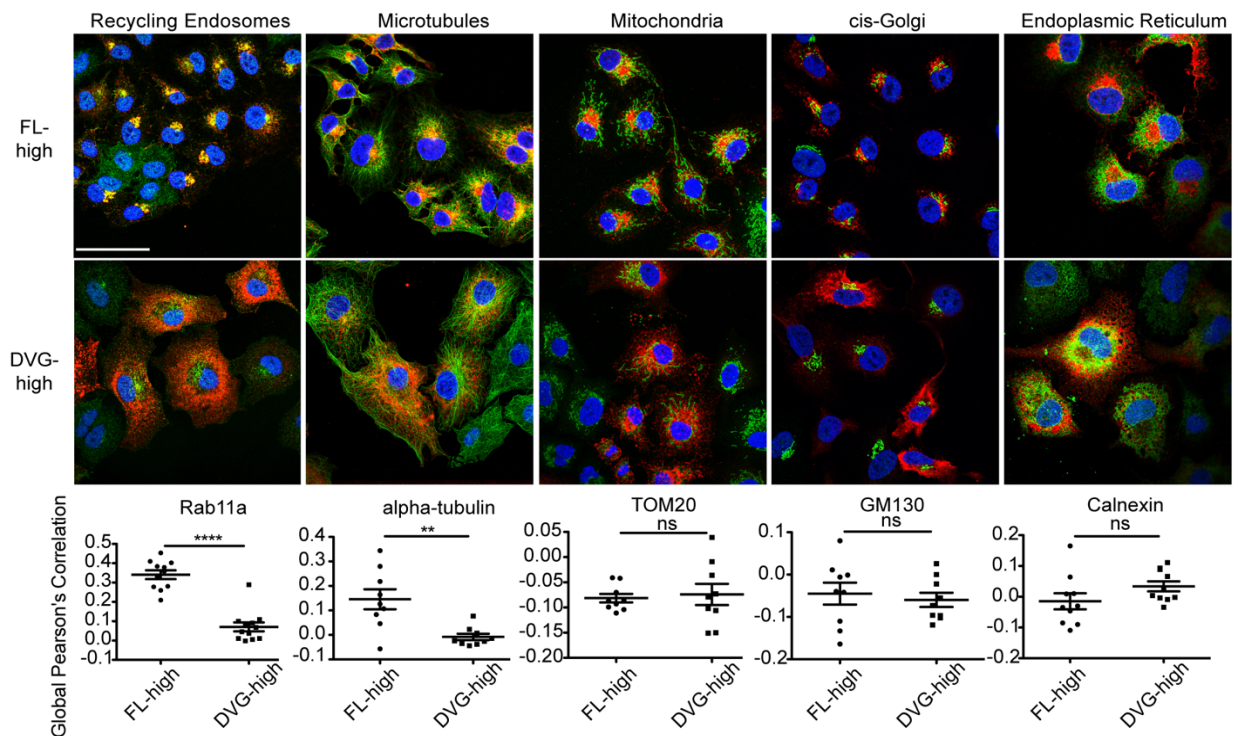
Figure 2.4. SeV NP colocalizes with Rab11a and microtubules in FL-high cells but not in DVG-high cells. A549 cells were infected with SeV-LD or SeV-HD for 24 h. Cells were fixed and subjected to immunofluorescence for viral protein SeV NP (red) and Rab11a (recycling endosomes), α-tubulin (microtubules), Tom-20 (mitochondria), GM130 (cis-Golgi), or Calnexin (endoplasmic reticulum) (all in green). Images captured at 100X, confocal. Single plane is shown. SeV LD infection was used to capture FL-high cells and DVG-high cells were captured from a SeV HD infection focusing on fields with cells containing majority cytoplasmically distributed SeV NP. Scalebar = 50μm. Global Pearson's Colocalization quantified by field for 3 independent experiments, >5 fields per experiment, ** = p < 0.005, **** = p < 0.0001 by student's t-test.

reticulum **(Fig 2.4)** indicating that DVG RNPs are likely not tethered to organelles within the cytoplasm. To further confirm that DVG RNPs do not interact with Rab11a in DVG-high cells, we used combined immunofluorescence and RNA-FISH on cells infected with SeV-HD to identify vRNPs and Rab11a in FL-high and DVG-high cells **(Fig 2.5A)**. For analysis, cells were binned as DVG-high or FL-high depending on their ratio of 5'-probe

to 3'-probe to the (-)-sense genome and Global Pearson's correlation of colocalization was assessed for individual cells **(Fig 2.5B)**. Similarly to what was observed when tracking NP (**Fig 2.4**), data indicate that within an infection in the presence of DVGs, viral genomes in the subpopulation of FL-high cells containing perinuclearly localized vRNPs interact with Rab11a, but in DVG-high cells with DVG RNPs distributed throughout the cytoplasm there is no significant co-localization of RNPs with Rab11a.
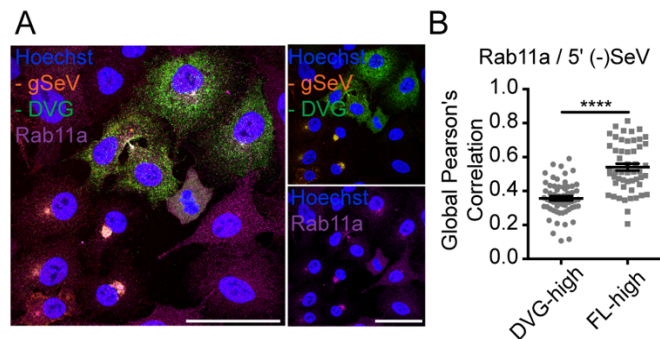
Figure 2.5. DVG-high cells show less colocalization with Rab11a than FL-high cells. (A) Immunofluoresence for Rab11a (magenta) with (-) sense viral RNA FISH of A549 cells infected with SeV-HD for 24 h with Hoechst staining nuclei (blue). Images captured at 63X, confocal, deconvolved, extended focus is shown, scalebar = 50µm. Single channel image of Rab11a (bottom) and RNA FISH (top) with Hoechst are shown to the right. (**B**) Global Pearson's Colocalization between Rab11a and 5' end of genome quantified per cell for 3 independent experiments, 5 fields per experiment. Cells were binned as DVG+ or FL+ based on ratio of 5'/3' probe intensity. Individual cells are plotted with a line at mean, error bar represents ± SEM, **** = $p < 0.0001$ by Mann-Whitney non-parametric U-test.

To next investigate whether the interaction of vRNPs with the microtubule/Rab11a machinery indicated functional interactions, we first disrupted

microtubule polymerization and tested if localization of viral genomes changed. To

disrupt microtubules, cells were infected with SeV-HD for 4 h to allow for virus entry and

then treated with the microtubule disrupting drug nocodazole. RNA FISH was performed

24 h post infection to assess viral genome distribution **(Fig 2.6A)**. Nocodazole disrupted

the localization of FL genomes in FL-high cells agreeing with their colocalization with

microtubules, but did not alter the localization of DVGs in DVG-high cells. FL genomes

redistributed to discrete cytoplasmic clusters while DVGs remained diffused throughout

the cytoplasm, indicating that they were not tethered to microtubules. Levels of SeV NP

transcripts **(Fig 2.6B)** and genomic SeV RNA **(Fig 2.6C)** did not change upon

nocodazole treatment, confirming that intracellular viral replication was not affected by

the drug; however, DVG replication levels were reduced upon nocodazole treatment (**Fig**

2.6C), potentially due to nocodazole's effects on tubulin, which has been shown to

influence SeV genomic and DVG RNA replication (188). Further, when cells depleted of

Rab11a by siRNA knockdown were infected with SeV-HD for 24 h, FL genomes failed to

localize to the perinuclear region and instead distributed throughout the cytoplasm, but

the distribution of DVGs remained the same (**Fig 2.6E**). Rab11a knockdown was

confirmed by testing for mRNA levels **(Fig 2.6F)** and protein expression using western

blot (**Fig 2.6J**). Viral replication was equivalent or increased in knockdown cells, likely

due to impaired particle production and consequent accumulation of viral genomes and

DVGs in the cell (**Fig 2.6G-I)**. As expected, Rab11a knockdown decreased levels of

infectious virus production compared to controls **(Fig 2.6K)**. In order to investigate

whether there was a similar impact on the production of defective particles, supernatant

from control or Rab11a-knockdown infected cells were added to LLCMK2 cells and

levels of intracellular DVGs were measured by RNA. Because Rab11a knockdown

reduced infectious virus production, LLCMK2 infections were adjusted to MOI 1 using

supplemented SeV LD. Interestingly, DVG-RNA levels in LLCMK2 cells treated with

supernatants from infected Rab11a knockdown cells were reduced compared to cells

treated with supernatants from infected control cells **(Fig 2.6L)** indicating that production

of defective particles were reduced in the absence Rab11a, while levels of SeV
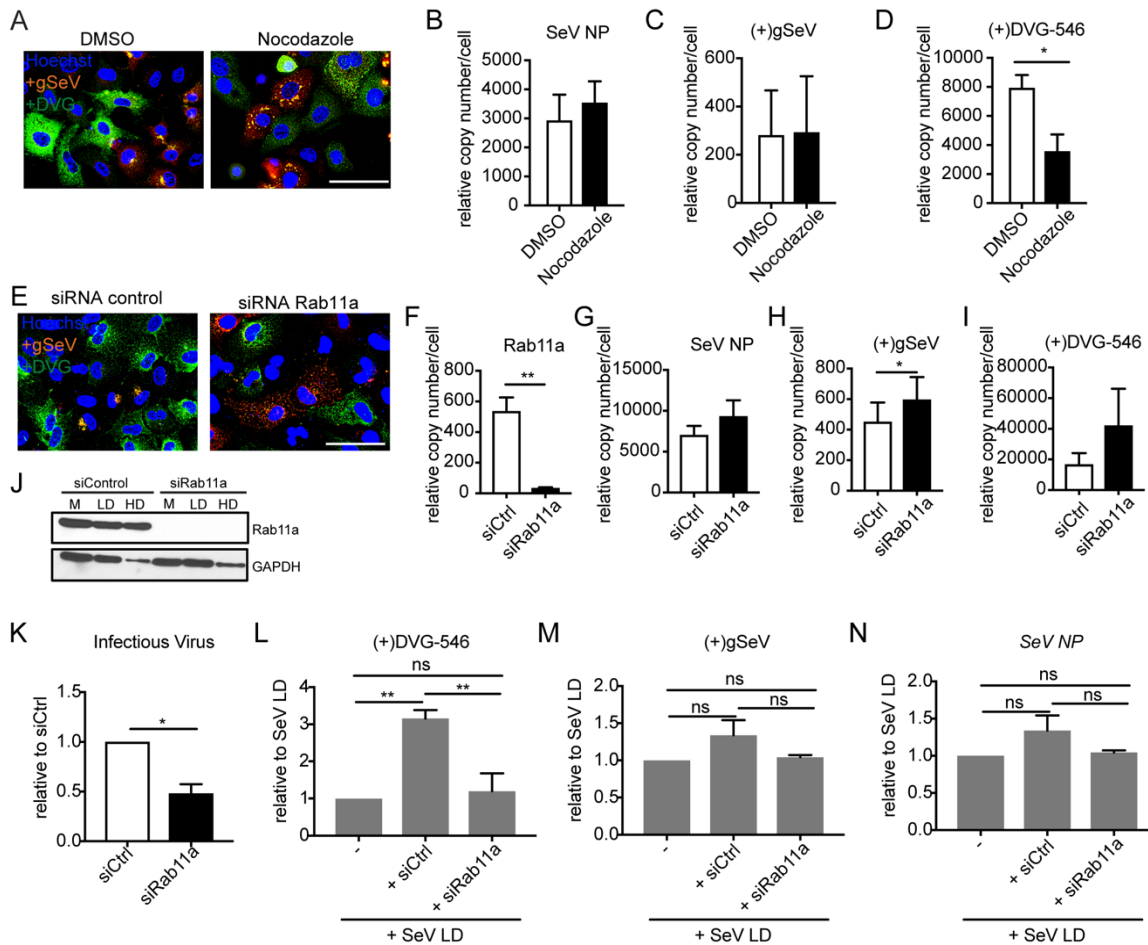
Figure 2.6. Cytoplasmic distribution of DVGs in DVG-high cells is independent of microtubule integrity and Rab11a expression. (A) A549 cells infected with SeV-HD, treated with nocodazole at 4 h post infection, (+) sense viral RNA FISH performed at 24 h post infection. Images captured at 63X, widefield, deconvolved. Extended focus is shown. Scalebar = 100μm. Images are representative of four independent experiments. RT-qPCR for **(B)** SeV NP, **(C)** (+)gSeV and **(D)** (+)DVG-546 transcripts relative to *GAPDH* at 24 h post infection. Data is represented as mean ± SEM of three independent experiments, * = p < 0.05 by paired t-test. **(C)** A549 cells transfected with siRNA targeting Rab11a or scrambled control siRNA (siCtrl) prior to infection, infected with SeV-HD for 24 h, then subjected to (+) sense viral RNA FISH. Images captured at 63X, widefield, deconvolved. Extended focus is shown. Scalebar = 100μm. Images are representative of four independent experiments. RT-qPCR for **(F)** Rab11a, **(G)** SeV NP **(H)** (+)gSeV, and **(I)** (+)DVG-546 transcripts relative to *GAPDH* at 24 h post infection, data is

represented as mean ± SEM of seven independent experiments, * = p < 0.05, ** = p < 0.005 by paired t-test. **(J)** Western blot for Rab11a protein with GAPDH loading control. **(K)** Relative levels of infectious virus by TCID50 normalized to siRNA control, data is represented as mean ± SEM of three independent experiments, * = p < 0.05 by paired t-test. Supernatant from control siRNA and Rab11a siRNA KD cells was adjusted to MOI 1 $TCID_{50}$/cell with SeV LD and LLCMK2 cells were infected for 24 h. RT-qPCR for Cantell specific DVG-546 **(L)**, (+)gSeV **(M)** and *SeV NP* **(N)** mRNA relative to GAPDH, data is represented as mean ± SEM of three independent experiments normalized to SeV LD alone. ** = p <0.005 by One-way ANOVA, Bonferroni post-hoc.

transcription and genomic SeV RNA were the same across infections **(Fig 2.6M-N)**.

Taken together, these results indicate that within an infection, vRNPs in FL-high cells interact with cellular trafficking machinery involved in virus packaging and budding, while RNPs in DVG-high cells are localized differently than in FL-high cells and fail to interact with the cellular machinery used for paramyxovirus budding and particle production.

2.4.5 Virions containing FL genomes or DVGs are produced by FL-high cells and not by DVG-high cells

Because of the documented importance of Rab11a/microtubule trafficking pathways for paramyxovirus particle production (45), we next asked if DVG-high cells produced defective viral genome containing particles (DPs). Taking into consideration the heterogeneity in viral genomic content among cells infected with SeV-HD (165) (**Fig 2.2**) we live sorted DVG-high and FL-high cells to obtain enriched populations. To do this, we took advantage of previous data from our laboratory that identified a subset of TNF-associated genes that are upregulated in DVG-high cells, including the cell surface molecule 4-1BB (165). In addition, the SeV HN protein is a surface protein whose content in infected cells surface is lower in DVG-high cells than FL-high cells (156). Notably however, even cells with lower levels of HN (HN-low gate) are sufficient to produce viral particles as sorted SeV-LD infected cells produce similar amounts of infectious particles from both gates **(Fig 2.7A-B)**. To study viral particle production, experiments were performed in LLCMK2 cells, which more robustly produce virus
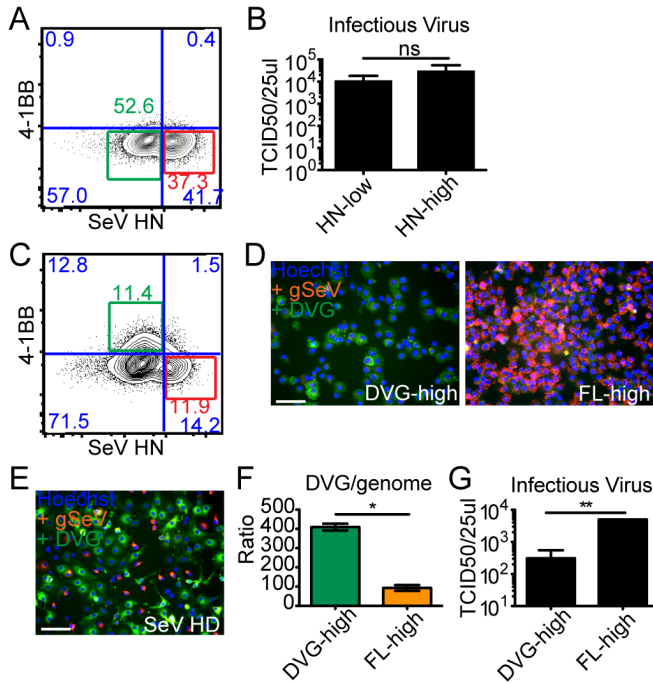
Figure 2.7. Infectious virus is produced by FL-virus high cells and not by DVG-high cells. (A) Representative flow cytometry plot of SeV LD infected LLCMK2 cells, 24 h post infection. HN-low shown in green, HN-high gate shown in red. **(B)** TCID$_{50}$/25ul of supernatant from indicated cell populations. **(C)** Representative flow cytometry plot of SeV HD infected LLCMK2 cells, 24 h post infection. DVG-high gate shown in green, FL-high gate shown in red. **(D)** cytospin of indicated populations post-sorting and **(E)** unsorted SeV HD infected LLCMK2 cells as control subjected to (+) sense RNA FISH, widefield, 20X. **(F)** Relative ratio of DVG to genome calculated by RT-qPCR for DVG-546 and +-sense genome in each population, relative to GAPDH, n = 4, Mann-Whitney non-parametric U-test, * = p<0.05. **(G)** TCID$_{50}$/25ul of supernatant from indicated cell populations, n = 3, student's t-test, ** = p<0.005.

compared to A549 cells. LLCMK2 cells were infected with SeV-HD, stained and gated based on their expression of 4-1BB and SeV HN for sorting **(Fig 2.7C)**. Sorted populations were characterized by RNA FISH **(Fig 2.7D)** and compared to unsorted population controls **(Fig 2.7E)** and relative genomic content was confirmed by RT-qPCR **(Fig 2.7F)**. Sorted cell populations were cultured for 24 h before analyzing their supernatant for presence of infectious virus and DPs. As expected, infectious virus was predominantly found in the supernatant of FL-high cells **(Fig 2.7G)**. Because low levels of DPs are not detectable by titration nor by hemagglutination, the content of DPs was assessed after amplification in LLCMK2 cells. To do this, LLCMK2 cells were infected with a combination of SeV-52-LD and supernatants from the cultured sorted populations. To confirm that SeV-52-LD was able to support replication of SeV Cantell DVG-546, purified DPs (HAU 20) were added to SeV-52-LD MOI 1.5 TCID$_{50}$ infections and levels of DVG-546 **(Fig 2.8A)** and genomic SeV **(Fig 2.8B)** were analyzed and showed an increase

47
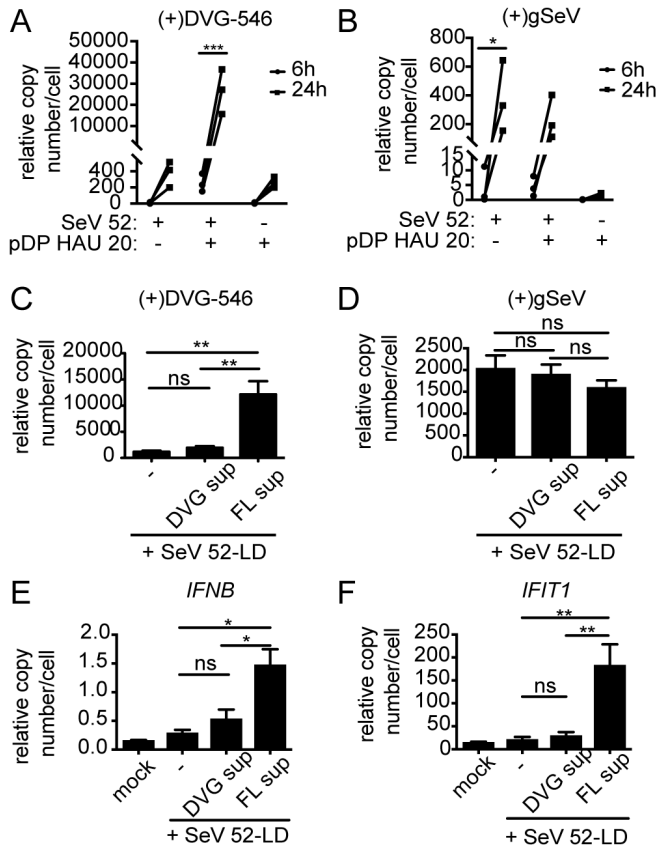
Figure 2.8. Defective particles are produced by FL-virus high cells and not by DVG-high cells. Purified defective particles added to SeV-52 and levels of **(A)** (+)DVG=546 and **(B)** (+)gSeV were measured at 6 and 24 h post infection. Three independent experiments are shown, * = p<0.05, *** = p < 0.001, by two-way ANOVA Sidak's multiple comparisons. Supernatant from sorted cells was mixed with SeV 52 at MOI 1.5 TCID$_{50}$/cell and LLCMK2 cells were infected for 24 h. RT-qPCR for **(C)** Cantell specific DVG-546, **(D)** (+)gSeV, **(E)** *IFNB,* and **(F)** *IFIT1* mRNA relative to GAPDH, n = 3, one-way ANOVA, Bonferroni post-hoc, ** = p <0.005.

over time. Upon infection of LLCMK2 with sorted cell supernatants, intracellular levels of SeV Cantell-specific DVG-546 were analyzed 24 h post infection by RT-qPCR. Interestingly, despite the abundance of intracellular DVGs, supernatant from purified DVG-high cells did not contain DVG-546 DPs, as there was no difference in the levels of DVGs in SeV-52-LD plus DVG supernatant compared to SeV-52-LD alone. Rather, DVG-546 DPs were present in the supernatant from purified FL-high infected cells (**Fig 2.8C**), however there was no difference in levels of genomic SeV RNA **(Fig 2.8D)**. Because we chose to amplify the supernatants in LLCMK2 cells to see robust virus replication, levels of *IFNB* and *IFIT1* are lower than in A549, as LLCMK2 cells are rather poor inducers of interferon. However, as expected, the presence of DPs correlated with increased expression of *IFNB* and *IFIT1* mRNA (**Fig 2.8E-F**) compared to mock levels. Together with published evidence of a critical role for DVG-high cells in engaging the antiviral response, these

data demonstrate the distinct functional properties of different cells during viral infections and identify viral particle production as a distinctive function of FL-high cells.

2.4.6 DVG cytoplasmic distribution is independent of antiviral signaling and cell type

DVGs from SeV Cantell strongly stimulate the RIG-I-like-receptor (RLR) pathway and induce the expression of type I and III IFNs and hundreds of interferon stimulated genes (164, 166, 167, 170). Agreeing with the well-known immunostimulatory activity of DVGs (90), SeV-HD infections showed robust induction of antiviral responses compared to SeV-LD infections, including high levels of expression of *IFNB* and the interferon stimulated gene *IFIT1* **(Fig 2.9A-B)**. To assess if these host responses impacted the differential distribution of FL genomes and DVGs and consequent different DP production levels (**Fig 2.8**), we used CRISPR knockout cell lines lacking the RLR signaling adaptor mitochondria antiviral signaling protein (MAVS KO), or lacking the type I IFN receptor (IFNAR KO). Intracellular distribution of FL-genomes and DVGs in knockout cell lines was similar to their distribution in control cells at 24 h post SeV infection **(Fig 2.9C-E)** indicating that cytoplasmic distribution of DVGs in DVG-high cells is independent of both RLR and IFN signaling. To investigate whether DVG distribution was dependent on other host factors, we tested a variety of cell lines from various host species. Infection of SeV in various adherent epithelial non-human cell lines, including monkey LLCMK2 cells, which support robust replication of virus and are traditionally used for virus growth and titration, Marine Darby Canine Kidney (MDCK), and Vero cell lines recapitulated the phenotype seen in A549 cells (**Fig 2.7E** and data not shown**)**. The independence on anti-viral signaling and host cell type indicate that the intracellular distribution of vRNPs in FL-high and DVG-high cells is likely virally driven process, the specifics of it are the subject of current investigations.

49
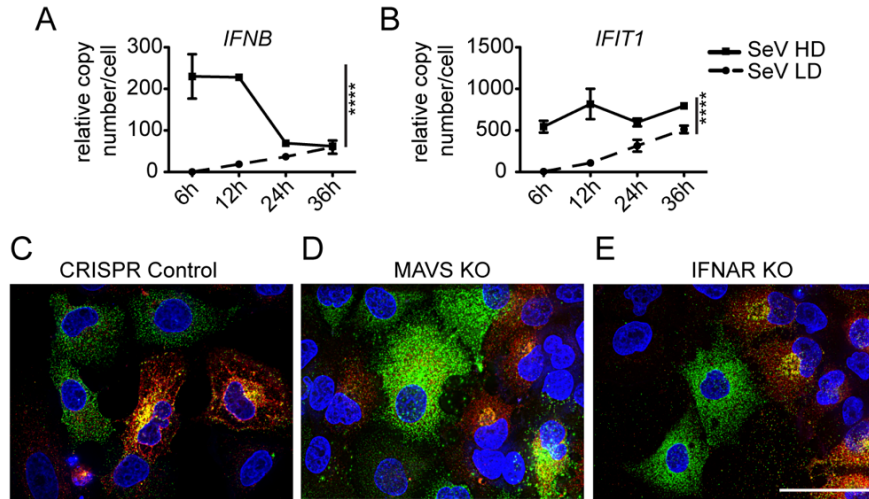
Figure 2.9. Differential distribution of viral genomes is independent of antiviral signaling.
(A) RT-qPCR for *IFNB* and *IFIT1* **(B)** mRNA relative to GAPDH, n = 3, one-way ANOVA, Bonferroni post-hoc, ** = p <0.005. **(C)** CRISPR control A549**, (D)** MAVS KO, and **(E)** IFNAR KO cell lines were infected with SeV-HD for 24 h then subjected to (+)-sense viral RNA FISH. Images captured at 63X, widefield, deconvolved. Extended focus is shown. Images are representative of three independent experiments, scalebar = 50μm.

2.5 Discussion

Our data indicate that cells that accumulate high levels of DVGs during an infection have a distinct cytoplasmic distribution of vRNPs compared to infected cells that do not accumulate high levels of DVGs, and these RNPs do not engage with the host cell to produce virions or DVG-containing defective particles (DPs). In contrast, FL-genome and DVG vRNPs in infected cells with low or no DVGs are efficiently packaged and released as standard virus or DPs. The differential interaction of virus and host proteins amongst infected cells in a population highlights the complexity and heterogeneity of viral infections. Most studies of the interactions of host proteins with viral components have relied on the purification or tagging of viral proteins or viral RNPs. However, we show that not all vRNPs across different cells within an infected population behave similarly, as DVG-high cells show differential distributions of viral components with distinct functional outcomes. The presence of DVGs within prepared viral stocks or

the accumulation of DVGs during an infection is near ubiquitous for viruses of the order *Mononegavirales*, orthomyxoviruses, and others (90, 91). Our results indicate that not only may DVGs shape the outcome of infection, but also the interaction of viral genomes with the intracellular trafficking machinery.

DVGs are important modulators of pathogenesis in many, but perhaps not all, infections as they ameliorate disease courses through the induction of antiviral immunity, particularly in paramyxovirus infections (140, 141). Additionally, DVG-high cells induce pro-survival pathways that extend their life span and facilitate the establishment of viral persistence (165). The differential distribution of DVGs within cells and their failure to form large perinuclear clusters, may be a clue to some of the functions that DVGs carry out in driving immunity and stimulating pro-survival pathways. Clustering of viral RNA into specialized structures in order to evade viral RNA sensing by RLRs has been described for a number of viruses including those of the paramyxovirus family (44). Though this specific proviral function has not been described for Sendai virus, the differential localization of DVGs and their correlation with immune stimulation may offer an additional explanation for why these viral products so actively engage with RLRs.

A widely described impact of DVGs on virus production is their ability to strongly interfere with viral protein expression and consequently broadly lower levels of standard virus replication and virion production (156, 189). However, our data indicate that the presence of defective particles in an infection led to a reduction in the proportion of cells able to produce virus rather than a global lowering of virus production in all cells and indicates the importance of moving away from bulk population analysis when studying the impact of DVGs on an infection. We show that the presence of high levels of DVGs within infected cells drastically limits the production of virions by such cell, and the

51

mechanisms leading to this reduction in virion production are of interest. Our data

indicates that the immunostimulatory nature of DVGs does not impact these differences

(Fig 2.9), and we presume that interference leading to reduction in certain viral proteins

may play a role. Interestingly, when analyzed on a per cell basis, levels of NP do not

decrease significantly with the accumulation of DVGs within cells, suggesting that not all

viral proteins are subject to stark interference. However, as NP is the first and most

abundantly produced mRNA and protein, there may be additional interfering affects on

subsequent proteins, which may influence viral particle assembly and production. While

DVG-high cells do have decreased levels of HN on the surface, we confirmed that this

level of HN is also found in a subpopulation of DVG-low cells that produces virions at

normal rates. These data suggest that the defect of DVG-high cells in producing DPs

cannot be explained by a reduction in the amount of HN. However, it is possible that

reductions in the amount of other proteins implicated in particle production may play a

role. For example, matrix protein bridges the interactions between viral glycoproteins,

including HN, and vRNPs, yet the details of how it functions in particle assembly are

unknown. Evidence indicates that matrix traffics to the cell surface together with viral

glycoproteins but independently of vRNPs (190) while other evidence suggests that

matrix interacts with cytoplasmic vRNPs and is critical for vRNP transport to the cell

membrane (191, 192). Regardless of how matrix works, high levels of DVGs during

infection can destabilizes matrix leading to failure of virus assembly (155). Whether

matrix interacts with recycling endosomes or facilitates recycling endosome interactions

with vRNPs is unknown. Our data suggest that defects in particle assembly in DVG-high

cells may originate prior to their assembly at the cell membrane, as we fail to see

interaction of DVGs with Rab11a and microtubules required for the trafficking of vRNPs

to the plasma membrane. It is possible that matrix plays an important role in these

interactions. Analysis of RNA from sorted cells shows that DVG-high cells contain lower levels of SeV M mRNA transcripts compared to FL-high cells, as expected. However, they do express SeV M mRNA and it is unclear how these lower levels impact protein amounts and whether this is a meaningfully lower level of viral protein. Unfortunately, due to limitations in tools available to study SeV M protein, we are currently unable to address these questions. Additionally, the non-structural viral protein C has been implicated in the formation of viral particles through mechanisms that remain controversial, and C protein is subject to additional regulations at a transcriptional level which may be altered in DVG-high cells (59, 69, 70). Further investigation into why DVG high cells fail to engage with these pathways should provide important insight into mechanisms mediating viral genome trafficking and egress, and possibly reveal additional roles of matrix or C protein in regulating virion formation.

The production of DPs and the transmission of DVGs during an infection can have large impacts on the infection outcome in cells (165), in animals (140, 141), and in humans (107). Here we show that cells accumulating the majority of DVGs during an infection are not the main producers of DPs. Rather, DPs and virus are produced from FL-high cells. Notably, FL-high cells die more promptly during infection (165) raising intriguing questions about the dynamics of virus spread and pathogenesis. The presence of DVG-high cells during infection occurs in the presence of high levels of DPs, however during natural infections there may be low levels of transmission of DPs. Therefore, a natural infection would presumably originally begin as low-DVG. Once DVGs accumulated in an LD infection **(Fig 2.1H)**, the production of DPs as well as standard virus could lead to a local area of high-DVG infection and produce DVG-high cells, which would then be capable of triggering antiviral immunity. The production of DVGs in vivo

has been established (140) and modeling of DVGs during transmission has been attempted (174, 193), but we believe that our updated model could yield more insights in to these infection dynamics. Additionally, the ability to separate and distinguish defective genomes from FL genomes has allowed us to further characterize properties of the viral genomes during an infection and reveal that cells enriched in DVGs do not engage with microtubules/Rab11a-driven viral production pathways. This dichotomy within a single population is a useful tool not only to understand the immunostimulatory functions of DVGs in infections, but also allows us to further investigate additional fundamental aspects of paramyxovirus biology.

2.6 Materials and Methods

Cells and Viruses

A549 cells (human type II pneumocytes, ATCC CCL-185) and LLCMK-2 (monkey kidney epithelial cells, ATTC CCL-7) were cultured in Tissue Culture Medium (DMEM (Invitrogen) supplemented with 10% Fetal Bovine Serum (Serum Source International), Gentamicin (ThermoFisher), Sodium Pyruvate (Invitrogen), L-glutamine (Invitrogen)) at 7% CO2, 37°C. Generation of A549 CRISPR cell lines is described in (8). Cells were treated with Mycoplasma Removal Agent (MP Biomedical) upon thawing and tested monthly for mycoplasma contamination using MycoAlert PLUS Mycoplasma testing kit (Lonza). Sendai Virus was grown in 8-day embryonated, specific pathogen free chicken eggs (Charles River) for 40 h before allantoic fluid was harvested. LD and HD stocks were produced as described previously (164). Viruses were characterized by ratio of $TCID_{50}$ to direct HA. In brief, $TCID_{50}$ was determined by 1:10 serial dilutions of virus in infection media (DMEM (Invitrogen) supplemented with 35% BSA (Sigma-Aldrich), Pen/Strep (Invitrogen), 5% $NaHCO_3$ (Sigma-Aldrich)) prior to infection of LLCMK2 cells

54

for 72 h in the presence of 2 µg/mL TPCK trypsin (Worthington Biochemicals), followed by hemagglutination of 0.5% chicken red blood cells (Lampire) to determine presence of virus in the supernatant. Titers were calculated using the Reed and Muench method (194). Total hemagglutinating (HA) titers were obtained by testing 1:2 serial dilutions of the virus in PBS for hemagglutination of 0.5% chicken RBCs. $TCID_{50}$/HA ratios were as follows: SeV Cantell LD = 195,776; SeV Cantell HD = 48,944; SeV 52 LD = 235,151; SeV 52 HD = 784. Infections were performed at an MOI of 1.5 $TCID_{50}$/cell with virus diluted in infection media. Cells were washed twice with PBS then incubated with infection media with virus at low volume at 37°C for 1 h. Cells were then supplemented with 2% FBS Tissue Culture Medium for indicated time periods. Defective Particles (DP) were purified from the allantoic fluid of SeV Cantell infected embryonated eggs by density ultracentrifugation on a 5-45% sucrose gradient, as previously described (140).

Immunofluorescence

Cells were seeded on No. 1.5 glass coverslips (Corning) prior to infection. At indicated time points, coverslips were briefly washed in PBS then fixed in 4% Paraformaldehyde (Electron Microscopy Sciences) for 10 min. Cells were permeabilized with 0.2% Triton-X (Sigma-Aldrich) for 10 min. Primary and secondary antibodies were diluted in 3% FBS/PBS and incubated at RT for 1.5 h and 1 h, respectively. Nuclei were stained with Hoechst for 10 min prior to mounting coverslips on slides using Fluoromount-G (ThermoFisher). Antibodies: SeV NP (clone M73/2 a kind gift from Alan Portner – directly conjugated with Dylight 594 NHS Ester (ThermoFisher)), Rab11a (Abcam, ab65200), alpha-tubulin (Abcam, ab52866), GM130 (Abcam, ab52649), calnexin (Abcam,

ab133615), TOM20 (Santa Cruz, sc-11414), AlexaFluor 647 Phalloidin
(Invitrogen, A22287), Goat anti-Rabbit IgG (H+L) Secondary Antibody, Alexa
Fluor 488 (Invitrogen, R37116)).

RNA FISH

Custom probe sets (described in Reference (165) and Table 1) conjugated to Quasar
570 and Quasar 670 dyes were purchased from LGC Biosearch. Cells were seeded on
No. 1.5 glass coverslips (Corning) prior to infection. At indicated time points, coverslips
were briefly washed in PBS then fixed in 3.7% formaldehyde (ThermoFisher) for 10 min.
Cells were permeabilized in 70% EtOH for 1 h, washed in wash buffer (2X SSC
(ThermoFisher), 10% formamide (ThermoFisher) in nuclease free water), and then
subjected to hybridization with FISH probes. In brief, probes were diluted to 2.5nM in
hybridization buffer (wash buffer + dextran sulfate) and applied to slides. Slides were
incubated with probe overnight at 37°C in a humidified chamber. Prior to imaging, slides
were washed in wash buffer twice (once with Hoechst to stain nuclei) then 2X SSC.
Cells were mounted in anti-fade buffer (2X SSC, 0.4% glucose (Sigma), Tris-HCL pH 8.0
(USB Corporation) with Catalase (Sigma) and Glucose Oxidase (Sigma)) and sealed
with rubber cement. RNA FISH combined with immunofluorescence includes the
following modifications: after fixation with EtOH, cells are stained with antibody in 1%
BSA (ThermoFisher) PBS with RnaseOUT (Invitrogen); 45 min for 1° Ab, 40 min for 2°
Ab. Cells were then post-fixed for 10 min in 3.7% formaldehyde prior to hybridization.

Microscopy and Image Analysis

Widefield images were acquired on a Leica DM1000 microscope with 40X (1.25-0.75
NA) and 63X (1.40-0.60 NA) oil-immersion objectives. Confocal images were acquired
on a Leica SP5-II Laser Scanning Confocal with 63X (1.40-0.60 NA) and 100X (1.46

NA) oil-immersion objectives with pixel size of 50.4nm x 50.4nm for immunofluorescence images and 120.2nm x 120.2 nm for FISH immunofluoresence. Images were deconvolved using Hugyens Essentials Deconvolution Wizard using theoretical point spread function and images were processed in Volocity (Perkins-Elmer). Global Pearson's Correlation was calculated in Volocity using automatic thresholding based on (195). For Rab11a/5'(-)SeV colocalization, non-specific nuclear staining was excluded using the Fiji software by subtracting signal from nuclear area defined by Hoechst staining. For individual cell measurements ROIs were defined manually for Global Pearson's Correlation. Measurements of nucleoprotein distribution and amount were done using MetaMorph (Molecular Devices) multiwavelength cell scoring application using phalloidin staining to define cellular boundaries. Single plane images were used for quantification and plane was determined by phalloidin staining in order to avoid bias.

RNA Extraction and PCR/RT-qPCR

RNA was extracted from Trizol (Invitrogen). Cellular and viral mRNA was reverse-transcribed using RNA-to-cDNA kit (Invitrogen). Viral RNA was reverse-transcribed using SuperScript III First Strand Synthesis System (Invitrogen) with primer 5'-GGTGAGGAATCTATACGTTATAC-3'. PCR was performed using Platinum Taq DNA polymerase (Invitrogen) the reverse transcription primer and 5'-ACCAGACAAGAGTTTAAGAGATATGTATT-3'. qPCR was performed with 1:40 dilution of cDNA, SYBR Green (Life Technologies) and 5uM forward/reverse primers (Invitrogen) on an Applied Biosystems ViiA 7 Real-Time System. Relative copy numbers per cell were calculated by delta-delta Ct and normalized to average cellular GAPDH expression levels. Primer sequences are: *SeV NP* (F: 5'-TGCCCTGGAAGATGAGTTAG-3', R: 5'-GCCTGTTGGTTTGTGGTAAG-3'), gSeV (F: 5'-GACCAGGAAATAAAGAGTGCA-3', R:

5'-CGATGTATTGGCATATAGCGT-3'), DVG-546 (F: 5'-

TCCAAGACTATCTTTATCTATGTCC -3', R: 5'-GGTGAGGAATCTATACGTTATAC-3'),

IFNB (F: 5'-GTCAGAGTGGAAATCCTAAG-3', R: 5'-ACAGCATCTGCTGGTTGAAG-3'),

IFIT1 (F: 5'- GGATTCTGTACAATACACTAGAAACCA-3', R: 5'-

CTTTTGGTTACTTTTCCCCTATCC-3')

siRNA

Cells ($3x10^4$) were transfected with 75µM On-TARGET Plus SMARTpool Rab11a

(Dharmacon GE), a mixture of four siRNA targeting Rab11a diluted in Opti-MEM, using

Lipofectamine RNAiMAX (Invitrogen). Transfection was performed 72 h prior to infection

to allow sufficient knockdown. Knockdown was assessed using immunofluorescence,

RT-qPCR, and Western Blot to confirm protein and mRNA levels. Control cells were

transfected with 75µM On-TARGET Plus non-targeting pool following identical

procedures.

Western Blot

Cells were lysed in NP-40 lysis buffer (Amresco) with proteinase inhibitors (Roche

Boehringer Mannheim), Rnase OUT (Invitrogen) and EDTA (ThermoFisher). Protein

concentration was measured using BCA Protein Assay (ThermoFisher). Protein (10µg)

was denatured by boiling for 10 min and loaded in a 10% Bis-Tris Gel (Bio-Rad) then

transferred to PVDF membrane (Millipore). Membranes were incubated overnight with

primary antibody in 5% milk (rabbit anti-Rab11a (Abcam) and mouse anti-GAPDH

(Sigma)). Membrane was incubated with anti-rabbit HRP-conjugated antibody (Cell

Signaling) or anti-mouse HRP-conjugated antibody (Jackson Immunologicals) in 5% milk

and developed using Lumi-light western blot substrate (Roche) to detect HRP.

Drug Treatment

Four h post infection, media was removed and replaced with 2% FBS tissue culture media containing 2µg/mL Nocodazole (Sigma-Aldrich) for duration of infection.

Flow Cytometry

Cells were stained with anti-4-1BB (Biolegend clone 4B4-1, #309819) and anti-SeV HN (Clone 6F11, kindly provided by T. Moran) followed by anti-IgG2a PE-/Cy7 (Biolegend clone RMG2a-62, #407113) at 24 h post infection. Cells were sorted on BD FACS Aria II SORP. Mock infected and SeV-LD infected cells were used to inform gating. Analysis was done using FlowJo_v9.9.4 (BD Biosciences).

Viral Production Analysis

Sorted cells (1.5×10^5 cells per population) were incubated for 30 min in 1% anti-SeV mouse serum twice to remove virus bound to the surface. Cells were then seeded in a 24-well plate in Infection Media (described above) and cultured for 24 h. 24 h post culture, media was collected and analyzed for virus particles. Detection of DPs was performed by infecting LLCMK2 cells with an inoculum containing 100µl of culture supernatants with 100ul of infection media containing SeV 52-LD to reach an MOI of 1 $TCID_{50}$/cell and 2µg/mL TPCK Trypsin (Worthington) for 24 h.

Statistics

Statistics were calculated using GraphPad Prism 5 for Mac.

Table 1. Probe sequences for SeV negative sense genome probes

Probe Sequence	Probe Set/Number
ctcttaaactcttgtctggt	DVG_Negative_1
tggaagtcttggacttatcc	DVG_Negative_2
gtgcagaacgatcgaagctc	DVG_Negative_3

gctcgtaataattagtccct	DVG_Negative_4
ggtgatatcgagccatatga	DVG_Negative_5
ccgtgattgatgatggatca	DVG_Negative_6
gccaggcaaaatgaatacac	DVG_Negative_7
aggggcagtcaagatgttcg	DVG_Negative_8
taacgtatagattcctcacc	DVG_Negative_9
ttattagacaggtttgagga	DVG_Negative_10
acctgagggttatcacaaaa	DVG_Negative_11
ttatcatcccgtgagatcag	DVG_Negative_12
cctgaccagaagtttgaagc	DVG_Negative_13
tctatgtccacaagattggt	DVG_Negative_14
cttggcagagatatctaggg	negSeV_1
acgattctggaatgcaggtg	negSeV_2
tcaaggatgtggaccttgag	negSeV_3
aagccactgatattgcactt	negSeV_4
gttgaaagatacggcaaccc	negSeV_5
tgctctaagacacgtcatgt	negSeV_6
tgactactctttctgtctca	negSeV_7
tcataggcttcaagtttcgg	negSeV_8
ctatacgagtgtcatgcagt	negSeV_9
tgacagggtatatcctaacc	negSeV_10
taagatcaggtctctgggta	negSeV_11
acatccacgatatctctcag	negSeV_12
tcagaagagcctgaatacct	negSeV_13
catataccacgacatcgtgt	negSeV_14
actgatgcttatccattgtc	negSeV_15

gtattcctaacccatgacaa	negSeV_16
atttcggaaccatcggagag	negSeV_17
gacacaaaatgccggtgttc	negSeV_18
cttgagaatgggtgcggaac	negSeV_19
taatggatgtgaatccccat	negSeV_20
gtcaatgggacatctctagg	negSeV_21
ctggtccagataagaaagcc	negSeV_22
cgtagatccaatctaccatc	negSeV_23
ggtggcaagactgacaacac	negSeV_24
agaggtacgaggaggtacat	negSeV_25
tacgaggcttcaaggtactt	negSeV_26
tgaatttgctccaggcaatt	negSeV_27
ggcccgatattaataagctt	negSeV_28
gagacaaagatggcagctct	negSeV_29

2.7 Acknowledgements

CHAPTER 3: The Viral Polymerase Complex Mediates the Interaction of vRNPs with Recycling Endosomes During Sendai Virus Assembly

3. 1 Abstract

Paramyxoviruses are negative sense single-stranded RNA viruses that comprise many important human and animal pathogens, including human parainfluenza viruses. These viruses bud from the plasma membrane of infected cells after the viral ribonucleoprotein complex (vRNP) is transported from the cytoplasm to the cell membrane via Rab11a marked recycling endosomes. The viral proteins that are critical for mediating this important initial step in viral assembly are unknown. Here we use the model paramyxovirus, Sendai virus (SeV), recently named murine parainfluenza virus 1, to investigate the roles of viral proteins in Rab11a-driven virion assembly. We previously reported that infection with SeV containing high levels of copy-back defective viral genomes (DVGs) generates heterogenous populations of cells, with cells enriched in full-length virus producing viral particles containing standard or defective viral genomes, while cells enriched in DVGs did not, despite high levels of defective viral genome replication. Here we take advantage of this heterogenous cell phenotype to identify proteins that mediate interaction of vRNPs with Rab11a. We examine the role of matrix protein and nucleoprotein and determine that they are not sufficient to drive interaction of vRNPs and recycling endosomes. Then, using a combination of mass spectrometry and comparative protein abundance and localization in DVG- and FL-high cells, we identify viral polymerase complex components L and, specifically, its cofactor C proteins as interactors with Rab11a. We find that accumulation of these proteins within the cell is the defining feature that differentiates cells that proceed to viral egress from cells which remain in replication phases.

4.2 Significance

Paramyxoviruses are a family of viruses that include a number of pathogens with significant burdens on human health. Particularly, human parainfluenza viruses are an important cause of pneumonia and bronchiolitis in children and do not have any vaccines or direct acting antivirals. These cytoplasmic replicating viruses bud from the plasma membrane and coopt cellular endosomal recycling pathways to traffic viral ribonucleoprotein complexes from the cytoplasm to the membrane of infected cells, yet the viral proteins required for viral engagement with the recycling endosome pathway is not known. Here we use the model paramyxovirus Sendai virus, or murine parainfluenza virus 1, to investigate the role of viral proteins in this initial step in viral assembly. We find that viral polymerase components large protein L and accessory C proteins are necessary for engagement with recycling endosomes. These findings are important in identifying viral targets for the development of antivirals.

4. 3 Introduction

Paramyxoviruses, as well as orthomyxoviruses and hantaviruses, use the recycling endosome pathway as a controlled mechanism of egress to traffic vRNPs from the infected cell cytoplasm to the cell membrane(45). Rab11a, a host GTPase associated with recycling endosomes, is critical for the transport of cargo from early endosomes to the perinuclear endocytic recycling complex and back to the plasma membrane(196). Paramyxoviruses that rely on Rab11a for intracellular transport and viral egress include SeV(47), measles(50), mumps(49), and HPIV1(47). While it is known that the vRNP interacts with Rab11a, it is not known which viral proteins are necessary to drive this critical interaction required for viral particle assembly. In fact, while multiple proteins including M and C have been investigated for their role in driving

viral assembly, their roles remain contested and poorly understood (20). For example, SeV M has been reported to interact with vRNPs in the cytoplasm and be required for recruitment of vRNPs to the membrane (191, 192) but has also been shown to traffic with surface proteins F and HN via the trans-golgi network (190). Whether the M protein is critical for engagement of SeV vRNPs with Rab11a marked endosomes is unknown. Further, in addition to the C proteins' roles in innate immune antagonism and polymerase function, they have also been reported to be enhancers of particle formation (68, 70). Data has suggested that C is critical in recruiting vRNPs to the membrane (70), and that C expression enhanced association of vRNPs to membranes. Additionally, both C and M proteins have been shown independently to recruit Aip1/Alix, a protein involved in endosomal sorting and vesicle budding, to the plasma membrane to enhance virion formation(67, 68). But the requirement for Aip1/Alix in paramyxovirus budding is contested with evidence that absence of Aip1/Alix in cells does not have any effect on SeV particle formation(69). Thus, while both C and M have been heavily studied in the context of particle assembly, a clear picture of how these proteins function in early steps of assembly is lacking.

We previously reported that upon infection with DVG-containing virus populations, cells display a heterogenous phenotype with the development of subpopulations of DVG-high cells and full-length (FL)-high cells(165, 197). DVG-high cells contain higher levels of DVGs than full length genomes, and FL-high cells contain higher levels of full-length genomes than DVGs. Not only do these subpopulations have distinct transcriptional profiles(165), but they have different intracellular localizations of viral RNA(vRNA) (197). The vRNA in FL-high cells interacts with recycling endosomes and this leads to the production of both standard and defective viral particles, while the

vRNA in DVG-high cells does not interact with recycling endosomes and consequently these cells do not produce significant amounts of viral particles. However, these DVG-high cells undergo robust levels of vRNA replication as evidenced by the large increase in DVG RNA by qPCR and vRNA fluorescent in situ hybridization (FISH) over time(165) (197). In this chapter, we take advantage of DVGs as a system to investigate early steps that differentiate viral replication from viral particle production, namely how vRNPs interact with Rab11a, and describe the viral polymerase components L and C as differentiating factors in FL-high cells that facilitate vRNP association with recycling endosomes and subsequent viral assembly.

3.4 Results

3.4.1 M protein interacts with NP primarily at the cell surface and does not localize with Rab11a

Though SeV matrix protein (M) is necessary for SeV particle assembly(20), whether it is required for the association of vRNPs to recycling endosomes is unknown. It has been proposed that M is targeted to the plasma membrane together with the F and HN proteins(190) and, conversely, to traffic with vRNPs from the cytoplasm to the plasma membrane(191). In order to investigate whether the M protein is responsible for the association of vRNPs with recycling endosomes, we created a recombinant SeV with an HA-tag on the N-terminus of the M protein (SeV-M-HA) to study its localization during infection. We characterized this virus to ensure that the HA-tag did not result in a dramatically different growth curve from the parental SeV F1R strain (SeV-F1R) and found that while viral output was slightly lower at later time points in infection, virion production was largely unimpaired (**Fig. 3.1A**). We then examined the localization of M during infection. Consistent with the fact that M lines the inside of virions and budding

occurs from the plasma membrane, we observed M at the plasma membrane of infected cells (**Fig. 3.1B-D**). Interestingly, single plane confocal images show little overlap of NP and M proteins (**Fig. 3.1B**).

As we previously reported, when Rab11a is knocked down by siRNA or when microtubule polymerization is disrupted, the perinuclear localization of viral RNA is altered(197). To ask if M interacted with the Rab11a/microtubule pathway, we assayed the localization of M upon treatment with nocodazole, a drug that prevents microtubule polymerization. In agreement with previously published data, nocodazole treatment of FL-high cells disrupted perinuclear clustering of the viral NP, indicating that vRNPs are tethered to microtubules via recycling endosomes(197). In contrast, M protein distribution was not drastically altered when cells were treated with nocodazole and it still localized at the plasma membrane (**Fig. 3.1C**). These data support a model whereby the M protein is trafficked to the cell plasma membrane independently of the microtubule network, implying that the M protein it is unlikely to be critical in driving interaction between vRNPs and recycling endosomes.

It has also been reported that DVGs lead to increased degradation and turnover of M(155). Therefore, if M is the protein responsible for tethering vRNPs to recycling endosomes, it is possible that DVGs in DVG-high cells fail to interact with Rab11a due to insufficient levels of M to drive this interaction. To address this possibility, we overexpressed M-FLAG in cells infected with SeV Cantell strain with a high level of DVGs (HD) which generates a heterogenous population of DVG-high and FL-high cells(165, 197) and asked whether high levels of M were sufficient to drive a perinuclear localization of DVGs. For these experiments we used 293T cells because they allow for infection and subsequent transfection of the same cell. We confirmed using vRNA FISH

to distinguish DVG from gSeV RNA (**Fig. 3.1D**) that the distinct intracellular distribution of FL-high and DVG-high cells was conserved in these cells. Overexpressed M localized to the membrane of infected cells, as expected. However, overexpression of M in DVG-high cells failed to recruit DVGs to the perinuclear region with DVGs remaining distributed throughout the host cell cytoplasm (**Fig. 3.1E**). These data indicate that M is not sufficient to drive association between vRNPs and recycling endosomes.

Finally, to confirm that M was not responsible for driving interactions between vRNPs and recycling endosomes, we infected A549 Rab11a-mcherry cells with SeV low DVG (LD) viruses, in which all vRNPs should interact with Rab11a(197), and performed immunofluorescence for various viral proteins (**Fig. 3.2A**) and compared their colocalization with Rab11a (**Fig. 3.2B**). As previously reported (197), in SeV LD infections NP and Rab11a colocalize in the perinuclear region. In contrast, M largely does not colocalize with Rab11a (**Fig. 3.2B**). We also examined the colocalization of Rab11a with other viral proteins, including the polymerase L and C proteins. We found that C also colocalizes with Rab11a to the same extent as NP, and that L colocalizes to an even higher degree than NP or C. This indicates that at this timepoint of infection, most or all L proteins are associated with recycling endosomes, while excess free NP and the pool of C proteins which antagonize innate immunity do not. Overall, these data support a model whereby vRNPs associate with Rab11a independent of M and likely through members of the polymerase complex L and C. In addition, our data support the model of interaction between M and the vRNPs occurring at the plasma membrane.

A

B   SeV NP/SeV M

SeV NP

SeV M

C   SeV NP/SeV M   SeV NP   SeV M

DMSO

Nocodazole

D   3'-Le ——————————//—————————— Tr-5' (-)gSeV

        Tr-5'
        ⊥⊥-3'   (-)DVG

E   SeV M/gSeV/DVG   gSeV/DVG   SeV M

mock +
SeV M-FLAG

SeV Cantell HD
non-transfected

SeV Cantell HD +
SeV M-FLAG
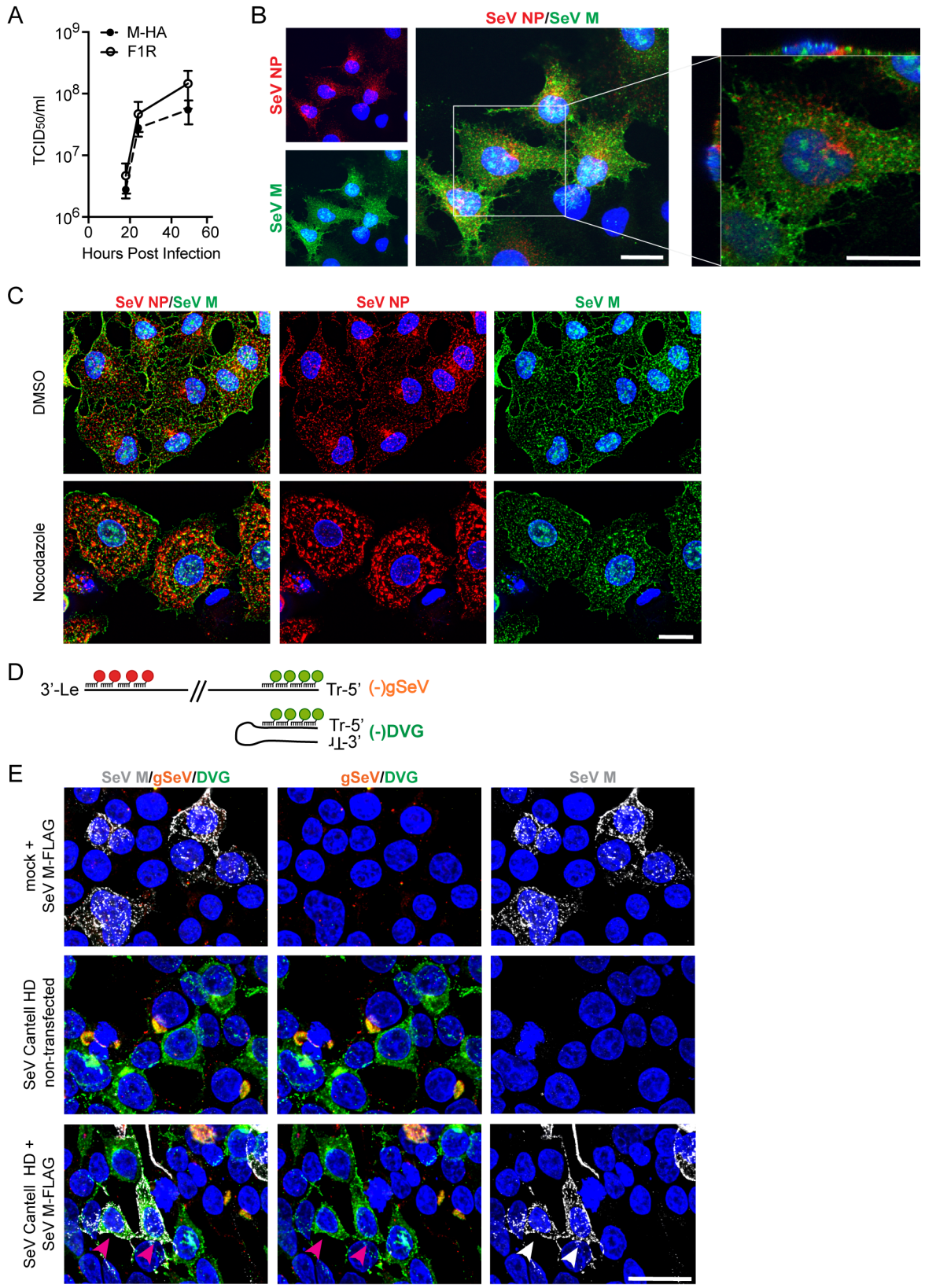
Figure 3.1. Matrix protein localization to the plasma membrane occurs independently of microtubules/Rab11a. A) TCID50/mL of supernatant from LLCMK2 cells infected with SeV-M-HA and SeV F1R (parental wildtype) at indicated timepoint, n = 3, graphed as mean ± SEM. **B)** A549 cells infected with SeV-M-HA for 24 hpi, immunofluorescence for SeV NP (red), HA (SeV M, green), Hoechst (nuclei, blue). Confocal 63x, 2x digital zoom. Panels 1-3 showing extended focus, panel 4 showing cropped single XY plane as well as XZ and YZ planes. **C)** A549 cells infected with SeV-M-HA, treated with nocodazole or DMSO vehicle control at 4hpi, immunofluorescence at 24 hpi for SeV NP (red), HA (SeV M, green), Hoechst (nuclei, blue). 63x widefield deconvoluted, max projection shown. **D)** Schematic of vRNA FISH to detect (-)gSeV and (-)DVG RNA, indicating red and green probe binding regions. **E)** 293T cells infected with SeV Cantell HD then transfected with SeV M-FLAG at 6hpi, vRNA FISH with immunofluorescence for FLAG (SeV M, gray) at 24hpi. 63x widefield deconvoluted, max projection shown. Magenta arrows indicate infected and transfected cells. All images are representative of 3 independent experiments, scale bar = 20µm.
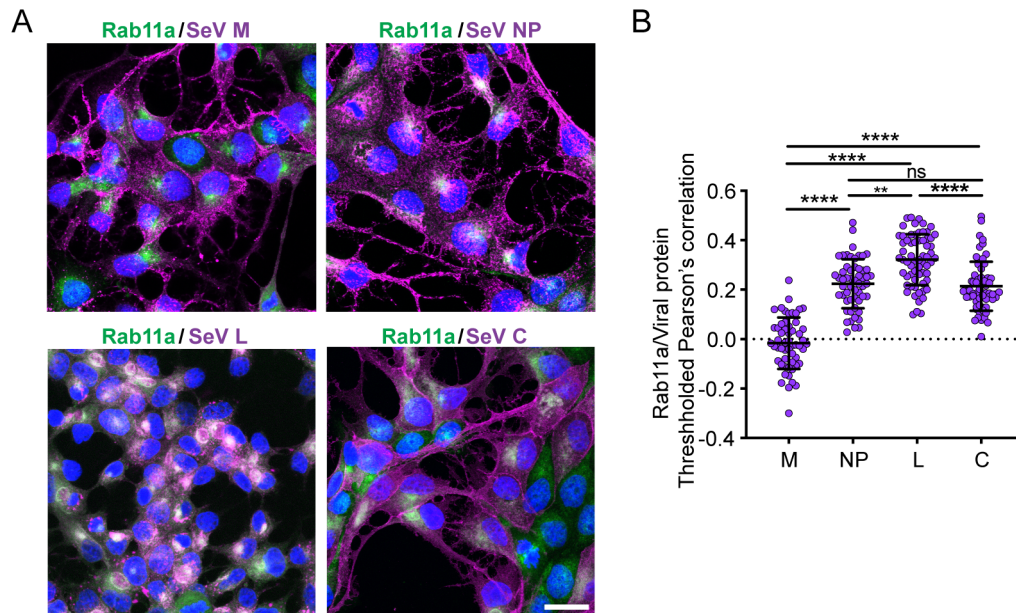
Figure 3.2. vRNP components colocalize with Rab11a but SeV M does not A) A549-Rab11-mcherry cells infected with SeV M-HA (M and NP), SeV Cantell LD (C), or SeV LeGFP (L) for 24 hours. Immunofluorescence for viral antigens (purple), mcherry-Rab11a shown in (green). Confocal 63x images, 1.5x zoom, max projection shown. All images are representative of 3 independent experiments, scale bar = 20µm. **B)** Quantification of colocalization between viral proteins and Rab11a, pooled from three independent experiments with >20 cells analyzed per experiment. Individual cells are plotted with line at the mean and error bars represent SD. ****= $p<0.0001$, ** = $p<0.01$ by One-way ANOVA with Sidak's multiple comparisons test.

3.4.2 Nucleoprotein coverage of vRNPs is not sufficient to drive interaction with Rab11a

Because we observed that NP, L, and C proteins all colocalized with Rab11a during infection, we next sought to address which of these proteins was important for the interaction of vRNPs with recycling endosomes. First, we asked whether NP was sufficient for driving this interaction. As the most abundant protein on the vRNP, it is possible that NP coverage of the viral genome dictates engagement with Rab11a. We reasoned that if NP coverage of vRNPs was critical for interaction with Rab11a, the lack of engagement of vRNPs with Rab11a in DVG-high cells may be explained by high levels of free or partially coated vRNA. In order to investigate whether viral RNA in DVG-high cells was coated in NP we tested for colocalization of these NP and viral genomes using RNA FISH combined with immunofluorescence for NP (**Fig. 3.3A**). To confirm the association of NP with DVG RNA, we quantified colocalization of 5'(-)SeV RNA with SeV NP (**Fig. 3.3B-D**). As shown in (**Fig. 3.1D**) the 5'(-)SeV probe set binds to all species of negative sense vRNA in cells. In DVG-high cells, the majority of vRNA recognized by 5'(-) SeV probe RNA corresponds to DVGs, but in FL-high cells it corresponds primarily to FL-genome RNA as indicated. We found that there was no significant difference in the colocalization between viral RNA and SeV NP in DVG-high and FL-high cells (**Fig. 3.3B**). Mander's overlap coefficient (MOC) indicates the portion of a signal that overlaps with the other signal in question, regardless of signal intensity. The MOC for NP with viral RNA showed that nearly all NP in DVG-high cells overlapped with viral genomes, but a lower fraction of SeV NP overlapped with vRNA in FL-high cells, presumably due to excess free NP that is not coating viral genomes (**Fig. 3.3C**). The MOC for 5'(-)SeV RNA overlap with NP was equivalent between DVG-high and FL-high cells, indicating that all equal portions of viral RNA colocalized with NP (**Fig. 3.3D**).

71
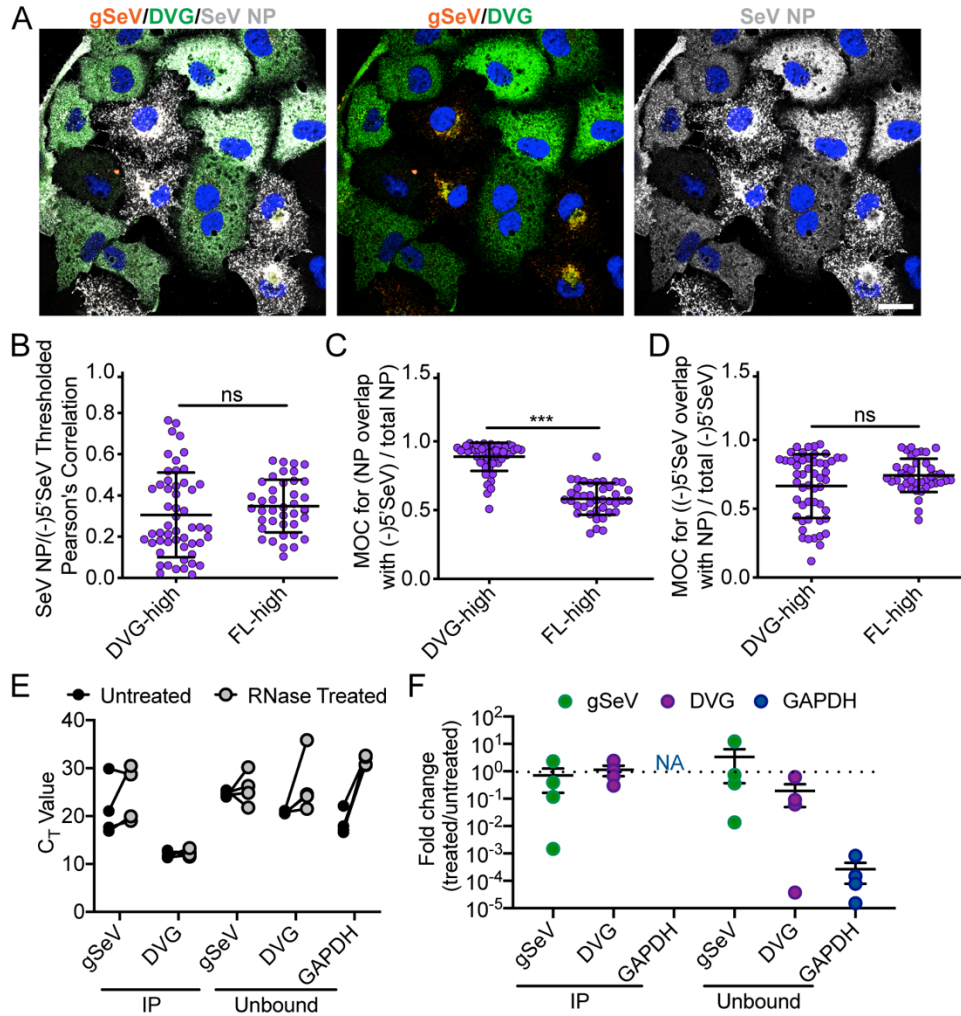
Figure 3.3. Nucleoprotein association is similar between full-length and defective viral genomes A) A549 cells infected with SeV Cantell HD for 24 hours and then subjected to RNA FISH with immunofluorescence for NP (gray), Hoechst (nuclei, blue). Confocal 63x image, 1.5x zoom, single plane image shown. Images are representative of three independent experiments, scale bar = 20μm. **B)** Costes's Pearson's correlation of colocalization between (-)5'SeV and SeV NP in individual DVG-high and FL-high cells. **C)** Mander's overlap coefficient of NP with 5' SeV in DVG-high and FL-high cells **D)** Mander's overlap coefficient of 5'SeV with NP in DVG-high and FL-high cells. Individual cells pooled from three independent experiments are plotted with line at the mean and error bars representing SD. **** = $p<0.0001$ by Mann-Whitney U-test. **E)** C_T values for qPCR for viral RNA, DVG RNA, and GAPDH with and without RNase A, V1, and T1 treatment after immunoprecipitation with anti-SeV NP. **F)** Fold change in RNA levels in RNase treated immunoprecipitation products relative to untreated. Data from four independent experiment are shown, with line at the mean and error bars representing SEM.

Though DVGs appear to be associated with NP, we wondered whether NP coating of DVGs was complete. We reasoned that there may be regions of exposed RNA that may disrupt the helical structure of the vRNP and therefore prevent interactions with host factors. To assess the integrity of the vRNP we performed an immunoprecipitation (IP) of NP from infected cells and subjected the IP product to RNase digestion with a combination of RNase A, V, and T1, targeting both single and double stranded RNA. RNA was then extracted and analyzed by RT-qPCR to compare levels of viral RNA to untreated controls. There was no significant difference in RNA quantities between DVG RNA and full-length vRNA in treated and untreated conditions (**Fig. 3.3E**). We also tested unbound fractions of the pulldown, reasoning that if there was any free RNA it would not be precipitated by anti-NP antibody. Both vRNA and DVG RNA where found in the unbound fraction indicating that the IP did not precipitate all of the vRNPs, but the RNA in this fraction was also not significantly different between treated and untreated conditions, particularly in comparison to an abundant cellular mRNA, GAPDH (**Fig. 3.3F**). These data do not preclude that there is some degree of uncoated RNA in DVG-high cells, but it indicates that the vast majority of vRNPs present during high DVG infections are sufficiently coated in NP. These data indicate that while NP and the vRNP associate with Rab11a in FL-high cells, NP coating of viral genomes is not sufficient to drive association with recycling endosomes and is likely not providing a direct link between viral genomes and Rab11a.

3.4.3 DVG driven interference leads to strong decrease in L transcripts and protein

Accumulation of DVGs leads to a decrease in standard viral genome replication and viral protein accumulation, a phenomenon known as interference. This interference is due to DVGs competing for viral polymerase and other proteins necessary for viral

replication (159, 175). In order to take a more systematic approach to the examination of the role of viral proteins in viral assembly, we investigated whether the interference effect resulting from high levels of DVGs had an equal impact across viral proteins or whether there were certain viral mRNAs and proteins most drastically impacted by interference. The hypothesis was that those proteins most interfered with by DVGs are essential for the localization of vRNPs to recycling endosomes and in their absence vRNPs, including DVG vRNPs, mislocalize within the cytoplasm.

The transcription of paramyxovirus mRNA is directed by the RdRP beginning at the 3' end of the genome and progressively losing processivity to generate a gradient of mRNA, with highest levels of the 3' proximal genes and lowest levels of the 5' genes(14, 27) produced (**Fig. 3.4A**). To determine whether interference with mRNA transcription by DVGs had a more drastic effect on some viral mRNAs compared to others, we performed qPCR on viral RNA from SeV LD and HD infected cell populations at 12 hours post infection, the time at which there is the highest rate of mRNA accumulation compared to genome accumulation(31, 197). As expected, we observed a gradient of transcription with higher levels of the 3' proximal transcripts and lowest amounts of L mRNA. Additionally, SeV HD infections had lower levels of viral mRNA levels across all genes (**Fig. 3.4B**). However, when comparing the levels of each mRNA across infections to normalize for differences in mRNA levels, it became clear that the levels of L mRNA were most significantly decreased (**Fig. 3.4C**). Because the SeV HD infections includes both FL-high and DVG-high cells, it is likely that levels of mRNA in DVG-high cells were even further reduced compared to levels of viral mRNA in LD infections, which contains mostly FL-high cells.

74
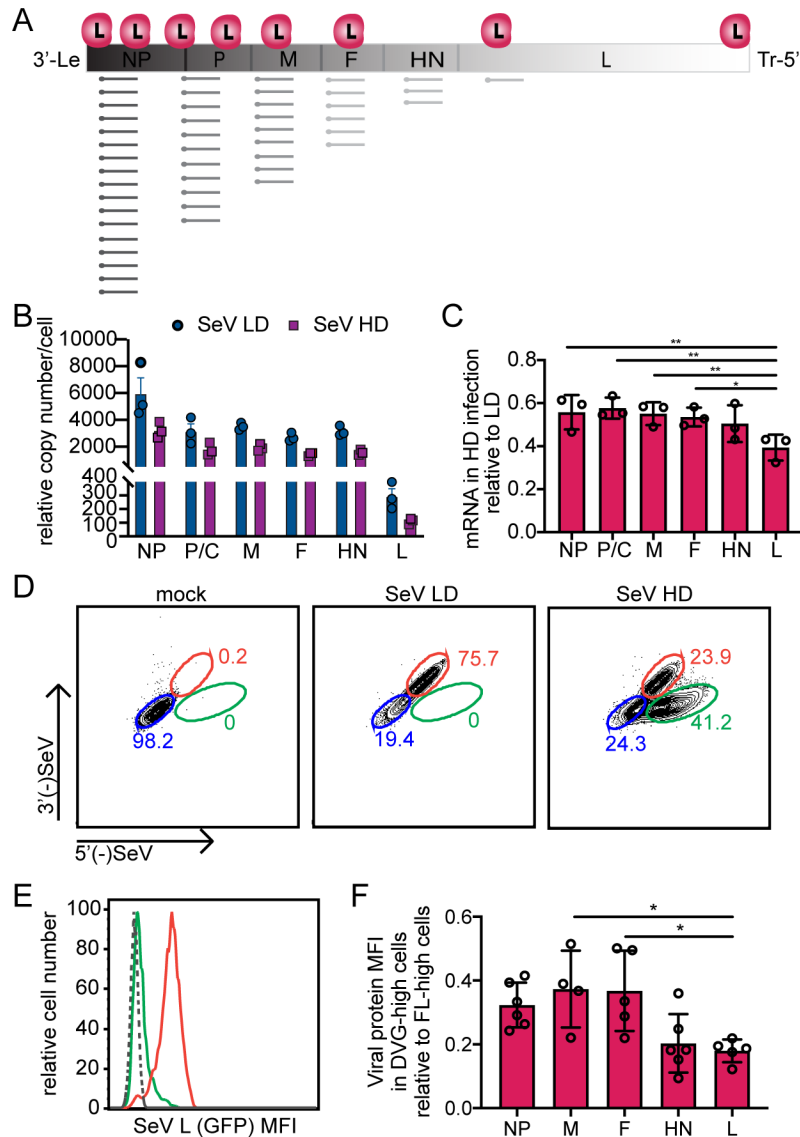
Figure 3.4 L mRNA and protein is significantly reduced in DVG-high cells compared to other viral proteins A) Schematic of gene organization and gradient mRNA transcription in SeV. **(B)** A549 cells infected with SeV Cantell LD and SeV Cantell HD for 12 hours, qPCR for viral genes shown as relative copy number compared to GAPDH and **(C)** relative amount in SeV HD infections compared to SeV LD infection for each viral gene. ** = p< 0.01, * = p<0.05 by One-way ANOVA with Sidak's multiple comparisons test. **(D-F)** A549 cells infected with SeV Cantell LD and SeV Cantell HD for 24 hours were subjected to RNA FISH combined with antibody staining for flow cytometry. **(D)** Representative flow plots for each condition with gates for DVG-high cells highlighted in green, and FL-high cells highlighted in red, and cells below limit of detection for viral RNA by flow in blue. **(E)** Representative MFI plot showing MFI of viral proteins in different cell populations in HD infected cells with FL-high cells shown in red and DVG-high cells shown in green, mock cells shown with dashed line. **(F)** relative MFI in DVG-high cells compared to FL-high cells in SeV HD infected conditions, four independent experiments are shown with bars

representing the mean and SD. * = p<0.05 by one-way ANOVA with Sidak's multiple comparison's test.

To determine whether decreases in viral mRNA transcription translate to lower levels of viral protein, we quantified protein levels in DVG-high and FL-high cells. SeV HD infections were subjected to RNA FISH flow coupled with immunostaining for different viral proteins. RNA FISH-flow cytometry allows for the identification of discrete cell populations based on intensity of 3'- and 5'- SeV probes in each cell, using the same strategy as in imaging (**Fig. 3.1D**). Using this method we are able to define DVG-high and FL-high populations (**Fig. 3.4D**) as validated in(165). We then calculated the mean fluorescence intensity as a proxy for viral protein amount in each of the identified populations (**Fig. 3.4E**). Levels of protein in DVG-high cells was normalized to FL-high cell levels (**Fig. 3.4F**). Levels of all viral proteins were lower in DVG-high cells compared to FL-high cells, recapitulating the mRNA data. These data show that the proteins that are the least abundant are most sensitive to DVG mediated interference as there is a much greater reduction of L protein in DVG-high cells than other viral proteins (**Fig. 3.4F**). This observation suggests that the L protein may be an important factor in regulating interactions of vRNPs with recycling endosomes, as this is the most strongly differentiating factor between DVG-high and FL-high cells.

3.4.4 SeV C proteins interact with Rab11a

We next used an unbiased approach to determine which viral proteins interact with Rab11a. To do this, we infected Rab11a-GFP A549 cells with SeV LD followed by immunoprecipitation (IP) of Rab11a using antibodies against GFP at 12 and 24 hours post infection to identify interacting proteins. By using SeV LD virus stocks we ensure that all cells are have vRNPs that are interacting with Rab11a. We also performed mass spectrometry on whole cell lysates. At 12 hours post infection, we identified viral proteins

present in a gradient of abundance with highest levels of NP and lowest levels of L and accessory proteins C and V (**Fig. 3.5A**) recapitulating the gradient of viral mRNA observed in (**Fig. 3.4B**). We identified high levels of NP, M, and C proteins in the Rab11a IP (**Fig. 3.5B**). C proteins are the most highly enriched viral proteins when normalized to levels of viral protein found in whole cell lysates **(Fig. 3.5C),** which was done to differentiate proteins that were enriched due to interactions with Rab11a from proteins simply increasing in abundance after viral infection. Similar results are observed at 24 hours post infection, with the magnitude of viral proteins increasing overall but trends staying the same (**Fig. 3.5D-F**). We also compared the log fold change of proteins identified by IP at both 12 hours post infection (**Fig. 3.5G**) and 24 hours post infection (**Fig. 3.5H**) and identified the C proteins as the most significantly enriched viral protein interacting with Rab11a compared to mock at both time points. Additionally, L protein is identified as significantly enriched at 24 hours post infection. To validate these results, we performed a western blot and probed for Rab11a and various viral proteins (**Fig. 3.5I**). As expected, Rab11a was enriched after IP, while the viral protein P was not seen, corresponding with its absence in the mass spectrometry analysis. C protein has the highest ratio of IP to input, strongly suggesting that the C protein most directly interacts with Rab11a. Both NP and M proteins are moderately present in the IP and likely represent high levels of protein in the cell (NP) and potential interactions between Rab11a and M which may occur at the plasma membrane in late stages of particle formation as shown in Figure 1. Because SeV generates 4 C proteins that are described to have discrete functions(198), we asked whether we could identify which C protein was interacting with Rab11a. The four C proteins range in size from 175 to 215 amino acids and share a common 175 amino acid C-terminus. We mapped the peptide reads

77
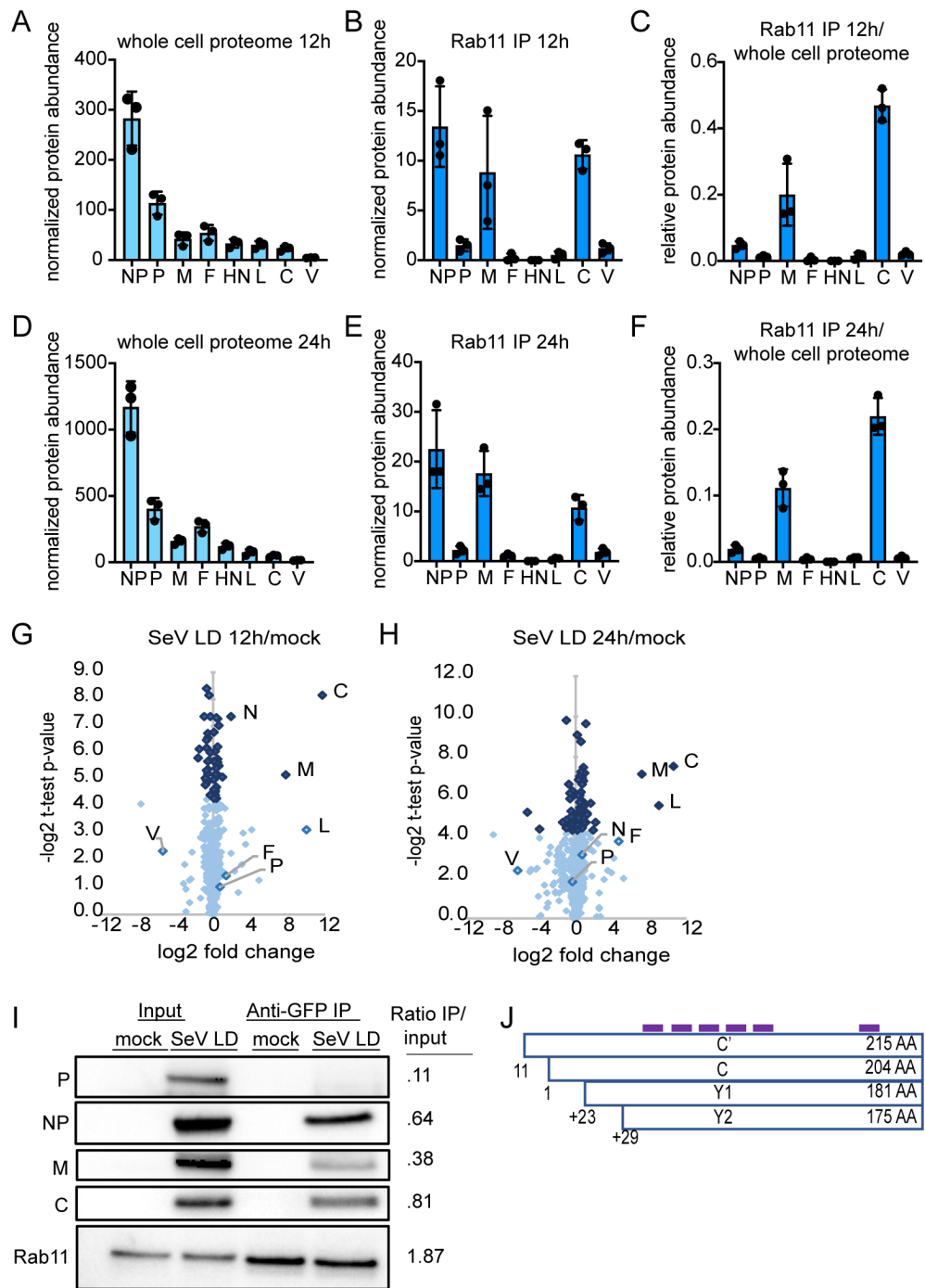
Figure 3.5. C proteins identified to interact with Rab11a by immunoprecipitation and mass spectrometry A) Normalized protein abundance for viral proteins identified by mass spectrometry at 12 hpi. **B)** Normalized protein abundance of viral proteins identified by IP of Rab11-GFP at 12 hpi. **C)** Relative protein abundance of proteins identified by IP to total protein abundance in whole cell lysates at 12hpi. **D)** Normalized protein abundance for viral proteins identified by mass spectrometry at 12 hpi. **E)** Normalized protein abundance of viral proteins identified by IP of Rab11-GFP at 12 hpi. **F)** Relative protein abundance of proteins identified by IP

to total protein abundance in whole cell lysates at 12hpi. A-F, three independent experiments are plotted with bar representing mean, error bar representing SD. **G**) Volcano plot comparing mock to 12 hpi and normalized to input or total abundance **H**) and comparing mock to 24 hours post infection and normalized to input. Data is pooled from three independent experiments. Viral proteins are indicated. Dark blue dots represent $p > 0.05$ and light blue dots represent $p < 0.05$ by student's t-test. **I**) Validation of mass spectrometry by western blot probing for Rab11a or viral proteins at 24 hours post infection and quantified for relative band intensity of IP over input. **J**) Schematic of C proteins with locations of peptides identified by mass spectrometry in IP samples marked in purple.

identified by in the IP by mass spectrometry to the C proteins (**Fig. 3.5J**) and found they were all from the shared 175 amino acid region, and therefore we could not conclude which specific protein(s) were identified. Overall, the identification of C proteins as a likely interactor of Rab11a by immunoprecipitation and subsequent mass spectrometry recapitulate results showing high degrees of colocalization as shown in (**Fig. 3.2A-B**) and suggests C proteins play an important role in directing interaction of vRNPs with recycling endosomes.

3.4.5 Occupancy of polymerase proteins on viral genomes is the differentiating factor in vRNPs that interact or fail to interact with Rab11a

Because we found that the L protein was lowest in DVG-high cells when comparing DVG-high and FL-high cells and identified its cofactor C by mass spectrometry as a Rab11a interacting partner, we considered whether differences in polymerase component levels may drive differences in engagement with Rab11a in DVG-high and FL-high cells. To ask whether polymerase was associated with viral RNA in DVG-high cells we performed RNA FISH combined with immunofluorescence. To visualize L we used a recombinant SeV with C-terminus fused GFP (SeV LeGFP) that has been previously described(48) and the addition of purified defective particles containing DVG-546, the dominant DVG in SeV Cantell. Previous studies have validated the ability of other strains of SeV to replicate DVGs from heterologous strains(197).

During infection with SeV LeGFP in the presence of purified defective particles (pDPs), we see the establishment of DVG-high cells, and strikingly these cells have very low levels of L protein (**Fig. 3.6A)**, recapitulating flow cytometry results that showed large differences in the amount of L protein in DVG- and FL-high cells. Additionally, it appears that a majority of DVG RNA in DVG-high cells is not bound by L protein. Indeed, colocalization of 5'(-)SeV RNA and L was significantly lower in DVG-high cells compare to FL-high cells (**Fig. 3.6B**). The MOC of L is equivalent in DVG-high and FL-high cells, indicating that the same proportion of L in each cell is interacting with vRNA, indicating that the small amount of polymerase present in those cells is colocalized with DVG RNA (**Fig. 3.6C**). However, the MOC of 5' (-) SeV RNA with SeV L was significantly lower in DVG-high cells compared to FL-high cells, indicating that a smaller fraction of viral RNA overlaps with L in DVG-high cells than in FL-high cells and that there are many DVG RNAs that are not occupied by a polymerase in DVG-high cells (**Fig. 3.6D**). The small amount of L protein in DVG-high cells is likely associated with DVGs for replication, but the majority of DVGs within the cytoplasm of DVG-high cells are not associated with L. This strong difference in L interaction with viral RNA in DVG-high and FL-high cells indicates that L protein may be critical in driving vRNPs to interact with Rab11a.

As levels of and engagement with the polymerase seems to be a differentiating factor between DVG-high and FL-high cells, we sought to investigate whether these differences were found with C protein as well. Upon RNA FISH combined with immunofluorescence for C protein, we observed similar results to those seen with SeV L, with low levels of C protein in DVG-high cells and a perinuclear localization of C protein in FL-high cells (**Fig. 7A**), indicating indeed that at later timepoints of infection, C protein
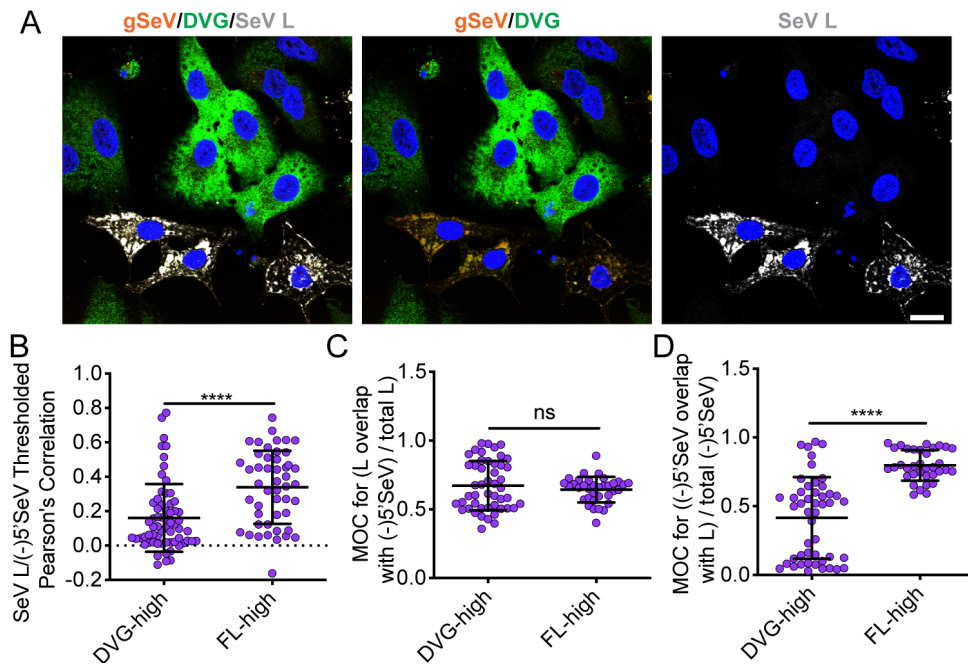
Figure 3.6. L protein interaction with vRNP distinguishes between DVG-high and FL-high cells A) A549 cells infected with SeV LeGFP supplemented with purified DPs (HAU 20) for 24 hours and then subjected to RNA FISH with immunofluorescence for GFP (L, gray), Hoechst (nuclei, blue). Confocal 63x image, 1.5x zoom, single plane image shown. Images are representative of four independent experiments, scale bar = 20μm. **B)** Costes's Pearson's correlation of colocalization between (-)5'SeV and SeV NP in individual DVG-high and FL-high cells. **C)** Mander's overlap coefficient of L (GFP) with 5' SeV in DVG-high and FL-high cells **D)** Mander's overlap coefficient of 5'SeV with L (GFP) in DVG-high and FL-high cells. Individual cells pooled from three independent experiments are plotted with line at the mean and error bars representing SD, **** = p<0.0001 by Mann-Whitney U-test.

associates with vRNA and presumably L. Quantification of colocalization revealed that there is a significantly greater degree of colocalization of C and 5'(-)SeV RNA in FL-high cells compared to DVG-high cells, indicating that like with L protein, many DVG vRNPs are not occupied by C protein (**Fig. 7B).** MOC of SeV C reveals that higher proportions of C are colocalized with 5' (-) SeV RNA in DVG-high cells than in FL-high cells (**Fig. 7C**). However, MOC of 5' (-) SeV RNA with SeV C indicates that in FL-high cells, a high proportion of vRNA overlaps with C, while in DVG-high cells, much of the vRNA does not

overlap with C proteins (**Fig. 7D**). These data indicate, that similarly to L protein, low levels of C proteins in DVG-high cells seem to colocalize with DVG-RNA but that very low levels of C protein in the cell leave many RNAs unbound by these proteins. Taken together, these data suggest that lack of accumulation of C and L proteins in DVG-high cells and therefore lack of C and L proteins bound to vRNPs precludes these vRNPs from interacting with Rab11a.
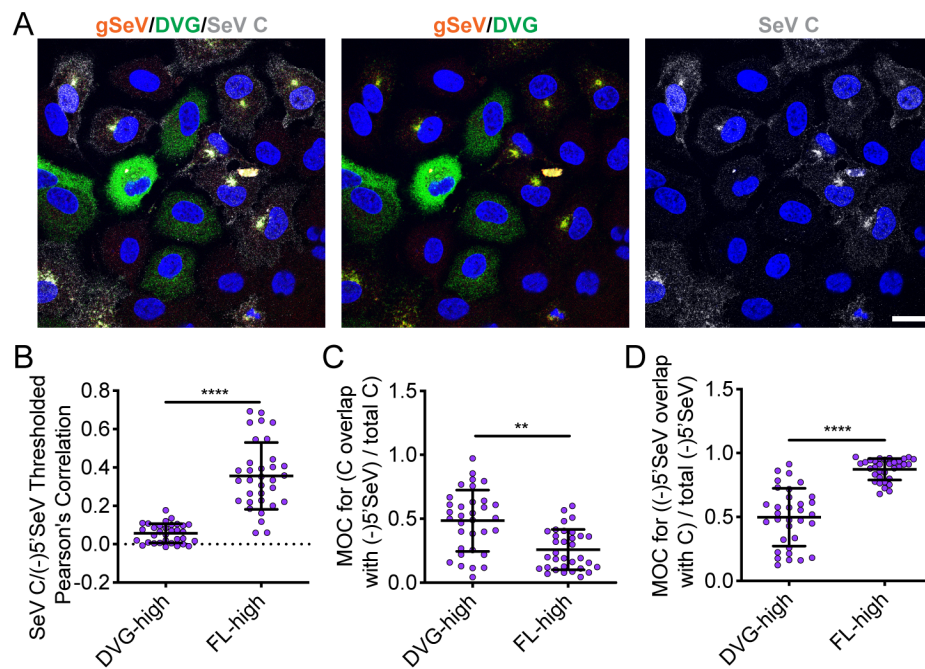
Figure 3.7. C protein interaction with vRNP distinguishes between DVG-high and FL-high cells A) A549 cells infected with SeV Cantell for 24 hours and then subjected to RNA FISH with immunofluorescence for C (gray), Hoechst (nuclei, blue). Confocal 63x image, 1.5x zoom, single plane image shown. Images are representative of four independent experiments, scale bar = 20µm. **B)** Costes's Pearson's correlation of colocalization between (-)5'SeV and SeV C in individual DVG-high and FL-high cells. **C)** Mander's overlap coefficient of C with 5' SeV in DVG-high and FL-high cells **D)** Mander's overlap coefficient of 5'SeV with C in DVG-high and FL-high cells. Individual cells pooled from two independent experiments are plotted with line at the mean and error bars representing SD **** = $p < 0.0001$ by Mann-Whitney U-test.

3.5 Discussion

We propose a model of Sendai virus assembly in which polymerase components including the viral polymerase L and its cofactor C are critical for the interaction between viral RNPs and Rab11a, a crucial initial step in viral particle production. In taking advantage of the difference in viral particle production in DVG-high and FL-high cells we parsed viral components that are critical for replication and those that are critical for viral assembly. DVG-high cells are able to carry out robust levels of viral genome replication using limited amounts of L but are unable to produce virions because they do not engage with host proteins critical for this process(197). We observed that DVG interference with viral protein expression critically diminishes levels of the viral polymerase L in DVG-high cells and we propose that L/C accumulation above a certain threshold is required for interaction of the vRNP with recycling endosomes and the cellular trafficking machinery. Further, we identified the C proteins as the most highly enriched viral proteins interacting with Rab11a by mass spectrometry. From these data we propose that recycling endosomes interacts with C proteins when it is bound to L, and that C-L polymerase complexes interact with vRNPs to tether then to recycling endosomes (**Fig. 3.8**).

It remains to be determined whether paramyxoviruses interact directly with recycling endosomes via endosomal membrane interactions, with the Rab11a GTPase itself, with family-interacting proteins (FIPs) associated with Rab11a or via another mechanism. The different Rab11-FIPs direct engagement of Rab11a-marked recycling endosomes with dynein or myosin Vb motor proteins, and specific FIPs have been identified as important for budding of different viruses. For example Rab11-FIP2 is important for respiratory syncytial virus budding(53) and influenza relies on Rab11-FIP3

for filamentous particle production(52). The Rab11a-FIPs used for trafficking of SeV are

unknown and identifying a viral protein that mediates interaction with recycling

endosomes will aid further study of these dynamics.
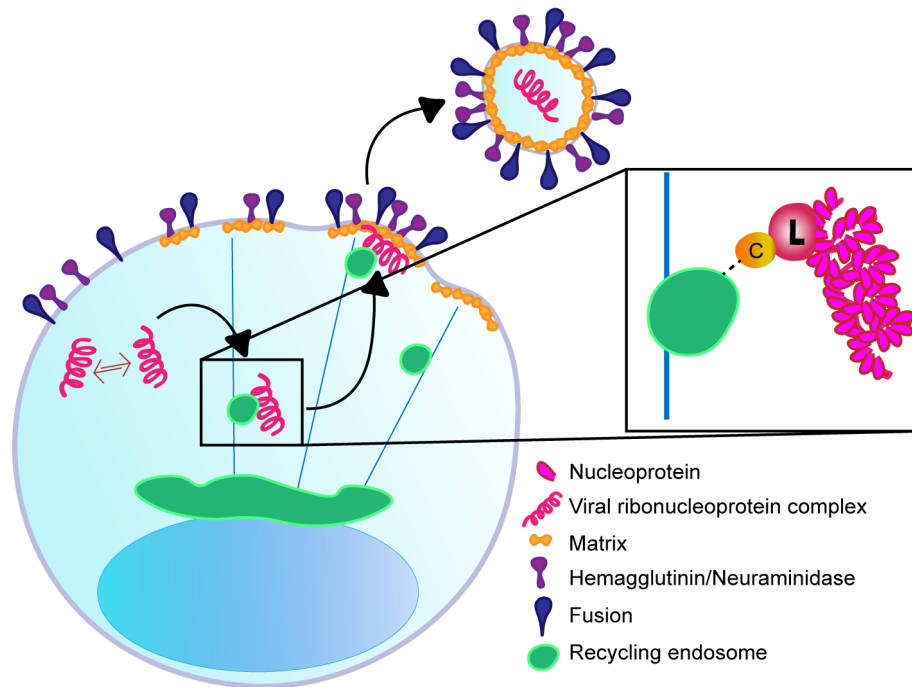
Figure 3.8. Model of SeV vRNP interaction with Rab11a. Viral replication occurs in the
cytoplasm and upon accumulation of sufficient levels of L and C proteins, vRNPs interact
with Rab11a-marked recycling endosomes via C and L proteins, in order to be trafficked to
the plasma membrane.

Negative-sense RNA viruses require packaging of RdRPs within virions to initiate

infection. Indeed, SeV L proteins have been shown to associate with viral nucleocapsids

isolated from virions(199). Additionally, C proteins have been found to be tightly

associated with nucleocapsid structures both inside the cell as well as when isolated

from SeV virions, with approximately 40 C proteins per vRNP(200). The observed role of

polymerase components in assembly are in accordance with what was observed in

infections with the orthomyxovirus influenza, where influenza virus RNPs interact with

Rab11a via one of its polymerase components PB2(201, 202). Like has been suggested for influenza, having the polymerase complex initiate packaging via interactions with Rab11a could be a mechanism to ensure that only vRNPs that contain a RdRP, and are thus infectious, can be packaged into virions.

Most paramyxoviruses encode a number of accessory proteins off of the P gene, either through RNA editing leading to interferon antagonist V and W families, or by translating alternate reading frames from the P mRNA(74) to generate C family members. While we propose that C proteins are critical for engagement with Rab11a, we believe that in the absence of accumulation of sufficient L protein, vRNPs would be unable to interact with Rab11a.Thus, even if, for example, levels of C protein were higher in DVG-high cells, we would not expect to see C interacting with vRNPs in the absence of L. Additionally, the specific mechanisms that dictate translation of the C proteins (C, C', Y1 and Y2) from the P mRNA are unknown. Therefore, how DVG-mediated interference affects C protein accumulation is unclear. Further, while the C proteins have been described to have discrete functions in regulating pathogenesis and mRNA and vRNA synthesis(198), our results are unable to distinguish if a specific C protein is required for interaction with Rab11a or if they are interchangeable. The specific C proteins required for SeV assembly, and whether C family proteins of other paramyxoviruses play similar or distinct roles in viral assembly are as of yet unknown. Discerning their function in assembly could provide specific targets for the development of direct acting antivirals.

We also investigated the role of SeV M in viral assembly. M lines the inside of virions and interacts directly with nucleoproteins(192, 203). These contacts between M and the nucleoproteins drive virus-specific viral particle production, as studies combining

M and nucleoproteins from the closely related SeV and HPIV1 fail to lead to particle production(58). While M-NP contacts are important for particle production, it is unknown whether M is delivered to the cell membrane with nucleoproteins or independently, and whether its transport relies on Rab11a (20). Our experiments indicate that M is independently trafficked to the plasma membrane and is not the key mediator in vRNP interactions with Rab11a. Our data is consistent with previous reports that indicate that M traffics with F and HN through the trans-golgi network (TGN) to the cell membrane(190). We also identify M in the Rab11a IP-mass spectrometry results. Though we don't see strong enrichment of M in the IP when validated by western blot, it is possible that interactions with Rab11a are occurring at the plasma membrane. Alternatively, if M is trafficked to the membrane with surface proteins F and HN as proposed by (190), Rab11a may be interacting with M near the TGN. There is evidence that the rhabdovirus vesicular stomatitis virus (VSV) glycoprotein, which is processed in the TGN, requires Rab11a for proper sorting to the plasma membrane(204). Therefore, it is possible that SeV M, F, and HN may interact with Rab11a during their transit from the TGN to the plasma membrane.

It is well established that DVGs exert effects on viral infections through interfering with standard viral genomes by competing for structural proteins or viral polymerase(92). DVGs have been reported to globally lower levels of viral proteins within infected cells and for that reason have been investigated as antivirals themselves(114). Whether all viral proteins are equally affected by interference has not been previously reported. While it has been shown that infections with SeV HD leads to lower levels of M protein, these lower levels were attributed to increased degradation of M(155). Presence of DVGs have also been shown to lead to lower levels of HN on the surface of infected

cells(156). We performed a systematic investigation of the effects of interference on levels of mRNA and protein levels by directly comparing FL-high cells and DVG-high cells from a heterogenous infection. Our results support previous finding of lower levels of M and HN in the presence of DVGs but reveal that DVG interference with L mRNA transcription leads to significantly lower amount of mRNA and subsequent lower protein translation in DVG-high cells. Because L is the lowest abundance mRNA and protein, DVG-driven interference has the highest impact on its abundance. The gradient expression of mRNA as well as copy-back DVGs are unique to single-stranded negative sense RNA viruses. However, other RNA viruses, such as influenza produce deletion DVGs and are known to be sensitive to DVG-driven interference. It has been shown that DVGs generated from certain segments can exert different levels of interference pressure(205), but not whether interference particularly affects the accumulation of certain mRNAs or proteins. The role that DVG-mediated interference may play in restricting viral progeny production via reduction of certain key proteins in other viral families remains to be investigated.

Overall, we have shown that polymerase cofactors may be critical in inducing primary steps of viral assembly using DVGs as a tool to understand differences in viral replication and viral assembly. While we propose that C and L proteins are essential for driving contact between vRNPs and Rab11a during SeV infection, whether intricacies of viral assembly are conserved across paramyxoviruses is unknown. Many studies suggest that there are at least subtle differences amongst the viruses in their intracellular localization, transport, and eventual assembly(20). Because DVGs have been identified from most paramyxoviruses, comparisons between DVG-high and FL-high cells during

87

infection may be useful in parsing proteins required for viral replication from those required to initiate virion assembly of other members of the viral family.

3.6 Materials and Methods

Cells

A549 (human type II pneumocytes, ATCC CCL-185) and LLCMK-2 (monkey kidney epithelial cells, ATTC CCL-7) were maintained in Tissue Culture Medium (DMEM (Invitrogen) supplemented with 10% Fetal Bovine Serum (Sigma), Gentamicin (ThermoFisher), Sodium Pyruvate (Invitrogen), L-glutamine (Invitrogen)) at 7% CO2, 37°C. A549 Rab11-GFP and A549 Rab11-mCherry cells were generated as described in (202). Cells were tested monthly for mycoplasma MycoAlert Mycoplasma detection kit (Lonza) and treated with Mycoplasma Removal Agent (MP Biomedical) upon thawing.

Viruses

Sendai virus Cantell was grown in 10-day embryonated specific pathogen free chicken eggs (Charles River) for 40 hours before allantoic fluid was collected. Low DVG and high DVG stocks were produced as previously described, and defective particles (pDPs) were purified from allantoic fluid infected with SeV Cantell by density ultracentrifugation on a 5-45% sucrose gradient. SeV-LeGFP is a recombinant Enders strain of virus described in(48). SeV-LeGFP cells was grown for 72 hours in LLCMK2 cells. SeV-M-HA virus was generated with an HA tag at the N-terminus of the M protein in a recombinant SeV F1R background. Virus was rescued by transfection in to BSRT7 cells as described(206) and passaged blindly three times. Virus was then grown for 5 days in LLCMK2 cells. All viruses were titrated using 1:10 serial dilution in triplicate in LLCMK2 cells in the presence of 2ug/mL TPCK trypsin (Worthington Biomedical) for 72 hours and $TCID_{50}$/mL

was determined by the Reed-Meunch method based on hemagluttination of 0.5% washed chicken red blood cells (Lampire) to indicate presence of infection.

Plasmids and Transfection

SeV-M-FLAG plasmid encodes codon optimized SeV Matrix with a 3X N-terminal FLAG tag in the pCMV-3Tag-1A vector. Cells in antibiotic free media (8×10^5/6-well) were transfected 6 hours post infection with 2ug plasmid and 6ul Lipofectamine 2000 (Invitrogen) per well diluted in Opti-MEM (Invitrogen).

Viral Infections

Infections were performed at a multiplicity of infection of 1.5 $TCID_{50}$/cell unless otherwise specified. Cells were seeded to reach 80% confluency upon day of infection (4×10^5 A549/well in 6 well plates). Prior to infection cells were washed twice with PBS. Virus was diluted in infection media (DMEM (Invitrogen) supplemented with 35% BSA (Sigma-Aldrich), Pen/Strep (Invitrogen), 5% $NaHCO_3$ (Sigma-Aldrich) and low volume inoculum was added to cells for 1 hour incubation at 37°C, with shaking every 15 minutes. Cells were then refed with 2% FBS Tissue Culture Medium.

Drug Treatment

Four h post infection, media was removed and replaced with 2% FBS tissue culture media containing 2μg/mL Nocodazole (Sigma-Aldrich) for duration of infection.

Immunofluorescence

Cells were seeded on No. 1.5 glass coverslips (Corning) overnight prior to infection. Post infection coverslips were rinsed in PBS then fixed for 10 minutes in 4% Paraformaldehyde in PBS (Electron Microscopy Sciences) for 10 min. Cells were permeabilized with 0.2% Triton-X in PBS (Sigma-Aldrich) for 10 min. Primary and

89

secondary antibodies were diluted in 3% FBS in PBS and incubated at RT for 1.5 h and 1 h, respectively. Nuclei were stained with Hoechst prior to mounting coverslips on slides using Fluoromount-G (ThermoFisher). Primary antibodies: mouse anti-SeV NP (clone M73/2 a kind gift from Alan Portner – directly conjugated with Dylight 594 NHS Ester (ThermoFisher)), rabbit Anti-HA-Tag (CST C29F4), mouse Anti-FLAG 9A3 (CST 8146), rabbit Anti-GFP (ab6556), mouse anti-C (clone P16, 96-6, from Toru Takimoto). Secondary antibodies: Goat anti-Rabbit IgG (H+L) Secondary Antibody, Alexa Fluor 488 (Invitrogen), Goat anti-mouse IgG (H+L) Secondary Antibody, Alexa Fluor 647 (Invitrogen); Goat anti-mouse IgG (H+L) Secondary Antibody, Alexa Fluor 488 (Invitrogen)

RNA-FISH

Custom probe sets were designed against the SeV genome (described in(197)) and conjugated to Quasar 570 (3'(-)SeV) and Quasar 670 (5'(-)SeV) dyes (LGC Biosearch). For RNA-FISH microscopy, cells were seeded on No. 1.5 glass coverslips (Corning) prior to infection. Post infection coverslips were rinsed with PBS then fixed in 3.7% formaldehyde (ThermoFisher) for 10 min. Cells were permeabilized in 70% EtOH for 1 h at room temperature then washed in wash buffer (2X SSC (ThermoFisher), 10% formamide (ThermoFisher) in nuclease free water), and then subjected to hybridization with FISH probes. For hybridization, probes were diluted to 2.5nM in hybridization buffer (wash buffer + dextran sulfate) and applied to slides. Slides were incubated with probe overnight at 37°C in a humidified chamber. Prior to imaging, slides were washed in wash buffer twice (once with Hoechst to stain nuclei) then 2X SSC. Cells were mounted in ProLong Diamond Antifade Mountant (ThermoFisher) and cured overnight at room temperature prior to imaging. RNA FISH combined with immunofluorescence was

modified by staining cells with antibody after permeabilization with EtOH. Cells are stained with antibody in 1% BSA (ThermoFisher) PBS with RNaseOUT (Invitrogen) for 45 min for 1° Ab and 40 min for 2° Ab. Cells were then post-fixed for 10 min in 3.7% formaldehyde prior to hybridization.

RNA FISH Flow Cytometry

Cells were harvested post infection by trypsinization (ThermoFisher) and centrifugation. Cell pellets were washed in 1% FBS in PBS one time. Cell pellets were then resuspended in 10mL ice cold methanol (ThermoFisher) and fixed and permeabilized on ice for 10 minutes before pelleting at 1500rpm for 5 minutes. Pellets were then resuspended in 1mL wash buffer per sample and transferred to a microcentrifuge tube where they were washed twice. For hybridization probes were diluted to 25nM in 100ul hybridization buffer (wash buffer + dextran sulfate) and cell pellets were resuspended in hybridization buffers and incubated overnight at 37°C. For antibody staining, primary antibodies were added to the hybridization buffer and incubated overnight. Post-hybridization cell pellets were washed in wash buffer twice, then washed in 2X SSC before being resuspended in anti-fade buffer (2X SSC, 0.4% glucose (Sigma), Tris-HCL pH 8.0 (USB Corporation) with Catalase (Sigma) and Glucose Oxidase (Sigma)). For secondary antibody staining, antibody was added to wash buffer prior to washing with 2X SSC and incubated at 37°C for 30 minutes. Flow cytometry was performed on a BD LSRFortessa and compensation and gating was done in FlowJo_v9.9.4 (BD Biosciences). Mock and SeV LD infections were used to inform gating of SeV HD DVG-high and FL-high populations.

Microscopy and Image Analysis

Images were acquired on a Leica SP5-II Laser Scanning Confocal with 63X (1.40-0.60 NA) and 100X (1.46 NA) oil-immersion objectives with pixel size 70x70nm for FISH immunofluorescence, with z-step size of 0.13um, with 15 slices total. Immunofluoresence images (Rab11a colocalization) were acquired with the same parameters except for a pixel size of 40x40nm. Images were processed in Volocity (Perkins-Elmer) and deconvolution when performed was done with Huygen's Essential Deconvolution Wizard using theoretical point spread function. Colocalization was quantified in Volocity with manually defined ROI's using automatic thresholding based on (195).

Immunoprecipitation

Cells were lysed in NP-40 lysis buffer (Amresco) with proteinase inhibitors (Roche Boehringer Mannheim), RNase OUT (Invitrogen) and EDTA (ThermoFisher). Protein concentration was measured using BCA Protein Assay (ThermoFisher). For anti-NP immunoprecipitation: 500ug of protein was incubated overnight with primary antibody (anti-SeV NP). Protein G Magnetic Beads (EMD Millipore), 30ul per sample, were blocked overnight with Salmon Sperm DNA (ThermoFisher) in 5% FBS/PBS. Beads were washed and incubated with lysate/antibody for 4 hours at 4°C while rotating. For anti-NP immunopreciptations, beads were added 3 times sequentially. Beads were then washed with high salt lysis buffer threes times, then low salt lysis buffer once. Samples for RNase treatment were stopped here, samples for other applications were boiled in sample buffer for 10 minutes. For Rab11-GFP immunoprecipitation: Anti-GFP immunoprecipitation was carried out using anti-GFP mAb magnetic beads. 500ug lysates were incubated overnight with beads, then washed five times with wash buffer (50 mM Tris-HCl (pH 7.5), 150 mM NaCl, 0.05% NP-40).

Sample preparation for proteomic analysis

All chemicals used for preparation of nanoflow liquid chromatography-tandem mass spectrometry (nLC-MS/MS) samples were sequencing grade and purchased from Sigma-Aldrich (St. Louis, MO), unless otherwise stated. Immunoprecipitated GFP-Rab11A interacting proteins (Rab11A IP) were eluted from the magnetic beads by the on-beads tryptic digestion. Briefly, the beads were resuspended in 50 μl of 50 mM triethylammonium bicarbonate, pH 8.5 (TEAB, Thermo Fisher Scientific, Waltham, MA) and proteins were reduced using 10 mM dithiothreitol (DTT) for 1 h at room temperature and alkylated with 20 mM iodoacetamide (IAA) in the dark for 30 min at room temperature. Proteins were digested with trypsin (Promega, Madison, WI) at an enzyme-to-substrate ratio of ~1:50 for 12 h in a thermomixer, shaking at 900 rpm, at room temperature. After digestion, the supernatant was removed and collected into fresh, labelled tubes. Beads were washed twice with 50 μl of the wash buffer (50 mM TEAB pH 8.5, 5% acetonitrile) and all supernatants were merged. The samples were concentrated to the volume of ~100 μl by lyophilization and acetified with trifluoroacetic acid (TFA) to a final concentration of 0.1%. The tryptic peptides were desalted using Poros Oligo R3 RP (PerSeptive Biosystems, Framingham, MA) P200 columns with C18 3 M plug (3 M Bioanalytical Technologies, St. Paul, MN) prior to nLC–MS/MS analysis.

The whole cell proteome samples were processed using the suspension trap (S-Trap, Protifi, Huntington, NY)(207) mini spin column digestion protocol with minor modifications. Briefly, cells were lysed in 300 μl of lysis buffer (5% SDS, 50 mM TEAB pH 7.55, Halt™ protease and phosphatase inhibitor cocktail (Thermo Fisher Scientific, Waltham, MA)) by vortexing and probe tip sonication at 4 °C. The lysate was clarified by centrifugation at 13,000×*g* for 10 min, at 4 °C. Protein concentration was measured by

93

Bradford protein assay (Thermo Fisher Scientific) and ~300 µg of reduced and alkylated proteins was subjected to trypsin digestion following the S-Trap manufacturer's procedure. The peptide solution was pooled, lyophilized, and desalted prior to nLC–MS/MS.

Nanoflow Liquid Chromatography Tandem Mass Spectrometry (nLC-MS/MS)

The peptide mixture was separated using a Dionex Ultimate 3000 high-performance liquid chromatography (HPLC) system (Thermo Fisher Scientific) equipped with a two-column setup, consisting of a reversed-phase trap column (Acclaim PepMap100 C18, 5 µm, 100 Å, 300 µm i.d. × 5 mm, Thermo Fisher Scientific) and a reversed-phase analytical column (30 cm, 75 µm i.d. 360 µm o.d., in-house packed with Pur C18AQ 3 µm; Dr Maisch). Loading buffer was 0.1% trifluoroacetic acid (Merck Millipore) in water. Buffer A was 0.1% formic acid, and Buffer B was 80% acetonitrile + 0.1% formic acid. The HPLC was coupled online with an Orbitrap Fusion mass spectrometer (Thermo Fisher Scientific, San Jose, CA). The gradient was 135 min from 2% to 36% buffer B at a flow rate of 300 nl/min for GFP-Rab11A samples, and 180 min for whole cell proteome samples. The MS instrument was controlled by the Xcalibur software (Thermo Fisher Scientific). The nanoelectrospray ion source (Thermo Fisher Scientific) was used with a spray voltage of 2.2 kV. The ion transfer tube temperature was 275°C. Data acquisition was performed in the Orbitrap for precursor ions. MS survey scans were obtained for the m/z range of 350-1200 in the Orbitrap with maximum ion injection time of 100 ms, automatic gain control target 5×10^5 and a mass resolution of 120,000. MS/MS was performed with a TopSpeed duty cycle set to 3 s. Dynamic exclusion was set to 4 sec. Charge state enabled was 2-6$^+$. Higher Collisional Dissociation (HCD) was set to 30.

MS/MS was acquired in the ion trap using the Rapid scan mode, an automatic gain control set to 10,000 and a maximum injection time set to 120 msec.

Proteins Identification and Quantification

The raw mass spectrometer files were processed for protein identification using the Proteome Discoverer (v2.4, Thermo Fisher Scientific) and the Sequest HT algorithm with a peptide mass tolerance of 10 ppm, fragment m/z tolerance of 0.25 Da, and a false discovery rate (FDR) of 1% for proteins and peptides. All peak lists were searched against the UniProtKB/Swiss-Prot database of Human (January 2020, 20,367 entries) and UniprotKB/TrEMBL Sendai Virus (Cantell); February 2020, 8 entries) sequences using the parameters as follows: enzyme, trypsin; maximum missed cleavages, 2; fixed modification, carbamidomethylation (C); variable modifications, oxidation (M), protein N-terminus acetylation. Protein quantifications were $\log_2$ transformed and normalized using the median of the distribution for each sample. Missing values were imputed using a distribution of values of 30% width and two standard deviations lower than the average of the distribution of valid values. Statistical analyses were performed on three different biological replicates. The sample size was chosen to provide enough statistical power to apply parametric tests (either homoscedastic or heteroscedastic one-tailed t test, depending on the statistical value of the F-test; heteroscedastic if F-test p value<0.05). The t test was considered as valuable statistical test because binary comparisons were performed, and the number of replicates was limited. No samples were excluded as outliers (this applies to all proteomics analyses described in this manuscript). Proteins with t test p value smaller than 0.05 were considered as significantly altered between the two tested conditions. Data distribution was assumed to be normal, but this was not formally tested.

Western Blot

Whole cell lysate (10µg) or immunoprecipitation products were denatured by boiling for 10 min and run on a 4-12% Gradient Bis-Tris Gel (Bio-Rad) before being transferred to a PVDF membrane (Millipore). Membranes were incubated overnight with primary antibody in 5% milk. Membranes was incubated secondary antibody for an hour in 5% milk and developed using Lumi-light western blot substrate (Roche) to detect HRP. Images were acquired using a ChemDoc biomimager (Bio-Rad) and quantified in ImageJ. Primary antibodies: rabbit anti-Rab11a (Invitrogen); mouse anti-C (clone p96-6, a kind gift from Toru Takimoto), chicken anti-SeV polyclonal. Secondary antibodies: anti-rabbit HRP-conjugated antibody (Cell Signaling), anti-mouse IgG for IP (Abcam), anti-chicken HRP-conjugated antibody.

RNase Treatment

Post immunoprecipitation unbound fractions or substrate bound to magnetic beads were subjected to treatment with a combination of 1U/mL RNase A, V, and T1 (Invitrogen) for 15 minutes at room temperature. RNase reaction was stopped by adding Trizol LS (Invitrogen) to the sample.

RNA Extraction and RT-qPCR

Cellular and viral RNA was harvested using Trizol (Invitrogen). RNA was reverse transcribed using SuperScript III First Strand Synthesis System (Invitrogen) with OligoDT for mRNA specific amplification or with primer 5'-GGTGAGGAATCTATACGTTATAC-3' for viral RNA. qPCR was performed with 1:40 dilution of cDNA, SYBR Green (Life Technologies) and 5uM forward/reverse primers (Invitrogen) on an Applied Biosystems ViiA 7 Real-Time System. Relative copy numbers per cell were calculated by delta-delta Ct and normalized to average cellular GAPDH expression levels. Primer sequences are:

SeV NP (F: 5' TGCCCTGGAAGATGAGTTAG-3' R: 5'-GCCTGTTGGTTTGTGGTAAG -3'); SeV P/C (F: 5'- GGATATCCGAGATCAGGTATTGA-3' R: 5'-GGCCCGGTGTATATTTTGTTT-3'); SeV M F: (5'- GCCATCCCCTACATCAGGAT-3' R: 5'- GTAACGACCCGGAGCCGCAT-3'); SeV F (F: 5'-CTCCTGAAGATCTCTAAGGCAT-3' R: 5'-GGATCCCACGAATCGAGGTA3'); SeV HN F: (5'-GACCAGGAAATAAAGAGTGCA-3' R: 5'-CGATGTATTGGCATATAGCGT-3'); SeV L (F: 5'- TGGTCAGAGATGCAACGAGA-3' R: 5'-ACCTTTCAAGGACTGGATGC-3'); gSeV (F: 5'-GACCAGGAAATAAAGAGTGCA-3', R: 5'-CGATGTATTGGCATATAGCGT-3'), DVG-546 (F: 5'-TCCAAGACTATCTTTATCTATGTCC -3', R: 5'-GGTGAGGAATCTATACGTTATAC-3').

3.7 Acknowledgements

CHAPTER 4: Conclusions and Future Directions

4.1 Summary of findings

      Defective viral genomes (DVGs) generated during paramyxovirus infections are able to alter the outcome of these infections primarily by inducing antiviral immunity and interfering with standard viral genome replication. This dissertation sought to address how different intracellular localizations of full-length (FL) and defective viral genomes during Sendai virus (SeV) infection influenced viral infections and asked what these differential localizations could teach us about paramyxovirus particle assembly. Chapter 2 describes the discrete localizations of SeV DVGs and FL genomes, with genomes in FL-high cells engaging with Rab11a marked recycling endosomes, and genomes in DVG-high cells failing to engage with the host in this way. We found that these distinct interactions contributed to differences in viral particle production with FL-high cells being the primary producers of both standard and defective viral particles, and DVG-high cells not contributing to the pool of infectious particles produced during infection(197). In Chapter 3, we addressed the viral determinants that drive FL-high cells to interact with Rab11a-containing recycling endosomes. We demonstrated that high levels of viral polymerase components including L and C, are differentiating factors in cells that proceed to viral assembly in contrast to DVG-high cells that solely carry out genomic replication. We propose that C and L proteins are critical in mediating viral genome engagement with recycling endosomes. Overall, this work has contributed to the understanding of how DVGs modulate infection outcomes by focusing on differential particle production in cells, as well as uncovered fundamental aspects of paramyxovirus assembly. This chapter will discuss broader implications and future directions for these areas of study.

4.2 DVG induced heterogeneity

The presence of defective particles during infection leads to heterogeneous accumulation of viral genomic material in infected cells, with some cells accumulating predominantly FL genomes (FL-high cells) and others accumulating predominantly DVGs (DVG-high cells). This type of heterogeneity has been observed for SeV(165) and described in depth in chapter 2, and has also been observed in influenza (208, 209) and respiratory syncytial virus(165) infections. The differences in viral product accumulation results in unique transcriptional responses of the infected cell populations and corroborates the role of DVGs as strong innate immune agonists. The work presented here, expands on impacts of this heterogeneity and indicates that the genomic accumulation influences particle production as well(197). Despite new appreciation that heterogeneity in DVG accumulation can influence cellular outcomes during infection, questions remain, including: What viral or cellular factors contribute to the heterogeneity that is observed? What does this heterogeneity look like in tissue or animals?

4.2.1 Drivers of heterogeneity

During SeV infection with high DVG (HD) stocks of virus, we observed heterogeneous accumulation of viral genomes amongst infected cells. Though the work presented here focused on descriptions of DVG-high and FL-high cells, which each comprise approximately 30% of the infected cell population, there are two other categories of cells which make up the rest of the population: intermediate cells, which fall between the phenotype of DVG-high and FL-high cells based on characterization of vRNA FISH probe binding, and cells with non-detectable (ND) levels of viral RNA based

on vRNA FISH(165). The factors that impact the distribution of these populations have yet to be characterized.

We hypothesize that the driving factor for determining a DVG-high or FL-high phenotype is the ratio of defective particles to standard virions that infect a particular cell. This hypothesis is supported by the ability to manipulate the proportions of DVG-high and FL-high cells in an infection by the addition of different amounts of purified defective particles (pDPs). The addition of increasing amounts of pDPs led to an increase in DVG-high cells (**Figure 2.2**). Interestingly, increasing the amount of pDPs past a certain threshold led to an increase in ND cells (**Figure 2.1**), suggesting that ND cells are the product of a single cell receiving an input with a high ratio of DVGs:standard genome, rather than due to lack of infection, particularly since infections are performed at an MOI 1.5 to ensure that at least 80% of the cells receive an infectious viral particle.

While the varying ratios of DPs:standard virions that cells receive is likely the driver of heterogeneity in infection, the precise ratios that lead to the development of each cell phenotype are not known. Use of new technologies available to more accurately measure the number of defective particles added to an infection could help define these ratios. Digital droplet PCR (ddPCR), which allows for quantification of RNA in the absence of a standard curve, could be used to perform sensitive quantification of viral RNA on both viral stocks and on purified DPs. In fact, ddPCR methods have been used to perform sensitive quantification of influenza virus(210) and Nipah virus DVGs(211), indicating that this would be a suitable method for quantification of DVGs in purified particle and virus stocks. With the ability to quantify numbers of DVGs in particles, we could perform infections with varying ratios of purified defective particles and standard virus and quantify cell populations by RNA FISH coupled with flow cytometry. These data sets would allow us to calculate the ratio of DPs:standard virions

101

that lend to the various cell phenotypes by quantifying ratios of cell phenotypes and fitting them with Poisson distributions of probability of cells receiving each particle ratio during infection.

Interestingly, FL-high cells in HD infections harbor DVGs and produce defective particles at a higher rate than FL-cells in low DVG (LD) infections (unpublished observation). In LD infections, DVGs must be generated *de novo* during infection and DPs are produced at much later timepoints than in HD infections, suggesting that FL-high cells in HD infections receive defective particles upon infection, but in insufficient quantities to lead to the development of a DVG-high cell phenotype. This suggests that a ratio greater than 1:1 DPs:standard virion is required to generate a DVG-high cell, in contrast to what has been reported for VSV, where even one defective particle was sufficient to suppress viral particle production(175). The ratios that lead to a DVG-high cell phenotype may vary in different viral infections or even in infections with the same standard virus but with different DVG species due to differences in DVG replication rates. Differences in DVG size or viral promoters may affect the ratios of DPs:standard that lead to different cell phenotypes.

We have also questioned whether cellular factors influence the development of DVG-high and FL-high cells during infection. The primary factor that may influence accumulation of viral products is which stage of the cell cycle cells are in during infection. Many DNA and RNA viruses employ diverse strategies to promote certain cell cycle stages to enhance their replication(212). For example, the M2/G stages of the cell cycle are more permissive to VSV replication(213). Whether cell cycle affects accumulation of DVGs or FL genomes can be addressed by synchronizing cells to different phases of the cell cycle prior to infection then performing vRNA-FISH flow cytometry and quantifying the proportions of DVG-high and FL-high cells generated

during infections at each phase of the cell cycle. Similar experiments have been done

with picornaviruses and have concluded that different cell cycle phases do not affect the

observed heterogeneity of infection(185). Additionally, given robust evidence that

varying input of defective particles can alter the number of DVG-high cells, we favor the

hypothesis that variations in cell cycle would minimally impact ratios of DVG-high and

FL-high cells.

4.2.2 Heterogeneity in tissue and animal models

The accumulation of heterogenous levels of viral genomes during infection has

primarily been observed in cell culture monolayers with synchronous infections using HD

stocks of virus. An outstanding question is whether these phenotypes will be

recapitulated *in vivo*. Large bottlenecks during natural transmission of infections mean

that likely very few virions initiate natural infections(144). As discussed in the

introduction, we hypothesize that during initial infection, a single virion seeds a local

focus of infection and that progressive rounds of amplification will eventually lead to

generation of DVGs which will be packaged into DPs. This would create a

microenvironment in which new cells may be infected by standard and defective

particles at varying ratios, eventually recapitulating HD infection phenotypes observed *in*

vitro. Because SeV is a natural murine pathogen and replicates robustly in the lungs of

infected mice, the question of whether we see this heterogeneity *in vivo* can be

addressed by performing RNA FISH on lung tissues of infected animals at different

timepoints of infection. Experiments can be performed where mice are infected with SeV

LD and development and expansion of foci of infection can be observed and assessed

for the appearance of DVG-high cells. Mice can also be infected with SeV HD and lungs

can be assayed for the presence of DVG-high cells. Preliminary data from the laboratory

shows that upon infection of mice with SeV HD, DVG-high cells are identifiable, but they are low in abundance. The primary issue with performing experiments using RNA-FISH in vivo has been difficulty in visualizing low levels of signal with high background of fluorescence in lung tissue, however new strategies to increase intensity of RNA-FISH probe signals including CLAMP-FISH(214), may be useful in visualizing early events of viral infection in the lung. Further, techniques to combine RNA-FISH with immunostaining developed in Chapter 3 could aid in identifying DVG-high populations in the lung.

The lung is composed of multiple cell types, including type I and type II pneumocytes that make up the alveoli, as well as structural cells and immune cells such as resident alveolar macrophages and others(215). During infection with SeV, there is rapid recruitment of immune cells, predominantly neutrophils followed by T and B cells required for infection clearance, all of which are able to be infected by SeV(140, 216, 217). Whether heterogeneity of genome accumulation as well as differences in intracellular distribution of DVGs and genomes, would be observed in different cells infected in the lung remains to be investigated. The majority of the data presented here is from infections performed in the tissue culture cell line A549 which are type II pneumocytes. However, all tissue culture cell lines investigated as well as primary lung fibroblasts have shown similar heterogeneity and intracellular distribution to that characterized in A549s. Based on these data, we hypothesize that *in vivo* pneumocytes and structural cells would display similar heterogeneity and intracellular distribution as described here. However, this may not be the case for immune cells. While we have measured high amounts of viral RNA in neutrophils, and plasmacytoid dendritic cells (pDCs) are also susceptible to viral infection, these cells are likely not sources of virions. Therefore, because intracellular distribution of RNA is directly related to virion

production, we would not expect to see these distinct intracellular distributions in these cell types. This could be confirmed by using RNA FISH on these cells either in in vivo tissue slices or by ex vivo cultures and subsequent infections of these cell types. We do know that DVG replication in pDCs is important for initiation and orchestration of immune responses(164). Therefore identifying whether different cell types develop DVG-high cells and whether these cells are the producers of DPs *in vivo* is important to better understand the initiation of an immune response.

4.3 Altered Infection Dynamics in the Presence of DVGs

In Chapter 2, we explored how the presence of DVGs alters which cells are able to produce DPs and standard virions and in Chapter 3, we investigated the impact of DVGs on interference with viral mRNA expression and viral protein accumulation. Overall, a better understanding of the dynamics of DVGs influence on infection can help address larger questions of the impact of DVGs during infection, including: Can we better model the impact of DVG interference during infection? How can this inform our models of pathogenesis at a tissue or animal level? How does this understanding impact the development of DVGs as therapeutics or antivirals?

4.3.1 DVG Impacts on Interference and Pathogenesis

DVGs have been well documented to exert influence on infection through interference with production of viral proteins through a number of mechanisms, as illustrated in (**Figure 1.4**)(92, 218). Competition and viral outgrowth assays in the presence of DPs have been extensively studied in vitro using VSV to inform mathematical models. Most often, the presence of DPs delayed, but did not shut down, viral protein expression in infected cells. Previous models suggested that low levels of DPs were sufficient to prevent infection(219), but updated models support a multi-hit

hypothesis whereby varying levels of input of DPs lead to divergent outcomes of infection: inhibition of total particle production, limited production of standard virus but high levels of DPs, and low levels of DPs but high levels of standard virus(220). Yet, these parameters may change based on the characteristics of the DVGs or standard virus used for these competition assays. Intriguingly, experiments performed using VSV found that while small numbers of DPs can completely shut down production of infectious virus, high levels of DPs prevented this inhibitory effect(175, 186). Further, virus production can be inhibited with a low input of DPs per infectious virus but cannot completely eliminate virus production even at very high rates of DPs(174, 221). Gaining a better understanding of the interplay between standard virus and DVGs at varying ratios could provide insight for the use of DPs as therapeutic particles or for understanding how interference modulates pathogenesis in vivo.

The delay in virus production and viral replication induced by DVGs is hypothesized to increase the time over which virus is produced and perhaps extend infection(186). Multiple models have been created to help researchers understand how the inclusion of DPs during infection impacts viral production, as mentioned above, and limits viral spread(221). However, the production of DPs and how it changes during infection have not been included in these models, leaving us wondering how these important aspects of the virus life cycle impact the dynamics. The data presented in Chapter 2 could aid in the inclusion of DPs in models of multicycle infections and better represent dynamics of infections in tissues or more complex landscapes.

Further, in chapter 3 we provide a comprehensive investigation into the effects of interference on the accumulation of multiple viral proteins in a comparative manor. We show that viral proteins that are least abundant, namely L, are most reduced when subjected to DVG-mediated interference. Based on our data of mRNA and genome

amounts over time, we can begin to build more informed mathematical models of viral replication rates and how the presence of DVGs affect replication and transcription rates. We have begun to develop mathematical models that reflect how interference by DVGs may affect protein accumulation and thus viral genome replication and virion production. Using these models we can vary the amounts of DVGs in the system upon input and ask how varying levels of DVGs can affect cell fate via interference with certain proteins. We could also include data from proposed experiments from section 4.2.1 on varying levels of input DPs, to understand the dynamic range of DPs/DVGs influence on infections. We can also expand these models to population based models, and combining the data from Chapter 3 on viral proteins critical for viral particle assembly and the data in Chapter 2 regarding viral particle production during DVG induced heterogeneity, we can begin to accurately model population dynamics in the presence of DVGs. Building these models will allow us to better understand the role of DVGs during infection and help guide the use of therapeutic DVG administration during disease.

4.3.2 Implications for prophylaxis and persistence

Therapeutic administration of DVGs either as a prophylaxis to induce a protective immune response or as a therapeutic to attenuate replication of virus has begun to be explored(114, 222-224). Results detailed in Chapter 2 indicate that high levels of defective particles can generate high percentages of DVG-high cells, and these DVG-high cells are incapable of generating either defective particles or standard virions. The inability of these cells to generate standard virions is protective and would achieve the goals of reducing viral loads by the administration of DVGs or pDPs. In addition, our lab has demonstrated that DVG-high cells initiate a unique pro-survival transcriptional profile as a result of MAVS-induced antiviral signaling. This pro-survival program protects these

cells from TNF-mediated cell death(165). While this work has not been expanded to *in vivo* experiments, the concept of cells being protected from cell death and unable to produce viral particles, seems like it would indeed bolster recovery from viral infection, as lung damage during respiratory infections is driven by death of infected cells(225).

However, we must also consider the long-appreciated role of DVGs in persistent infections. DVGs and DPs from many viruses, including paramyxoviruses, have been associated with the establishment of persistent infections in both tissue culture and animal models(226). Recently, our lab associated this with the pro-survival pathway upregulated by DVG-high cells and posited that these DVG-high cells may survive past the acute phase of infection and act as reservoirs for virus which may become activated due to immunosuppression or periods of stress later in life(165). Therefore, it is important to fully understand the dynamics between DVG-high and FL-high cells and reach an appropriate balance of these cells during prophylactic or therapeutic administration of DVGs/DPs to maximize disease amelioration and minimize long-term consequences.

4.4 Paramyxovirus Interactions with Recycling Endosomes During Assembly

In Chapter 3 we suggest that polymerase components, namely the polymerase L and polymerase cofactor C are important in initiating contact between viral genomes or viral ribonucleoproteins (vRNPs) and recycling endosomes for the production of infectious particles. We also explore the role of the matrix protein (M) in regulating viral assembly. However, there are many areas of this research which should be expanded to more comprehensively understand the role of polymerase components in paramyxovirus assembly, including: What molecular characteristics of C protein allow for interaction with recycling endosomes and how is C protein affected by interference? How is M

trafficked to the plasma membrane and when does it interact with Rab11a? Which host

proteins are required for vRNP trafficking and how are host cells impacted by viral

assembly? Are the mechanisms described here conserved for other paramyxoviruses?

And what are the implications for these findings in the development of antivirals?

4.4.1. Further characterization of polymerase components required for assembly

Our current model for interactions between vRNPs and Rab11a is that in FL-high

cells when there is accumulation of polymerase to sufficiently high levels, all vRNPs are

occupied by multiple copies of the viral polymerase (approximately 40 copies as

determined by the amount seen on vRNPs recovered from infectious virions)(199, 200).

C protein is covalently attached to L protein(227), presumably acting as a regulator of

polarity of genome replication, favoring production of negative strand genomes at this

time point of infection(31, 73, 119). This C protein is in turn interacting with Rab11a,

either directly or through one another host protein.

Because C proteins are generated from P mRNA, instead of as an independent

gene product, it is not straightforward to generate a virus which does not generate C

proteins without disrupting expression of P. There have been multiple independent

attempts to create a SeV that lacks the four C proteins(72, 228). The SeVΔC virus

generated by the Kolakofsky lab was generated by altering the C and C' protein start

codons(72). We obtained this virus to test for the involvement of C protein in intracellular

genome localization, however validation in our hands revealed that some version of C

protein was present as a fusion with P protein, as detectable by western blot and

immunofluorescence with an anti-SeV C monoclonal antibody. The Nagai group has also

created a recombinant virus, SeV 4C(-), through the creation of four consecutive stop

codons after all four C proteins(228). We could infect cells with this virus to directly study

the impact of C proteins on the intracellular localization of viral genomes. I hypothesize that in the absence of C proteins, viral genomes in FL-high cells will fail to interact with Rab11a. Indeed, a profound decrease in peak viral titers is observed when cells or embryonated chicken eggs are infected with 4C(-) viruses(31, 70, 228) and C has been thus hypothesized to play a role in particle formation(68, 70). If indeed infections with 4C(-) showed defects in vRNP engagement with recycling endosomes, we could identify which C protein family member which may be essential in interacting with Rab11a, and further map which regions or residues are essential in this interaction. Paramyxoviruses tolerate insertion of additional proteins in their genomes, and indeed additional copies of C have been added to the paramyxovirus genome in the presence of C ablation to confirm the role of C protein during infection (118). We could create recombinant viruses that expressed only one C protein at a time and RNA FISH combined with immunofluorescence could be used to assay for interaction between viral RNA and Rab11a in the presence of the expression of single C proteins. If a specific C protein is been identified, similar experiments could be repeated with the insertion of distinct regions of this C protein or C protein with deletions or mutations and assayed similarly to identify which regions of C are critical for mediating the interaction with recycling endosomes. The residues required for C protein to antagonize innate immunity and to regulate genome polarity have been mapped by mutation (229) and the first 98 amino acid residues have been deemed dispensable for these functions(230), indicating they perhaps serve other functions such as bridging interactions between vRNPs and Rab11.

Completing these experiments would further define the interactions of Sendai virus and the host via its C protein and confirm the role of polymerase components as essential in regulating the interactions between vRNPs and Rab11a during infection.

4.4.2 Effects of interference on C proteins

While we were able to measure and compare accumulation of viral RNA over time in LD and HD infections, we are unable to perform similar measurements for C because the protein is generated from the P mRNA. Levels of P mRNA are reduced in HD infections compared to LD infections at 12 hours post infection, but not to a significantly greater degree than any other viral transcript. We could investigate whether there are differences in C proteins in FL-high and DVG-high cells. Preliminary data from immunofluorescence microscopy indicates that there is less C proteins in DVG-high cells than FL-high cells. We attempted to quantify this using RNA FISH combined with flow cytometry, but extremely low levels of C proteins are hard to detect by this method. An alternate strategy would be simply to compare the levels of C proteins by flow cytometry in SeV LD and SeV HD infections and ask whether levels of C proteins are globally reduced to the same extent that L proteins are during infection, or whether they are less significantly reduced similar to the effects on NP proteins. Because P mRNA levels are not significantly reduced, the levels of C in DVG-high and FL-high cells might be similar. We do not understand the factors that induce ribosomal skipping or shunting that result in usage of alternative start codons to produce C proteins. However, it may be that these fairly rare events cause C levels to be more sensitive to reduced P mRNA levels. Understanding how alternately translated proteins are affected by interference may shed light on mechanisms that drive alternate translation of mRNAs during viral infection as well as add to our understanding of how low abundance proteins are influenced by interference.

111

4.4.3 Further characterization of matrix proteins role in viral assembly

In Chapter 3, we also characterize the role of the viral matrix protein (M) in SeV assembly. We propose a model whereby L and C proteins are essential in driving association of vRNPs with Rab11a and that M is trafficked independently and interacts with vRNPs at the plasma membrane of infected cells. These conclusions rely on the characterization of the intracellular localization of M at 24 hours post infection, a time of robust viral particle production. In order to fully characterize the important role that M plays during infection and fully elucidate where and how it functions during assembly, we could perform a number of experiments. First, more detailed time courses of M localization during infection using the already generated recombinant virus would help clarify when and how M accumulates at the plasma membrane during infection. Immunofluorescence to detect M via HA tag in combination with other viral proteins such as C protein could illuminate the sites of their interactions. Additionally, localization of SeV F or HN proteins and M could be used to determine whether M interacts with these proteins during trafficking through the trans-golgi network (TGN). Though our results indicated that SeV M did not have large degrees of colocalization with Rab11a, M is identified by mass spectrometry to immunoprecipitate with Rab11a. We have yet to investigate whether we see interactions between M and the TGN, which would support interactions with cytoplasmic tails of surface proteins during their transit and explain some level of interaction between M and Rab11a. Further, while time course studies could help detail the dynamics of M during infection, the creation of a recombinant virus with a fluorescent protein tag could enhance our ability to study the dynamics of M during infection. M is an oligomeric protein and does not tolerate a tag at the C-terminal of the protein and may not tolerate a large tag at the N terminus, but rescue of a virus

with a GFP or mCherry protein fused to the N-terminus could be attempted using reverse genetics. Infections using a virus with a fluorescent tagged M protein could be observed using a spinning-disc confocal over periods of time to observe protein movement during infection. These infections could also be observed in fluorescently tagged Rab11a cell lines in order to observer real-time interplay between virus and host proteins.

Additional experiments to confirm the absence of a role for M in the association of vRNPs to recycling endosomes could be carried out by creating a virus that lacks M protein and observing the intracellular localization of vRNPs during infection with this virus. A single-cycle replication competent virus could be generated that lacks the M protein in its genome as long as recombinant virus rescue was performed in cells that stably expressed M protein. This would allow for the creation of virions which could then be used to infect cells but would not be able to express M protein. In the absence of M protein, I hypothesize that viral genomes would still interact with Rab11a, confirming the absence of a role for M in driving this interaction.

Completing these studies would help to understand how matrix functions in assembly and define the spatiotemporal aspects of its interaction with host cells.

4.4.4 Further characterization of host proteins involved in paramyxovirus assembly

While it is well-established that viral genomes interact with Rab11a to produce new virions(45, 231), it is still not known whether this is a direct interaction between viral components and the Rab11a protein itself or whether viral proteins interact with other host proteins which in turn interact with Rab11a.It has been suggested that viral genomes may interact with Rab11a family interacting proteins (FIPs) which are a family of proteins that tether Rab11a to the cell cytoskeleton to direct different types of

movement. There are five described FIPs which direct different types of motion within the cell (232). In order to investigate whether any of these FIPs are important in bridging interactions between vRNPs and Rab11a, we could perform an siRNA screen targeting the different FIPs. After knock down by siRNA, cells could be infected with SeV LD and immunofluorescence for NP or vRNA FISH for genomes could be applied to determine whether perinuclear clustering of viral genomes is disrupted. If there is an observed change in the localization phenotype in any of the knock down conditions, then this could indicate that either this FIP is essential for bridging interactions between vRNPs and Rab11a or that this FIP is necessary for the movement that directs the clustering of Rab11a at the endocytic recycling compartment during viral infection. Different viruses have been shown to coopt different FIPs, for example FIP2 has been identified as important for the production of respiratory syncytial virus virions (53), while budding of filamentous influenza relies on FIP3(52). In order to investigate whether candidate FIPs are important for bridging interactions with Rab11a or directing movement of Rab11a, we could perform colocalization assays of SeV NP and Rab11a during FIP siRNA knockdowns that yielded changes in localization. If we see decreases in colocalization between SeV NP and Rab11a during FIP knockdown this indicates that this FIP was important in bridging the vRNP-Rab11a interaction. If we do not see changes in colocalization but see changes in Rab11a or NP distribution this indicates that this FIP is being utilized for Rab11a movement during infection. Performing these experiments would help to identify elements of host pathways that are coopted during SeV infection and understand how the virus alters host cell dynamics during infection.

     We have also observed that infection with SeV drastically changes the dynamics of the host cytoskeleton and recycling kinetics (unpublished observations). Drastic changes in cytoskeleton networks have been observed during infection across many

types of viruses including DNA, RNA, and retrovirus infections for entry, replication, and assembly(233). We observe large changes in microtubule dynamics during infection with SeV LD, decreased transferrin recycling, as well as changes in motor proteins associated with Rab11a by mass spectrometry. Preliminary experiments have indicated that disruptions to transferrin recycling are blunted in SeV HD infections compared to changes seen in SeV LD infections, presumably due to DVG-high cells not disrupting normal transferrin recycling rates. Finally, mass spectrometry to identify proteins interacting with Rab11a during infection showed large changes in the proteins that associate with Rab11a, particularly an increase in proteins that are associated with membrane trafficking, indicating that the virus alters the cell in a way that promotes particle production. Changes such as these have been identified in other viruses that coopt Rab11a pathways during infection, particularly influenza(202, 234). Investigation into how these proteins and cellular processes are altered during SeV infection could be pursued to get a more complete picture of how SeV alters normal cell physiology during infection.

4.4.5 Assembly mechanisms in other paramyxoviruses

While this work has focused on assembly of paramyxoviruses using SeV as a model, it could be easily expanded to ask whether the principles uncovered in SeV infection are conserved in other viruses. The first virus that ought to be investigated is HPIV1 as it is the most closely related human pathogen to SeV. HPIV1 has been demonstrated to use Rab11a during viral particle formation(47), and HPIV1 expresses C proteins that have 69% protein identity to Sendai virus C proteins,. They also have similar described functions in innate immune antagonism (235). Therefore, we could ask whether HPIV1 C proteins are involved in regulating engagement of vRNPs with Rab11a

using similar approaches as those described in Chapter 3. Similar to experiments performed with SeV C proteins, HPIV3 viruses with mutated C proteins have been used to map residues that are critical for antagonizing the immune response or regulating viral replication(236), therefore it would be reasonable to carry out similar experiments to identify residues that are critical for regulating interactions with Rab11a.

In addition to the closely related human parainfluenza viruses which are part of the respirovirus genus, other paramyxoviruses in the morbillivirus and henipavirus genuses also encode C proteins that are multifunctional. The C proteins of measles have been well characterized as interferon antagonists(237) and as polymerase cofactors that regulate polarity of genome transcription(238, 239). However, the role of measles virus C proteins in particle production has yet to be investigated. Likewise, the C proteins of NiV have also been described to be polyfunctional, both acting to enhance pathogenesis through the antagonism of IFN responses and to participate in enhancing particle formation(63, 240). The C protein of NiV has been shown to enhance the recruitment of ESCRT proteins to drive budding in the presence of expression of M(63). Whether C may also interact with Rab11a in NiV infection is yet to be investigated.

In contrast, viruses in the rubulavirus genus, such as Mumps, do not express C proteins. While mumps uses Rab11a for particle formation, it differs in requirements of host proteins during budding, relying on expression of fusion proteins to form VLPs and is dependent on ESCRT, unlike respiroviruses(65), indicating that there may be different mechanisms of particle productions used by viruses that do not express C proteins. Members of the avulavirus genus such as NDV also do not express C proteins. There are no reports on whether NDV requires Rab11a for particle formation, but there is evidence that VLP formation requires expression of F and HN for homogenous particle

formation like for mumps(241), arguing that these viruses have different requirements for particle formation than those that express C proteins.

4.4.6 Implications for development of therapeutics/antivirals

Completion of experiments detailed above will help to elucidate the molecular mechanisms of paramyxovirus assembly. With a better understanding of how viral proteins interact to assemble particles, we can develop virus directed small molecules to that prevent the virus from interacting with the host. Identifying residues and regions of C proteins in SeV that are critical for regulating these interactions is useful for identifying whether there are conserved regions in C proteins that behave similarly across paramyxovirus species or genuses. Further, completing more detailed studies of the role of M in SeV infection will help to elucidate a previously contested role of this viral protein in assembly. A better and more nuanced understanding of this proteins' role in viral assembly will be helpful in the development of antiviral drugs, since, as an oligomeric protein, it may be efficiently targeted(242). Additionally, having a better understanding of proteins in the host that are manipulated by the virus could give rise to host directed therapies that may be more broadly acting than virus directed therapies.

4.5 Concluding Remarks

Overall this work provides a better understanding of how DVG induced heterogeneity contributes to viral population dynamics. These insights can be used to better understand complex interactions between virus, DVG, and the host and model viral infections in tissues, as well as inform uses of defective particles as prophylactics or therapeutic interventions. Additionally, this work uses DVGs as a tool to expand our knowledge on basic paramyxovirus biology and understand critical elements that drive

117

viral genome assembly. The identification of viral polymerase components as critical for

virion assembly provides additional targets for antiviral therapy.

BIBLIOGRAPHY

1.   Anonymous. 2011. Chapter 17 - Paramyxoviridae, p 299-325. *In* MacLachlan NJ, Dubovi EJ (ed), Fenner's Veterinary Virology (Fourth Edition) doi:https://doi.org/10.1016/B978-0-12-375158-4.00017-1. Academic Press, San Diego.

2.   Maykowski P, Smithgall M, Zachariah P, Oberhardt M, Vargas C, Reed C, Demmer RT, Stockwell MS, Saiman L. 2018. Seasonality and clinical impact of human parainfluenza viruses. Influenza Other Respir Viruses 12:706-716.

3.   Pawelczyk M, Kowalski ML. 2017. The Role of Human Parainfluenza Virus Infections in the Immunopathology of the Respiratory Tract. Curr Allergy Asthma Rep 17:16.

4.   Jain S, Self WH, Wunderink RG, Fakhran S, Balk R, Bramley AM, Reed C, Grijalva CG, Anderson EJ, Courtney DM, Chappell JD, Qi C, Hart EM, Carroll F, Trabue C, Donnelly HK, Williams DJ, Zhu Y, Arnold SR, Ampofo K, Waterer GW, Levine M, Lindstrom S, Winchell JM, Katz JM, Erdman D, Schneider E, Hicks LA, McCullers JA, Pavia AT, Edwards KM, Finelli L, Team CES. 2015. Community-Acquired Pneumonia Requiring Hospitalization among U.S. Adults. N Engl J Med 373:415-27.

5.   Pneumonia Etiology Research for Child Health Study G. 2019. Causes of severe pneumonia requiring hospital admission in children without HIV infection from Africa and Asia: the PERCH multi-country case-control study. Lancet 394:757-779.

6.   Weatherman S, Feldmann H, de Wit E. 2018. Transmission of henipaviruses. Curr Opin Virol 28:7-11.

7.   Field HE. 2016. Hendra virus ecology and transmission. Curr Opin Virol 16:120-125.

8.   Kumar B, Manuja A, Gulati BR, Virmani N, Tripathi BN. 2018. Zoonotic Viral Diseases of Equines and Their Impact on Human and Animal Health. Open Virol J 12:80-98.

9.   Ochani RK, Batra S, Shaikh A, Asad A. 2019. Nipah virus - the rising epidemic: a review. Infez Med 27:117-127.

10.   Kenmoe S, Demanou M, Bigna JJ, Nde Kengne C, Fatawou Modiyinji A, Simo FBN, Eyangoh S, Sadeuh-Mba SA, Njouom R. 2019. Case fatality rate and risk factors for Nipah virus encephalitis: A systematic review and meta-analysis. J Clin Virol 117:19-26.

11.   Thibault PA, Watkinson RE, Moreira-Soto A, Drexler JF, Lee B. 2017. Zoonotic Potential of Emerging Paramyxoviruses: Knowns and Unknowns. Adv Virus Res 98:1-55.

12.   Greenwood B. 2014. The contribution of vaccination to global health: past, present and future. Philos Trans R Soc Lond B Biol Sci 369:20130433.

13.   Bankamp B, Hickman C, Icenogle JP, Rota PA. 2019. Successes and challenges for preventing measles, mumps and rubella by vaccination. Curr Opin Virol 34:110-116.

14.   Noton SL, Fearns R. 2015. Initiation and regulation of paramyxovirus transcription and replication. Virology 479-480:545-54.

15. Kolakofsky D, Roux L, Garcin D, Ruigrok RWH. 2005. Paramyxovirus mRNA editing, the "rule of six" and error catastrophe: a hypothesis. J Gen Virol 86:1869-1877.
16. Egelman EH, Wu SS, Amrein M, Portner A, Murti G. 1989. The Sendai virus nucleocapsid exists in at least four different helical states. J Virol 63:2233-43.
17. Horikami SM, Curran J, Kolakofsky D, Moyer SA. 1992. Complexes of Sendai virus NP-P and P-L proteins are required for defective interfering particle genome replication in vitro. J Virol 66:4901-8.
18. Curran J, Marq JB, Kolakofsky D. 1995. An N-terminal domain of the Sendai paramyxovirus P protein acts as a chaperone for the NP protein during the nascent chain assembly step of genome replication. J Virol 69:849-55.
19. Ke Z, Strauss JD, Hampton CM, Brindley MA, Dillard RS, Leon F, Lamb KM, Plemper RK, Wright ER. 2018. Promotion of virus assembly and organization by the measles virus matrix protein. Nat Commun 9:1736.
20. El Najjar F, Schmitt AP, Dutch RE. 2014. Paramyxovirus glycoprotein incorporation, assembly and budding: a three way dance for infectious particle production. Viruses 6:3019-54.
21. Cox RM, Plemper RK. 2017. Structure and organization of paramyxovirus particles. Curr Opin Virol 24:105-114.
22. Harrison MS, Sakaguchi T, Schmitt AP. 2010. Paramyxovirus assembly and budding: building particles that transmit infections. Int J Biochem Cell Biol 42:1416-29.
23. Ogino T, Kobayashi M, Iwama M, Mizumoto K. 2005. Sendai virus RNA-dependent RNA polymerase L protein catalyzes cap methylation of virus-specific mRNA. J Biol Chem 280:4429-35.
24. Parks GD, Alexander-Miller MA. 2013. Paramyxovirus activation and inhibition of innate immune responses. J Mol Biol 425:4872-92.
25. Chang A, Dutch RE. 2012. Paramyxovirus fusion and entry: multiple paths to a common end. Viruses 4:613-36.
26. Haywood AM. 2010. Membrane uncoating of intact enveloped viruses. J Virol 84:10946-55.
27. Wignall-Fleming EB, Hughes DJ, Vattipally S, Modha S, Goodbourn S, Davison AJ, Randall RE. 2019. Analysis of Paramyxovirus Transcription and Replication by High-Throughput Sequencing. J Virol 93.
28. Vidal S, Kolakofsky D. 1989. Modified model for the switch from Sendai virus transcription to replication. J Virol 63:1951-8.
29. Le Mercier P, Garcin D, Garcia E, Kolakofsky D. 2003. Competition between the Sendai virus N mRNA start site and the genome 3'-end promoter for viral RNA polymerase. J Virol 77:9147-55.
30. Whelan SP, Barr JN, Wertz GW. 2004. Transcription and replication of nonsegmented negative-strand RNA viruses. Curr Top Microbiol Immunol 283:61-119.
31. Irie T, Okamoto I, Yoshida A, Nagai Y, Sakaguchi T. 2014. Sendai virus C proteins regulate viral genome and antigenome synthesis to dictate the negative genome polarity. J Virol 88:690-8.
32. Wulan WN, Heydet D, Walker EJ, Gahan ME, Ghildyal R. 2015. Nucleocytoplasmic transport of nucleocapsid proteins of enveloped RNA viruses. Front Microbiol 6:553.

33. Pentecost M, Vashisht AA, Lester T, Voros T, Beaty SM, Park A, Wang YE, Yun TE, Freiberg AN, Wohlschlegel JA, Lee B. 2015. Evidence for ubiquitin-regulated nuclear and subnuclear trafficking among Paramyxovirinae matrix proteins. PLoS Pathog 11:e1004739.

34. Lahaye X, Vidy A, Pomier C, Obiang L, Harper F, Gaudin Y, Blondel D. 2009. Functional characterization of Negri bodies (NBs) in rabies virus-infected cells: Evidence that NBs are sites of viral transcription and replication. J Virol 83:7948-58.

35. Hoenen T, Shabman RS, Groseth A, Herwig A, Weber M, Schudt G, Dolnik O, Basler CF, Becker S, Feldmann H. 2012. Inclusion bodies are a site of ebolavirus replication. J Virol 86:11779-88.

36. Cifuentes-Munoz N, Branttie J, Slaughter KB, Dutch RE. 2017. Human Metapneumovirus Induces Formation of Inclusion Bodies for Efficient Genome Replication and Transcription. J Virol 91.

37. Rincheval V, Lelek M, Gault E, Bouillier C, Sitterlin D, Blouquit-Laye S, Galloux M, Zimmer C, Eleouet JF, Rameix-Welti MA. 2017. Functional organization of cytoplasmic inclusion bodies in cells infected by respiratory syncytial virus. Nat Commun 8:563.

38. Kubo T, Kagawa Y, Taniyama H, Hasegawa A. 2007. Distribution of inclusion bodies in tissues from 100 dogs infected with canine distemper virus. J Vet Med Sci 69:527-9.

39. Carlos TS, Fearns R, Randall RE. 2005. Interferon-induced alterations in the pattern of parainfluenza virus 5 transcription and protein synthesis and the induction of virus inclusion bodies. J Virol 79:14112-21.

40. Ma D, George CX, Nomburg JL, Pfaller CK, Cattaneo R, Samuel CE. 2018. Upon Infection, Cellular WD Repeat-Containing Protein 5 (WDR5) Localizes to Cytoplasmic Inclusion Bodies and Enhances Measles Virus Replication. J Virol 92.

41. Koga R, Sugita Y, Noda T, Yanagi Y, Ohno S. 2015. Actin-Modulating Protein Cofilin Is Involved in the Formation of Measles Virus Ribonucleoprotein Complex at the Perinuclear Region. J Virol 89:10524-31.

42. Ringel M, Heiner A, Behner L, Halwe S, Sauerhering L, Becker N, Dietzel E, Sawatsky B, Kolesnikova L, Maisner A. 2019. Nipah virus induces two inclusion body populations: Identification of novel inclusions at the plasma membrane. PLoS Pathog 15:e1007733.

43. Nikolic J, Le Bars R, Lama Z, Scrima N, Lagaudriere-Gesbert C, Gaudin Y, Blondel D. 2017. Negri bodies are viral factories with properties of liquid organelles. Nat Commun 8:58.

44. Lifland AW, Jung J, Alonas E, Zurla C, Crowe JE, Jr., Santangelo PJ. 2012. Human respiratory syncytial virus nucleoprotein and inclusion bodies antagonize the innate immune response mediated by MDA5 and MAVS. J Virol 86:8245-58.

45. Bruce EA, Stuart A, McCaffrey MW, Digard P. 2012. Role of the Rab11 pathway in negative-strand virus assembly. Biochem Soc Trans 40:1409-15.

46. Naslavsky N, Caplan S. 2018. The enigmatic endosome - sorting the ins and outs of endocytic trafficking. J Cell Sci 131.

47. Stone R, Hayashi T, Bajimaya S, Hodges E, Takimoto T. 2016. Critical role of Rab11a-mediated recycling endosomes in the assembly of type I parainfluenza viruses. Virology 487:11-8.

48.   Chambers R, Takimoto T. 2010. Trafficking of Sendai virus nucleocapsids is mediated by intracellular vesicles. PLoS One 5:e10994.

49.   Katoh H, Nakatsu Y, Kubota T, Sakata M, Takeda M, Kidokoro M. 2015. Mumps Virus Is Released from the Apical Surface of Polarized Epithelial Cells, and the Release Is Facilitated by a Rab11-Mediated Transport System. J Virol 89:12026-34.

50.   Nakatsu Y, Ma X, Seki F, Suzuki T, Iwasaki M, Yanagi Y, Komase K, Takeda M. 2013. Intracellular transport of the measles virus ribonucleoprotein complex is mediated by Rab11A-positive recycling endosomes and drives virus release from the apical membrane of polarized epithelial cells. J Virol 87:4683-93.

51.   Nturibi E, Bhagwat AR, Coburn S, Myerburg MM, Lakdawala SS. 2017. Intracellular Colocalization of Influenza Viral RNA and Rab11A Is Dependent upon Microtubule Filaments. J Virol 91.

52.   Bruce EA, Digard P, Stuart AD. 2010. The Rab11 pathway is required for influenza A virus budding and filament formation. J Virol 84:5848-59.

53.   Utley TJ, Ducharme NA, Varthakavi V, Shepherd BE, Santangelo PJ, Lindquist ME, Goldenring JR, Crowe JE, Jr. 2008. Respiratory syncytial virus uses a Vps4-independent budding mechanism controlled by Rab11-FIP2. Proc Natl Acad Sci U S A 105:10209-14.

54.   Nanbo A, Ohba Y. 2018. Budding of Ebola Virus Particles Requires the Rab11-Dependent Endocytic Recycling Pathway. J Infect Dis 218:S388-S396.

55.   Rowe RK, Suszko JW, Pekosz A. 2008. Roles for the recycling endosome, Rab8, and Rab11 in hantavirus release from epithelial cells. Virology 382:239-49.

56.   Chazal N, Gerlier D. 2003. Virus entry, assembly, budding, and membrane rafts. Microbiol Mol Biol Rev 67:226-37, table of contents.

57.   Liu Q, Chen L, Aguilar HC, Chou KC. 2018. A stochastic assembly model for Nipah virus revealed by super-resolution microscopy. Nat Commun 9:3050.

58.   Coronel EC, Takimoto T, Murti KG, Varich N, Portner A. 2001. Nucleocapsid incorporation into parainfluenza virus is regulated by specific interaction with matrix protein. J Virol 75:1117-23.

59.   Sugahara F, Uchiyama T, Watanabe H, Shimazu Y, Kuwayama M, Fujii Y, Kiyotani K, Adachi A, Kohno N, Yoshida T, Sakaguchi T. 2004. Paramyxovirus Sendai virus-like particle formation by expression of multiple viral proteins and acceleration of its release by C protein. Virology 325:1-10.

60.   Coronel EC, Murti KG, Takimoto T, Portner A. 1999. Human parainfluenza virus type 1 matrix and nucleoprotein genes transiently expressed in mammalian cells induce the release of virus-like particles containing nucleocapsid-like structures. J Virol 73:7035-8.

61.   Re GG, Kingsbury DW. 1988. Paradoxical effects of Sendai virus DI RNA size on survival: inefficient envelopment of small nucleocapsids. Virology 165:331-7.

62.   Chen BJ, Lamb RA. 2008. Mechanisms for enveloped virus budding: can some viruses do without an ESCRT? Virology 372:221-32.

63.   Park A, Yun T, Vigant F, Pernet O, Won ST, Dawes BE, Bartkowski W, Freiberg AN, Lee B. 2016. Nipah Virus C Protein Recruits Tsg101 to Promote the Efficient Release of Virus in an ESCRT-Dependent Pathway. PLoS Pathog 12:e1005659.

64.   Schmitt AP, Leser GP, Morita E, Sundquist WI, Lamb RA. 2005. Evidence for a new viral late-domain core sequence, FPIV, necessary for budding of a paramyxovirus. J Virol 79:2988-97.

65. Li M, Schmitt PT, Li Z, McCrory TS, He B, Schmitt AP. 2009. Mumps virus matrix, fusion, and nucleocapsid proteins cooperate for efficient production of virus-like particles. J Virol 83:7261-72.

66. Salditt A, Koethe S, Pohl C, Harms H, Kolesnikova L, Becker S, Schneider-Schaulies S. 2010. Measles virus M protein-driven particle production does not involve the endosomal sorting complex required for transport (ESCRT) system. J Gen Virol 91:1464-72.

67. Irie T, Nagata N, Yoshida T, Sakaguchi T. 2008. Recruitment of Alix/AIP1 to the plasma membrane by Sendai virus C protein facilitates budding of virus-like particles. Virology 371:108-20.

68. Sakaguchi T, Kato A, Sugahara F, Shimazu Y, Inoue M, Kiyotani K, Nagai Y, Yoshida T. 2005. AIP1/Alix is a binding partner of Sendai virus C protein and facilitates virus budding. J Virol 79:8933-41.

69. Gosselin-Grenet AS, Marq JB, Abrami L, Garcin D, Roux L. 2007. Sendai virus budding in the course of an infection does not require Alix and VPS4A host factors. Virology 365:101-12.

70. Hasan MK, Kato A, Muranaka M, Yamaguchi R, Sakai Y, Hatano I, Tashiro M, Nagai Y. 2000. Versatility of the accessory C proteins of Sendai virus: contribution to virus assembly as an additional role. J Virol 74:5619-28.

71. Loney C, Mottet-Osman G, Roux L, Bhella D. 2009. Paramyxovirus ultrastructure and genome packaging: cryo-electron tomography of sendai virus. J Virol 83:8191-7.

72. Garcin D, Latorre P, Kolakofsky D. 1999. Sendai virus C proteins counteract the interferon-mediated induction of an antiviral state. J Virol 73:6559-65.

73. Cadd T, Garcin D, Tapparel C, Itoh M, Homma M, Roux L, Curran J, Kolakofsky D. 1996. The Sendai paramyxovirus accessory C proteins inhibit viral genome amplification in a promoter-specific fashion. J Virol 70:5067-74.

74. Curran J, Latorre P, Kolakofsky D. Translational gymnastics on the Sendai virus P/C mRNA, p 351-357. *In* (ed), Elsevier,

75. Sakaguchi T, Irie T, Kuwayama M, Ueno T, Yoshida A, Kawabata R. 2011. Analysis of interaction of Sendai virus V protein and melanoma differentiation-associated gene 5. Microbiol Immunol 55:760-7.

76. Komatsu T, Tanaka Y, Kitagawa Y, Koide N, Naiki Y, Morita N, Gotoh B, Yokochi T. 2018. Sendai Virus V Protein Inhibits the Secretion of Interleukin-1beta by Preventing NLRP3 Inflammasome Assembly. J Virol 92.

77. Sanchez-Aparicio MT, Feinman LJ, Garcia-Sastre A, Shaw ML. 2018. Paramyxovirus V Proteins Interact with the RIG-I/TRIM25 Regulatory Complex and Inhibit RIG-I Signaling. J Virol 92.

78. Kato A, Kiyotani K, Sakai Y, Yoshida T, Nagai Y. 1997. The paramyxovirus, Sendai virus, V protein encodes a luxury function required for viral pathogenesis. EMBO J 16:578-87.

79. Kato A, Kiyotani K, Kubota T, Yoshida T, Tashiro M, Nagai Y. 2007. Importance of the anti-interferon capacity of Sendai virus C protein for pathogenicity in mice. J Virol 81:3264-71.

80. Tashiro M, Yokogoshi Y, Tobita K, Seto JT, Rott R, Kido H. 1992. Tryptase Clara, an activating protease for Sendai virus in rat lungs, is involved in pneumopathogenicity. J Virol 66:7211-6.

81. Markwell MA, Paulson JC. 1980. Sendai virus utilizes specific sialyloligosaccharides as host cell receptor determinants. Proc Natl Acad Sci U S A 77:5693-7.

82. Parker JC, Reynolds RK. 1968. Natural history of Sendai virus infection in mice. Am J Epidemiol 88:112-25.

83. Chen Y, Webster RG, Woodland DL. 1998. Induction of CD8+ T cell responses to dominant and subdominant epitopes and protective immunity to Sendai virus infection by DNA vaccination. J Immunol 160:2425-32.

84. Hou S, Doherty PC. 1995. Clearance of Sendai virus by CD8+ T cells requires direct targeting to virus-infected epithelium. Eur J Immunol 25:111-6.

85. Kim WK, Jain D, Sanchez MD, Koziol-White CJ, Matthews K, Ge MQ, Haczku A, Panettieri RA, Jr., Frieman MB, Lopez CB. 2014. Deficiency of melanoma differentiation-associated protein 5 results in exacerbated chronic postviral lung inflammation. Am J Respir Crit Care Med 189:437-48.

86. Garcia GL, Valenzuela A, Manzoni T, Vaughan AE, Lopez CB. 2020. Distinct Chronic Post-Viral Lung Diseases upon Infection with Influenza or Parainfluenza Viruses Differentially Impact Superinfection Outcome. Am J Pathol 190:543-553.

87. Profeta ML, Lief FS, Plotkin SA. 1969. Enzootic sendai infection in laboratory hamsters. Am J Epidemiol 89:316-24.

88. Hara H, Hara H, Hironaka T, Inoue M, Iida A, Shu T, Hasegawa M, Nagai Y, Falsey AR, Kamali A, Anzala O, Sanders EJ, Karita E, Mwananyanda L, Vasan S, Lombardo A, Parks CL, Sayeed E, Krebs M, Cormier E, Ackland J, Price MA, Excler JL. 2011. Prevalence of specific neutralizing antibodies against Sendai virus in populations from different geographic areas: implications for AIDS vaccine development using Sendai virus vectors. Hum Vaccin 7:639-45.

89. Pathak KB, Nagy PD. 2009. Defective Interfering RNAs: Foes of Viruses and Friends of Virologists. Viruses 1:895-919.

90. Lopez CB. 2014. Defective viral genomes: critical danger signals of viral infections. J Virol 88:8720-3.

91. Rezelj VV, Levi LI, Vignuzzi M. 2018. The defective component of viral populations. Curr Opin Virol 33:74-80.

92. Genoyer E, Lopez CB. 2019. The Impact of Defective Viruses on Infection and Immunity. Annu Rev Virol 6:547-566.

93. Li D, Aaskov J. 2014. Sub-genomic RNA of defective interfering (D.I.) dengue viral particles is replicated in the same manner as full length genomes. Virology 468-470:248-55.

94. Duhaut S, Dimmock NJ. 2000. Approximately 150 nucleotides from the 5' end of an influenza A segment 1 defective virion RNA are needed for genome stability during passage of defective virus in infected cells. Virology 275:278-85.

95. Li D, Lott WB, Lowry K, Jones A, Thu HM, Aaskov J. 2011. Defective interfering viral particles in acute dengue infections. PLoS One 6:e19447.

96. Poirier EZ, Mounce BC, Rozen-Gagnon K, Hooikaas PJ, Stapleford KA, Moratorio G, Vignuzzi M. 2015. Low-Fidelity Polymerases of Alphaviruses Recombine at Higher Rates To Overproduce Defective Interfering Particles. J Virol 90:2446-54.

97. Liao WY, Ke TY, Wu HY. 2014. The 3'-terminal 55 nucleotides of bovine coronavirus defective interfering RNA harbor cis-acting elements required for both negative- and positive-strand RNA synthesis. PLoS One 9:e98422.

98. McLaren LC, Holland JJ. 1974. Defective interfering particles from poliovirus vaccine and vaccine reference strains. Virology 60:579-83.

99. Xiao CT, Liu ZH, Yu XL, Ge M, Li RC, Xiao BR, Zhou HR. 2011. Identification of new defective interfering RNA species associated with porcine reproductive and respiratory syndrome virus infection. Virus Res 158:33-6.

100. Kuge S, Saito I, Nomoto A. 1986. Primary structure of poliovirus defective-interfering particle genomes and possible generation mechanisms of the particles. J Mol Biol 192:473-87.

101. Davis AR, Hiti AL, Nayak DP. 1980. Influenza defective interfering viral RNA is formed by internal deletion of genomic RNA. Proceedings of the National Academy of Sciences of the United States of America 77:215-9.

102. Patel AH, Elliott RM. 1992. Characterization of Bunyamwera virus defective interfering particles. J Gen Virol 73 (Pt 2):389-96.

103. Sheng Z, Liu R, Yu J, Ran Z, Newkirk SJ, An W, Li F, Wang D. 2018. Identification and characterization of viral defective RNA genomes in influenza B virus. J Gen Virol 99:475-488.

104. Saira K, Lin X, DePasse JV, Halpin R, Twaddle A, Stockwell T, Angus B, Cozzi-Lepri A, Delfino M, Dugan V, Dwyer DE, Freiberg M, Horban A, Losso M, Lynfield R, Wentworth DN, Holmes EC, Davey R, Wentworth DE, Ghedin E. 2013. Sequence analysis of in vivo defective interfering-like RNA of influenza A H1N1 pandemic virus. Journal of virology 87:8064-74.

105. Jennings PA, Finch JT, Winter G, Robertson JS. 1983. Does the higher order structure of the influenza virus ribonucleoprotein guide sequence rearrangements in influenza viral RNA? Cell 34:619-27.

106. Boni MF, Zhou Y, Taubenberger JK, Holmes EC. 2008. Homologous recombination is very rare or absent in human influenza A virus. J Virol 82:4807-11.

107. Vasilijevic J, Zamarreno N, Oliveros JC, Rodriguez-Frandsen A, Gomez G, Rodriguez G, Perez-Ruiz M, Rey S, Barba I, Pozo F, Casas I, Nieto A, Falcon A. 2017. Reduced accumulation of defective viral genomes contributes to severe outcome in influenza virus infected patients. PLoS Pathog 13:e1006650.

108. Fodor E, Mingay LJ, Crow M, Deng T, Brownlee GG. 2003. A single amino acid mutation in the PA subunit of the influenza virus RNA polymerase promotes the generation of defective interfering RNAs. J Virol 77:5017-20.

109. Kolakofsky D. 1976. Isolation and characterization of Sendai virus DI-RNAs. Cell 8:547-55.

110. Schubert M, Keene JD, Lazzarini RA, Emerson SU. 1978. The complete sequence of a unique RNA species synthesized by a DI particle of VSV. Cell 15:103-12.

111. Meier E, Harmison GG, Keene JD, Schubert M. 1984. Sites of copy choice replication involved in generation of vesicular stomatitis virus defective-interfering particle RNAs. J Virol 51:515-21.

112. Sun Y, Kim EJ, Felt SA, Taylor LJ, Agarwal D, Grant GR, Lopez CB. 2019. A specific sequence in the genome of respiratory syncytial virus regulates the generation of copy-back defective viral genomes. PLoS Pathog 15:e1007707.

113. Kupke SY, Riedel D, Frensing T, Zmora P, Reichl U. 2019. A Novel Type of Influenza A Virus-Derived Defective Interfering Particle with Nucleotide Substitutions in Its Genome. J Virol 93.

114. Dimmock NJ, Easton AJ. 2014. Defective Interfering Influenza Virus RNAs: Time To Reevaluate Their Clinical Potential as Broad-Spectrum Antivirals? Journal of virology 88:5217-27.
115. Ngunjiri JM, Buchek GM, Mohni KN, Sekellick MJ, Marcus PI. 2013. Influenza virus subpopulations: exchange of lethal H5N1 virus NS for H1N1 virus NS triggers de novo generation of defective-interfering particles and enhances interferon-inducing particle efficiency. Journal of interferon & cytokine research : the official journal of the International Society for Interferon and Cytokine Research 33:99-107.
116. Ngunjiri JM, Lee CW, Ali A, Marcus PI. 2012. Influenza virus interferon-inducing particle efficiency is reversed in avian and mammalian cells, and enhanced in cells co-infected with defective-interfering particles. Journal of interferon & cytokine research : the official journal of the International Society for Interferon and Cytokine Research 32:280-5.
117. Brinton MA. 1983. Analysis of extracellular West Nile virus particles produced by cell cultures from genetically resistant and susceptible mice indicates enhanced amplification of defective interfering particles by resistant cultures. J Virol 46:860-70.
118. Sanchez-Aparicio MT, Garcin D, Rice CM, Kolakofsky D, Garcia-Sastre A, Baum A. 2017. Loss of Sendai virus C protein leads to accumulation of RIG-I immunostimulatory defective interfering RNA. J Gen Virol 98:1282-1293.
119. Pfaller CK, Mastorakos GM, Matchett WE, Ma X, Samuel CE, Cattaneo R. 2015. Measles Virus Defective Interfering RNAs Are Generated Frequently and Early in the Absence of C Protein and Can Be Destabilized by Adenosine Deaminase Acting on RNA-1-Like Hypermutations. J Virol 89:7735-47.
120. Odagiri T, Tobita K. 1990. Mutation in NS2, a nonstructural protein of influenza A virus, extragenically causes aberrant replication and expression of the PA gene and leads to generation of defective interfering particles. Proceedings of the National Academy of Sciences of the United States of America 87:5988-92.
121. Marcus PI, Gaccione C. 1989. Interferon induction by viruses. XIX. Vesicular stomatitis virus--New Jersey: high multiplicity passages generate interferon-inducing, defective-interfering particles. Virology 171:630-3.
122. White CL, Thomson M, Dimmock NJ. 1998. Deletion analysis of a defective interfering Semliki Forest virus RNA genome defines a region in the nsP2 sequence that is required for efficient packaging of the genome into virus particles. J Virol 72:4320-6.
123. Xie Q, Cao Y, Su J, Wu J, Wu X, Wan C, He M, Ke C, Zhang B, Zhao W. 2017. Two deletion variants of Middle East respiratory syndrome coronavirus found in a patient with characteristic symptoms. Arch Virol 162:2445-2449.
124. Zhong P, Agosto LM, Munro JB, Mothes W. 2013. Cell-to-cell transmission of viruses. Curr Opin Virol 3:44-50.
125. Salinas Y, Roux L. 2005. Replication and packaging properties of short Paramyxovirus defective RNAs. Virus Res 109:125-32.
126. Ziegler CM, Eisenhauer P, Bruce EA, Weir ME, King BR, Klaus JP, Krementsov DN, Shirley DJ, Ballif BA, Botten J. 2016. The Lymphocytic Choriomeningitis Virus Matrix Protein PPXY Late Domain Drives the Production of Defective Interfering Particles. PLoS Pathog 12:e1005501.
127. Ziegler CM, Eisenhauer P, Bruce EA, Beganovic V, King BR, Weir ME, Ballif BA, Botten J. 2016. A novel phosphoserine motif in the LCMV matrix protein Z

regulates the release of infectious virus and defective interfering particles. J Gen Virol 97:2084-9.

128. Von Magnus P. 1954. Incomplete forms of influenza virus. Advances in virus research 2:59-79.

129. Magnus Pv. 1947. Studies on interference in experimental influenza. Ark Kemi Mineral Geol 24.

130. Paucker K, Cantell K. 1963. QUANTITATIVE STUDIES ON VIRAL INTERFERENCE IN SUSPENDED L CELLS. V. PERSISTENCE OF PROTECTION IN GROWING CULTURES. Virology 21:22-9.

131. Sokol F, Neurath AR, Vilcek J. 1964. FORMATION OF INCOMPLETE SENDAI VIRUS IN EMBRYONATED EGGS. Acta Virol 8:59-67.

132. Huang AS, Greenawalt JW, Wagner RR. 1966. Defective T particles of vesicular stomatitis virus. I. Preparation, morphology, and some biologic properties. Virology 30:161-72.

133. Mims CA. 1956. Rift Valley Fever virus in mice. IV. Incomplete virus; its production and properties. Br J Exp Pathol 37:129-43.

134. Kennedy SI, Bruton CJ, Weiss B, Schlesinger S. 1976. Defective interfering passages of Sindbis virus: nature of the defective virion RNA. J Virol 19:1034-43.

135. Cole CN, Smoler D, Wimmer E, Baltimore D. 1971. Defective interfering particles of poliovirus. I. Isolation and physical properties. Journal of virology 7:478-85.

136. Barrett AD, Dimmock NJ. 1984. Modulation of a systemic Semliki Forest virus infection in mice by defective interfering virus. The Journal of general virology 65 (Pt 10):1827-31.

137. Crouch CF, Mackenzie A, Dimmock NJ. 1982. The effect of defective-interfering Semliki Forest virus on the histopathology of infection with virulent Semliki Forest virus in mice. J Infect Dis 146:411-6.

138. Rabinowitz SG, Huprikar J. 1979. The influence of defective-interfering particles of the PR-8 strain of influenza A virus on the pathogenesis of pulmonary infection in mice. The Journal of infectious diseases 140:305-15.

139. Gamboa ET, Harter DH, Duffy PE, Hsu KC. 1976. Murine influenza virus encephalomyelitis. III. Effect of defective interfering virus particles. Acta Neuropathol (Berl) 34:157-69.

140. Tapia K, Kim WK, Sun Y, Mercado-Lopez X, Dunay E, Wise M, Adu M, Lopez CB. 2013. Defective viral genomes arising in vivo provide critical danger signals for the triggering of lung antiviral immunity. PLoS pathogens 9:e1003703.

141. Sun Y, Jain D, Koziol-White CJ, Genoyer E, Gilbert M, Tapia K, Panettieri RA, Jr., Hodinka RL, Lopez CB. 2015. Immunostimulatory Defective Viral Genomes from Respiratory Syncytial Virus Promote a Strong Innate Antiviral Response during Infection in Mice and Humans. PLoS Pathog 11:e1005122.

142. Poirier EZ, Goic B, Tome-Poderti L, Frangeul L, Boussier J, Gausson V, Blanc H, Vallet T, Loyd H, Levi LI, Lanciano S, Baron C, Merkling SH, Lambrechts L, Mirouze M, Carpenter S, Vignuzzi M, Saleh MC. 2018. Dicer-2-Dependent Generation of Viral DNA from Defective Genomes of RNA Viruses Modulates Antiviral Immunity in Insects. Cell Host Microbe 23:353-365.e8.

143. Pesko KN, Fitzpatrick KA, Ryan EM, Shi PY, Zhang B, Lennon NJ, Newman RM, Henn MR, Ebel GD. 2012. Internally deleted WNV genomes isolated from exotic birds in New Mexico: function in cells, mosquitoes, and mice. Virology 427:10-7.

144. McCrone JT, Lauring AS. 2018. Genetic bottlenecks in intraspecies virus transmission. Curr Opin Virol 28:20-25.

145. Cuevas JM, Duran-Moreno M, Sanjuan R. 2017. Multi-virion infectious units arise from free viral particles in an enveloped virus. Nat Microbiol 2:17078.
146. Aguilera ER, Erickson AK, Jesudhasan PR, Robinson CM, Pfeiffer JK. 2017. Plaques Formed by Mutagenized Viral Populations Have Elevated Coinfection Frequencies. mBio 8.
147. Mottet G, Curran J, Roux L. 1990. Intracellular stability of nonreplicating paramyxovirus nucleocapsids. Virology 176:1-7.
148. Cane C, McLain L, Dimmock NJ. 1987. Intracellular stability of the interfering activity of a defective interfering influenza virus in the absence of virus multiplication. Virology 159:259-64.
149. Noppornpanth S, Smits, S.L., Lien, T.X., Poovorawan, Y., Osterhaus, A.D.M.E., Haagmans, B.L. 2007. Characterization of Hepatitis C Virus Deletion Mutants Circulating in Chronically Infected Patients. Journal of Virology 81:7.
150. Nuesch JP, de Chastonay J, Siegl G. 1989. Detection of defective genomes in hepatitis A virus particles present in clinical specimens. The Journal of general virology 70 (Pt 12):3475-80.
151. Sidhu MS, Crowley, J., Lowenthal, A., Karcher, D., Menonna, J., Cook, S., Udem, S., Dowling, P. 1994. Defective Measles Virus in Human Subacute Sclerosing Panencephalitis Brain. Virology 202:10.
152. Sun Y, López CB. 2016. Preparation of Respiratory Syncytial Virus with High or Low Content of Defective Viral Particles and Their Purification from Viral Stocks. Bio-protocol 6.
153. Calain P, Roux L. 1995. Functional characterisation of the genomic and antigenomic promoters of Sendai virus. Virology 212:163-73.
154. Fonville JM, Marshall N, Tao H, Steel J, Lowen AC. 2015. Influenza Virus Reassortment Is Enhanced by Semi-infectious Particles but Can Be Suppressed by Defective Interfering Particles. PLoS Pathog 11:e1005204.
155. Tuffereau C, Roux L. 1988. Direct adverse effects of Sendai virus DI particles on virus budding and on M protein fate and stability. Virology 162:417-26.
156. Roux L, Waldvogel FA. 1983. Defective interfering particles of Sendai virus modulate HN expression at the surface of infected BHK cells. Virology 130:91-104.
157. Adachi T, Lazzarini RA. 1978. Elementary aspects of autointerference and the replication of defective interfering virus particles. Virology 87:152-63.
158. Brinton MA, Fernandez AV. 1983. A replication-efficient mutant of West Nile virus is insensitive to DI particle interference. Virology 129:107-15.
159. McLain L, Armstrong SJ, Dimmock NJ. 1988. One defective interfering particle per cell prevents influenza virus-mediated cytopathology: an efficient assay system. J Gen Virol 69 (Pt 6):1415-9.
160. Fuller FJ, Marcus PI. 1980. Interferon induction by viruses. IV. Sindbis virus: early passage defective-interfering particles induce interferon. The Journal of general virology 48:63-73.
161. Fuller FJ, Marcus PI. 1980. Interferon induction by viruses. Sindbis virus: defective-interfering particles temperature-sensitive for interferon induction. The Journal of general virology 48:391-4.
162. van den Hoogen BG, van Boheemen S, de Rijck J, van Nieuwkoop S, Smith DJ, Laksono B, Gultyaev A, Osterhaus AD, Fouchier RA. 2014. Excessive production and extreme editing of human metapneumovirus defective interfering RNA is associated with type I IFN induction. J Gen Virol 95:1625-33.

163. Yount JS, Gitlin L, Moran TM, Lopez CB. 2008. MDA5 Participates in the Detection of Paramyxovirus Infection and Is Essential for the Early Activation of Dendritic Cells in Response to Sendai Virus Defective Interfering Particles. J Immunol 180:4910-8.

164. Yount JS, Kraus TA, Horvath CM, Moran TM, Lopez CB. 2006. A novel role for viral-defective interfering particles in enhancing dendritic cell maturation. J Immunol 177:4503-13.

165. Xu J, Sun Y, Li Y, Ruthel G, Weiss SR, Raj A, Beiting D, Lopez CB. 2017. Replication defective viral genomes exploit a cellular pro-survival mechanism to establish paramyxovirus persistence. Nat Commun 8:799.

166. Xu J, Mercado-Lopez X, Grier JT, Kim WK, Chun LF, Irvine EB, Del Toro Duany Y, Kell A, Hur S, Gale M, Jr., Raj A, Lopez CB. 2015. Identification of a Natural Viral RNA Motif That Optimizes Sensing of Viral RNA by RIG-I. MBio 6.

167. Baum A, Sachidanandam R, Garcia-Sastre A. 2010. Preference of RIG-I for short viral RNA molecules in infected cells revealed by next-generation sequencing. Proceedings of the National Academy of Sciences of the United States of America 107:16303-8.

168. Mura M, Combredet C, Najburg V, Sanchez David RY, Tangy F, Komarova AV. 2017. Nonencapsidated 5' Copy-Back Defective Interfering Genomes Produced by Recombinant Measles Viruses Are Recognized by RIG-I and LGP2 but Not MDA5. J Virol 91.

169. Ho TH, Kew C, Lui PY, Chan CP, Satoh T, Akira S, Jin DY, Kok KH. 2015. PACT- and RIG-I-Dependent Activation of Type I Interferon Production by a Defective Interfering RNA Derived from Measles Virus Vaccine. J Virol 90:1557-68.

170. Strahle L, Garcin D, Kolakofsky D. 2006. Sendai virus defective-interfering genomes and the activation of interferon-beta. Virology 351:101-11.

171. Yoshida A, Kawabata R, Honda T, Sakai K, Ami Y, Sakaguchi T, Irie T. 2017. A single amino acid substitution within the Paramyxovirus Sendai virus nucleoprotein is a critical determinant for production of IFN-beta-inducing copyback-type defective interfering genomes. J Virol doi:10.1128/JVI.02094-17.

172. Russell AB, Trapnell C, Bloom JD. 2018. Extreme heterogeneity of influenza virus infection in single cells. Elife 7.

173. Killip MJ, Jackson D, Perez-Cidoncha M, Fodor E, Randall RE. 2017. Single-cell studies of IFN-beta promoter activation by wild-type and NS1-defective influenza A viruses. J Gen Virol 98:357-363.

174. Akpinar F, Inankur B, Yin J. 2016. Spatial-Temporal Patterns of Viral Amplification and Interference Initiated by a Single Infected Cell. J Virol 90:7552-66.

175. Sekellick MJ, Marcus PI. 1980. Viral interference by defective particles of vesicular stomatitis virus measured in individual cells. Virology 104:247-52.

176. Calain P, Monroe MC, Nichol ST. 1999. Ebola Virus Defective Interfering Particles and Persistent Infection. Virology 262:114-128.

177. Whistler T, Bellini WJ, Rota PA. 1996. Generation of defective interfering particles by two vaccine strains of measles virus. Virology 220:480-4.

178. Santak M, Markusic M, Balija ML, Kopac SK, Jug R, Orvell C, Tomac J, Forcic D. 2015. Accumulation of defective interfering viral particles in only a few passages in Vero cells attenuates mumps virus neurovirulence. Microbes Infect 17:228-36.

179.	Murphy DG, Dimock K, Kang CY. 1987. Defective interfering particles of human parainfluenza virus 3. Virology 158:439-43.
180.	Frey TK, Hemphill ML. 1988. Generation of defective-interfering particles by rubella virus in Vero cells. Virology 164:22-9.
181.	Treuhaft MW, Beem MO. 1982. Defective interfering particles of respiratory syncytial virus. Infect Immun 37:439-44.
182.	Hall WW, Martin SJ, Gould E. 1974. Defective interfering particles produced during the replication of measles virus. Med Microbiol Immunol 160:155-64.
183.	Perrault J. 1981. Origin and replication of defective interfering particles. Curr Top Microbiol Immunol 93:151-207.
184.	Zanini F, Pu SY, Bekerman E, Einav S, Quake SR. 2018. Single-cell transcriptional dynamics of flavivirus infection. Elife 7.
185.	Guo F, Li S, Caglar MU, Mao Z, Liu W, Woodman A, Arnold JJ, Wilke CO, Huang TJ, Cameron CE. 2017. Single-Cell Virology: On-Chip Investigation of Viral Infection Dynamics. Cell Rep 21:1692-1704.
186.	Akpinar F, Timm A, Yin J. 2015. High-Throughput Single-Cell Kinetics of Virus Infections in the Presence of Defective Interfering Particles. J Virol 90:1599-612.
187.	Ruigrok RW, Crepin T, Kolakofsky D. 2011. Nucleoproteins and nucleocapsids of negative-strand RNA viruses. Curr Opin Microbiol 14:504-10.
188.	Moyer SA, Baker SC, Lessard JL. 1986. Tubulin: a factor necessary for the synthesis of both Sendai virus and vesicular stomatitis virus RNAs. Proc Natl Acad Sci U S A 83:5405-9.
189.	Roux L, Beffy P, Portner A. 1984. Restriction of cell surface expression of Sendai virus hemagglutinin-neuraminidase glycoprotein correlates with its higher instability in persistently and standard plus defective interfering virus infected BHK-21 cells. Virology 138:118-28.
190.	Sanderson CM, McQueen NL, Nayak DP. 1993. Sendai virus assembly: M protein binds to viral glycoproteins in transit through the secretory pathway. J Virol 67:651-63.
191.	Stricker R, Mottet G, Roux L. 1994. The Sendai virus matrix protein appears to be recruited in the cytoplasm by the viral nucleocapsid to function in viral assembly and budding. J Gen Virol 75 (Pt 5):1031-42.
192.	Iwasaki M, Takeda M, Shirogane Y, Nakatsu Y, Nakamura T, Yanagi Y. 2009. The matrix protein of measles virus regulates viral RNA synthesis and assembly by interacting with the nucleocapsid protein. J Virol 83:10374-83.
193.	Neil RC, Tapia KA, Dandapani A, MacArthur BD, López C, Ma'ayan A. 2011. Stochastic model of virus and defective interfering particle spread across mammalian cells with immune response. arXiv arXiv:1108.4901.
194.	Reed LJ MH. 1938. A simple method of estimating fifty per cent endpoints. Am J Hyg 27:493-497.
195.	Costes SV, Daelemans D, Cho EH, Dobbin Z, Pavlakis G, Lockett S. 2004. Automatic and quantitative measurement of protein-protein colocalization in live cells. Biophys J 86:3993-4003.
196.	Grant BD, Donaldson JG. 2009. Pathways and mechanisms of endocytic recycling. Nat Rev Mol Cell Biol 10:597-608.
197.	Genoyer E, Lopez CB. 2019. Defective Viral Genomes Alter How Sendai Virus Interacts with Cellular Trafficking Machinery, Leading to Heterogeneity in the Production of Viral Particles among Infected Cells. J Virol 93.

198.   Latorre P, Cadd T, Itoh M, Curran J, Kolakofsky D. 1998. The various Sendai virus C proteins are not functionally equivalent and exert both positive and negative effects on viral RNA accumulation during the course of infection. J Virol 72:5984-93.

199.   Portner A, Murti KG, Morgan EM, Kingsbury DW. 1988. Antibodies against Sendai virus L protein: distribution of the protein in nucleocapsids revealed by immunoelectron microscopy. Virology 163:236-9.

200.   Yamada H, Hayata S, Omata-Yamada T, Taira H, Mizumoto K, Iwasaki K. 1990. Association of the Sendai virus C protein with nucleocapsids. Arch Virol 113:245-53.

201.   Amorim MJ, Bruce EA, Read EK, Foeglein A, Mahen R, Stuart AD, Digard P. 2011. A Rab11- and microtubule-dependent mechanism for cytoplasmic transport of influenza A virus viral RNA. J Virol 85:4143-56.

202.   Bhagwat AR, Le Sage V, Nturibi E, Kulej K, Jones J, Guo M, Tae Kim E, Garcia BA, Weitzman MD, Shroff H, Lakdawala SS. 2020. Quantitative live cell imaging reveals influenza virus manipulation of Rab11A transport through reduced dynein association. Nat Commun 11:23.

203.   Liljeroos L, Huiskonen JT, Ora A, Susi P, Butcher SJ. 2011. Electron cryotomography of measles virus reveals how matrix protein coats the ribonucleocapsid within intact virions. Proc Natl Acad Sci U S A 108:18085-90.

204.   Chen W, Feng Y, Chen D, Wandinger-Ness A. 1998. Rab11 is required for trans-golgi network-to-plasma membrane transport and a preferential target for GDP dissociation inhibitor. Mol Biol Cell 9:3241-57.

205.   Laske T, Heldt FS, Hoffmann H, Frensing T, Reichl U. 2016. Modeling the intracellular replication of influenza A virus in the presence of defective interfering RNAs. Virus Res 213:90-99.

206.   Beaty SM, Park A, Won ST, Hong P, Lyons M, Vigant F, Freiberg AN, tenOever BR, Duprex WP, Lee B. 2017. Efficient and Robust Paramyxoviridae Reverse Genetics Systems. mSphere 2.

207.   HaileMariam M, Eguez RV, Singh H, Bekele S, Ameni G, Pieper R, Yu Y. 2018. S-Trap, an Ultrafast Sample-Preparation Approach for Shotgun Proteomics. J Proteome Res 17:2917-2924.

208.   Russell AB, Elshina E, Kowalsky JR, Te Velthuis AJW, Bloom JD. 2019. Single-Cell Virus Sequencing of Influenza Infections That Trigger Innate Immunity. J Virol 93.

209.   Wang C, Forst CV, Chou TW, Geber A, Wang M, Hamou W, Smith M, Sebra R, Zhang B, Zhou B, Ghedin E. 2020. Cell-to-Cell Variation in Defective Virus Expression and Effects on Host Responses during Influenza Virus Infection. mBio 11.

210.   Schwartz SL, Lowen AC. 2016. Droplet digital PCR: A novel method for detection of influenza virus defective interfering particles. J Virol Methods 237:159-165.

211.   Welch SR, Tilston NL, Lo MK, Whitmer SLM, Harmon JR, Scholte FEM, Spengler JR, Duprex WP, Nichol ST, Spiropoulou CF. 2020. Inhibition of Nipah Virus by Defective Interfering Particles. J Infect Dis doi:10.1093/infdis/jiz564.

212.   Bagga S, Bouchard MJ. 2014. Cell cycle regulation during viral infection. Methods Mol Biol 1170:165-227.

213.   Bressy C, Droby GN, Maldonado BD, Steuerwald N, Grdzelishvili VZ. 2019. Cell Cycle Arrest in G2/M Phase Enhances Replication of Interferon-Sensitive Cytoplasmic RNA Viruses via Inhibition of Antiviral Gene Expression. J Virol 93.

214. Rouhanifard SH, Mellis IA, Dunagin M, Bayatpour S, Jiang CL, Dardani I, Symmons O, Emert B, Torre E, Cote A, Sullivan A, Stamatoyannopoulos JA, Raj A. 2018. ClampFISH detects individual nucleic acid molecules using click chemistry-based amplification. Nat Biotechnol doi:10.1038/nbt.4286.

215. Cohen M, Giladi A, Gorki AD, Solodkin DG, Zada M, Hladik A, Miklosi A, Salame TM, Halpern KB, David E, Itzkovitz S, Harkany T, Knapp S, Amit I. 2018. Lung Single-Cell Signaling Interaction Map Reveals Basophil Role in Macrophage Imprinting. Cell 175:1031-1044 e18.

216. Mostafa HH, Vogel P, Srinivasan A, Russell CJ. 2016. Non-invasive Imaging of Sendai Virus Infection in Pharmacologically Immunocompromised Mice: NK and T Cells, but not Neutrophils, Promote Viral Clearance after Therapy with Cyclophosphamide and Dexamethasone. PLoS Pathog 12:e1005875.

217. Lopez CB, Yount JS, Hermesh T, Moran TM. 2006. Sendai virus infection induces efficient adaptive immunity independently of type I interferons. J Virol 80:4538-45.

218. Vignuzzi M, Lopez CB. 2019. Defective viral genomes are key drivers of the virus-host interaction. Nat Microbiol 4:1075-1087.

219. Khan SR, Lazzarini RA. 1977. The relationship between autointerference and the replication of defective interfering particle. Virology 77:189-201.

220. Stauffer Thompson KA, Rempala GA, Yin J. 2009. Multiple-hit inhibition of infection by defective interfering particles. The Journal of General Virology 90:888-899.

221. Baltes A, Akpinar F, Inankur B, Yin J. 2017. Inhibition of infection spread by co-transmitted defective interfering particles. PLoS One 12:e0184029.

222. Easton AJ, Scott PD, Edworthy NL, Meng B, Marriott AC, Dimmock NJ. 2011. A novel broad-spectrum treatment for respiratory virus infections: influenza-based defective interfering virus provides protection against pneumovirus infection in vivo. Vaccine 29:2777-84.

223. Smith CM, Scott PD, O'Callaghan C, Easton AJ, Dimmock NJ. 2016. A Defective Interfering Influenza RNA Inhibits Infectious Influenza Virus Replication in Human Respiratory Tract Cells: A Potential New Human Antiviral. Viruses 8.

224. Tanner EJ, Kirkegaard KA, Weinberger LS. 2016. Exploiting Genetic Interference for Antiviral Therapy. PLoS Genet 12:e1005986.

225. Atkin-Smith GK, Duan M, Chen W, Poon IKH. 2018. The induction and consequences of Influenza A virus-induced cell death. Cell Death Dis 9:1002.

226. Manzoni TB, Lopez CB. 2018. Defective (interfering) viral genomes re-explored: impact on antiviral immunity and virus persistence. Future Virol 13:493-503.

227. Pfaller CK, Bloyet LM, Donohue RC, Huff AL, Bartemes WP, Yousaf I, Urzua E, Claviere M, Zachary M, de Masson d'Autume V, Carson S, Schieferecke AJ, Meyer AJ, Gerlier D, Cattaneo R. 2020. The C Protein Is Recruited to Measles Virus Ribonucleocapsids by the Phosphoprotein. J Virol 94.

228. Kurotani A, Kiyotani K, Kato A, Shioda T, Sakai Y, Mizumoto K, Yoshida T, Nagai Y. 1998. Sendai virus C proteins are categorically nonessential gene products but silencing their expression severely impairs viral replication and pathogenesis. Genes Cells 3:111-24.

229. Kato A, Cortese-Grogan C, Moyer SA, Sugahara F, Sakaguchi T, Kubota T, Otsuki N, Kohase M, Tashiro M, Nagai Y. 2004. Characterization of the amino acid residues of sendai virus C protein that are critically involved in its interferon antagonism and RNA synthesis down-regulation. J Virol 78:7443-54.

230. Kato A, Ohnishi Y, Hishiyama M, Kohase M, Saito S, Tashiro M, Nagai Y. 2002. The amino-terminal half of Sendai virus C protein is not responsible for either counteracting the antiviral action of interferons or down-regulating viral RNA synthesis. J Virol 76:7114-24.

231. Vale-Costa S, Amorim MJ. 2016. Recycling Endosomes and Viral Infection. Viruses 8:64.

232. Baetz NW, Goldenring JR. 2013. Rab11-family interacting proteins define spatially and temporally distinct regions within the dynamic Rab11a-dependent recycling system. Mol Biol Cell 24:643-58.

233. Taylor MP, Koyuncu OO, Enquist LW. 2011. Subversion of the actin cytoskeleton during viral infection. Nat Rev Microbiol 9:427-39.

234. Vale-Costa S, Alenquer M, Sousa AL, Kellen B, Ramalho J, Tranfield EM, Amorim MJ. 2016. Influenza A virus ribonucleoproteins modulate host recycling by competing with Rab11 effectors. J Cell Sci 129:1697-710.

235. Schomacker H, Hebner RM, Boonyaratanakornkit J, Surman S, Amaro-Carambot E, Collins PL, Schmidt AC. 2012. The C proteins of human parainfluenza virus type 1 block IFN signaling by binding and retaining Stat1 in perinuclear aggregates at the late endosome. PLoS One 7:e28382.

236. Wells G, Addington-Hall M, Malur AG. 2012. Mutations within the human parainfluenza virus type 3 (HPIV 3) C protein affect viral replication and host interferon induction. Virus Res 167:385-90.

237. Patterson JB, Thomas D, Lewicki H, Billeter MA, Oldstone MB. 2000. V and C proteins of measles virus function as virulence factors in vivo. Virology 267:80-9.

238. Ito M, Iwasaki M, Takeda M, Nakamura T, Yanagi Y, Ohno S. 2013. Measles virus nonstructural C protein modulates viral RNA polymerase activity by interacting with host protein SHCBP1. J Virol 87:9633-42.

239. Reutter GL, Cortese-Grogan C, Wilson J, Moyer SA. 2001. Mutations in the measles virus C protein that up regulate viral RNA synthesis. Virology 285:100-9.

240. Mathieu C, Guillaume V, Volchkova VA, Pohl C, Jacquot F, Looi RY, Wong KT, Legras-Lachuer C, Volchkov VE, Lachuer J, Horvat B. 2012. Nonstructural Nipah virus C protein regulates both the early host proinflammatory response and viral virulence. J Virol 86:10766-75.

241. Pantua HD, McGinnes LW, Peeples ME, Morrison TG. 2006. Requirements for the assembly and release of Newcastle disease virus-like particles. J Virol 80:11062-73.

242. Tanner EJ, Liu HM, Oberste MS, Pallansch M, Collett MS, Kirkegaard K. 2014. Dominant drug targets suppress the emergence of antiviral resistance. Elife 3.